TURUN
YLIOPISTO
UNIVERSITY
OF TURKU

IMAGING OF NEUROINFLAMMATION IN MULTIPLE SCLEROSIS BRAIN

A positron emission tomography and diffusion tensor imaging study

Jouni Tuisku

TURUN YLIOPISTON JULKAISUJA – ANNALES UNIVERSITATIS TURKUENSIS
SARJA – SER. D OSA – TOM. 1557 | MEDICA – ODONTOLOGICA | TURKU 2021

TURUN
YLIOPISTO
UNIVERSITY
OF TURKU

IMAGING OF NEUROINFLAMMATION IN MULTIPLE SCLEROSIS BRAIN

A positron emission tomography and diffusion tensor imaging study

Jouni Tuisku

TURUN YLIOPISTON JULKAISUJA – ANNALES UNIVERSITATIS TURKUENSIS
SARJA – SER. D OSA – TOM. 1557 | MEDICA – ODONTOLOGICA | TURKU 2021

University of Turku

Faculty of Medicine
Department of Neurology
Drug Research Doctoral Programme
Turku PET centre

Supervised by

Professor Laura Airas, MD, Ph.D
Turku PET Centre
University of Turku
Clinical Neurosciences
Turku University Hospital
Turku, Finland

Professor Juha Rinne, MD, Ph.D
Turku PET Centre
University of Turku
Clinical Neurosciences
Turku University Hospital
Turku, Finland

Docent Jussi Hirvonen, MD, Ph.D
Department of Radiology
Intensive Care, Emergency Care and
Pain Medicine
Turku University Hospital
Turku, Finland

Reviewed by

Professor Olli Gröhn, Ph.D
A. I. Virtanen Institute for Molecular Sciences
University of Eastern Finland
Kuopio, Finland

Assistant Professor Yeona Kang, Ph. D
Department of Mathematics
Howard University
Washington, DC, USA

Opponent

Professor Federico Turkheimer, Ph.D
Institute of Psychiatry
King's College
London, UK

ISBN 978-951-29-8484-8 (PRINT)
ISBN 978-951-29-8485-5 (PDF)
ISSN 0355-9483 (Print)
ISSN 2343-3213 (Online)
Painosalama Oy, Turku, Finland 2021

UNIVERSITY OF TURKU
Faculty of Medicine
Department of Neurology
Turku PET centre
JOUNI TUISKU: Imaging of neuroinflammation in multiple sclerosis brain: A positron emission tomography and diffusion tensor imaging study
Doctoral Dissertation, 119 pp.
Drug Research Doctoral Programme
May 2021

ABSTRACT

Multiple sclerosis (MS) is an autoimmune disease of the central nervous system, where the immune system attacks the protective myelin sheet surrounding the nerve cell axons, causing neuroinflammation and neurodegeneration. In this thesis, molecular and microstructural brain changes were evaluated in MS patients using diffusion tensor imaging (DTI) and positron emission tomography (PET) with translocator protein (TSPO) binding radioligand. In MS, TSPO is expressed mainly in activated microglia and therefore TSPO is considered as a marker of inflammation. The aim of this thesis was to evaluate the association between TSPO PET radioligand uptake and DTI macroparameters, as well as their association to clinical disability, in normal appearing white matter (NAWM). Moreover, the aim was to study if the individual physiological properties including age, body mass index (BMI) and sex have influence on the observed variability, which has been reported in previous clinical PET studies.

The results showed that increased TSPO uptake in NAWM was associated with altered NAWM DTI macroparameters, their regional correspondence was consistent, and they both were associated with advanced clinical disability. Increased age was associated with higher TSPO uptake in NAWM and in thalamus of MS patients, whereas in healthy control subjects, higher age was associated with higher cortical TSPO uptake. However, a multicenter data analysis of healthy volunteers revealed that higher age was associated with higher cortical and subcortical TSPO uptake only in male subjects. Additionally, higher TSPO uptake was associated with lower BMI, and females showed higher TSPO uptake compared to males.

The results demonstrate that PET and DTI can be used as complementary imaging modalities in clinical MS studies. TSPO levels may be associated with age, BMI and sex suggesting that they can be confounding factors in clinical designs. Subtle microglial activation may be initially related to normal ageing but is accentuated following neuroinflammation.

KEYWORDS: [^{11}C](R)-PK11195, [^{11}C]PBR28, ageing, body mass index, BMI, DTI, microglia, multiple sclerosis, PET, sex, TSPO

TURUN YLIOPISTO
Lääketieteellinen tiedekunta
Neurologia
Valtakunnallinen PET-keskus
JOUNI TUISKU: Neuroinflammaation aivokuvantaminen ms-taudissa:
Positroniemissiotomografia ja diffuusiotensorikuvantamistutkimus
Väitöskirja, 119 s.
Lääketutkimuksen tohtoriohjelma
Toukokuu 2021

TIIVISTELMÄ

Multippeliskleroosi (MS-tauti) on keskushermoston autoimmuunisairaus, jossa immuunijärjestelmä hyökkää hermosoluja suojaavaa myeliiniä vastaan aiheuttaen tulehdusreaktiota ja hermosolujen rappeutumista. Tässä tutkimuksessa tarkasteltiin MS-tautiin liittyviä aivojen molekulaarisia ja rakenteellisia muutoksia käyttämällä diffuusiotensorikuvantamista (DTI) ja positroniemissiotomografiaa (PET) translokaattoriproteiiniin (TSPO) sitoutuvalla merkkiaineella. MS-taudissa TSPO esiintyy pääosin aktivoituneissa mikroglia-soluissa ja siksi sitä pidetään tulehdusreaktion markkerina. Tämän tutkimuksen tarkoituksena oli arvioida TSPO-sitoutumisen yhteyttä DTI-kuvantamisen makroparametreihin ja kummankin yhteyttä kliinisiin mittaustuloksiin. Koska aiemmissa kliinisissä tutkimuksissa on havaittu runsaasti yksilöllistä vaihtelua TSPO-sitoutumisessa, oli tavoitteena tarkastella yksilöllisten fysiologisten tekijöiden, kuten iän, painoindeksin ja sukupuolen yhteyttä TSPO-sitoutumiseen.

Tulosten mukaan kohonnut TSPO-sitoutuminen terveessä valkeassa aineessa (NAWM) oli yhteydessä muuttuneisiin DTI-makroparametreihin, alueellinen vastaavuus oli yhtenevää ja kummankin menetelmän tulokset olivat yhteydessä kliinisiin mittaustuloksiin. Ikääntyminen oli yhteydessä kohonneeseen TSPO-sitoutumiseen NAWM:ssa ja talamuksissa MS-potilailla, kun taas terveillä koehenkilöillä ikääntyminen oli yhteydessä korkeampaan kortikaaliseen TSPO-sitoutumiseen. Laajempi monikeskustutkimus osoitti kuitenkin, että ikääntyminen oli yhteydessä korkeampaan kortikaaliseen ja subkortikaaliseen TSPO-sitoutumiseen vain miehillä. Lisäksi korkeampi TSPO-sitoutuminen oli yhteydessä matalampaan painoindeksiin ja naisilla TSPO-sitoutuminen oli korkeampaa miehiin verrattuna.

Tulokset osoittavat, että PET- ja DTI-kuvantaminen ovat toisiaan täydentäviä menetelmiä MS-taudin kuvantamisessa. Ikä, painoindeksi ja sukupuoli voivat olla sekoittavia tekijöitä kliinisissä TSPO-tutkimuksissa. TSPO-sitoutuminen liittyy normaaliin ikääntymiseen, mutta se korostuu tulehdusreaktion yhteydessä.

AVAINSANAT: [11C](R)-PK11195, [11C]PBR28, DTI, ikääntyminen, mikroglia, MS-tauti, PET, painoindeksi, sukupuoli, TSPO

Table of Contents

Abbreviations

AAL	Automated anatomical labelling
ABSS	Arterial blood sampling system
AD	Axial diffusivity
ANOVA	Analysis of variance
ANCOVA	Analysis of covariance
B_{avail}	Number of available receptors
BBB	Blood brain barrier
BET	Brain extraction tool
BMI	Body mass index
BP_{ND}	Non-displaceable binding potential
CIS	Clinically isolated syndrome
CNS	Central nervous system
COX-2	Cyclooxygenase-2
CSF	Cerebrospinal fluid
DIS	Dissemination of lesions in space
DIT	Dissemination of lesions in time
DMT	Disease modifying treatment
DTI	Diffusion tensor imaging
DVR	Distribution volume ratio
DWI	Diffusion weighted imaging
EDSS	Expanded disability status scale
EPI	Echo planar imaging
FA	Fractional anisotropy
FDR	False discovery rate
FLAIR	Fluid attenuated inversion recovery
f_p	free radioligand fraction in plasma
f_{ND}	Fraction of free radioligand in non-displaceable compartment
FWHM	Full width at half maximum
Gd	Gadolinium
GM	Gray matter
HAB	High affinity binder

HC	Healthy control
HLA	Human leukocyte antigen
HSD	Honestly significant difference
HRRT	High resolution research tomograph
K_D	Receptor dissociation constant
KI	Karolinska institutet
kDa	KiloDalton
kEV	Kilo-electronvolts
LAB	Low affinity binder
LOR	Line of response
LST	Lesion segmentation toolbox
Ma1	Ichise's multilinear analysis 1
MAB	Mixed affinity binder
MBq	Megabecquerel
MD	Mean diffusivity
MR	Magnetic resonance
MRI	Magnetic resonance imaging
MS	Multiple sclerosis
MSSS	Multiple sclerosis severity score
NAWM	Normal appearing white matter
NAGM	Normal appearing gray matter
OP-OSEM	Ordinary Poisson ordered subset estimation maximization
PET	Positron emission tomography
PGSE	Pulse-gradient spin echo
PPMS	Primary progressive multiple sclerosis
PVE	Partial volume effect
RD	Radial diffusivity
RESTORE	Robust estimation of tensors by outlier rejection
rmANCOVA	Repeated measures analysis of covariance
RRMS	Relapsing remitting multiple sclerosis
ROI	Region of interest
SCA	Supervised clustering algorithm
SD	Standard deviation
SPM	Statistical parametric mapping
SPMS	Secondary progressive multiple sclerosis
SRTM	Simplified reference tissue model
SUV	Standardized uptake value
TAC	Time-activity curve
T	Tesla
TBSS	Tract based spatial statistic

TSPO	Translocator protein
TPC	Turku PET centre
V_{ND}	Volume of distribution of non-displaceable radioligand
V_S	Volume of distribution of specifically bound radioligand
V_T	Volume of distribution
WM	White matter
WMIC	Wolfson molecular imaging centre

List of Original Publications

This dissertation is based on the following original publications, which are referred to in the text by their Roman numerals I-III:

I Rissanen E, Tuisku J, Vahlberg T, Sucksdorff M, Paavilainen T, Parkkola R, Rokka J, Gerhard A, Hinz R, Talbot PS, Rinne JO, Airas L. (2018). Microglial activation, white matter tract damage, and disability in MS. Neurology: Neuroimmunology & Neuroinflammation, Mar 6;5(3):e443

II Bezukladova S, Tuisku J, Matilainen M, Vuorimaa A, Nylund MK, Smith S, Sucksdorff MLK, Mohammadian M, Saunavaara V, Laaksonen S, Rokka J, Rinne JO, Rissanen R, Airas L. (2020). Insights into disseminated MS brain pathology with multimodal diffusion tensor and PET imaging. Neurology: Neuroimmunology & Neuroinflammation, Mar 2;7(3):e691

III Tuisku J, Plavén-Sigray P, Gaiser EC, Airas L, Al-Abdulrasul H, Brück A, Carson RE, Chen MK, Cosgrove KP, Ekblad L, Esterlis I, Farde L, Forsberg A, Halldin C, Helin S, Hilmer A, Kosek E, Lekander M, Lindgren N, Marjamäki P, Rissanen E, Sucksdorff M, Varrone A, HRRT [11C]PBR28 study group, Collste K, Gallezot JD, Hillmer A, Huang Y, Höglund CO, Johansson J, Jucaite A, Lampa J, Nabulsi N, Pittman B, Sandiego CM, Stenkrona P, Rinne JO, Matuskey D, Cervenka S. (2019). Effects of age, BMI and sex on the glial cell marker TSPO - a multicentre [11C]PBR28 HRRT PET study. European Journal of Nuclear Medicine and Molecular Imaging, Oct;46(11):2329-2338

1 Introduction

Multiple sclerosis (MS) is a chronic inflammatory autoimmune disease of the central nervous system (CNS), which causes irreversible disability for most of the patients. The origin of MS is still unknown, but it is suggested to be a result of genetic and environmental factors. In most cases, MS begins with relapsing-remitting form (RRMS), where episodes of symptoms alternate with periods of no signs of disease activity. Eventually, for majority of the patients the disease proceeds into the secondary progressive phase (SPMS), where the attacks worsen by time leading to permanent disability. Current hypothesis is that the disease progression is a result of chronic neuroinflammation associated with diffuse demyelination, axonal injury, mitochondrial dysfunction, and neurodegeneration. (Compston and Coles, 2008; Lassmann, van Horssen and Mahad, 2012).

Although conventional magnetic resonance imaging (MRI) has enabled earlier MS diagnosis and provided means for monitoring disease progression and treatment response, it is limited by the low sensitivity to detect diffuse damage in normal appearing white matter (NAWM) and gray matter (NAGM). To overcome these limitations, diffuse tensor imaging (DTI) and positron emission tomography (PET) are used to reveal the microstructural and cellular changes occurring due to the pathogenic events.

These advanced imaging methods are particularly useful in the clinical trials enabling to observe the efficacy of treatments, as curative therapy for MS is still missing. (Inglese and Bester, 2010; Baecher-Allan, Kaskow and Weiner, 2018).

The aim of this thesis was to investigate the in vivo neuroinflammation imaging in MS brain with PET and DTI. Particularly, this thesis concentrated on PET radioligands binding to translocator protein (TSPO), which shows increased brain expression in response to immune activation (Lavisse et al., 2012). The sub-studies investigated if the TSPO uptake in NAWM of MS patients would be associated with microstructural changes observed with DTI in NAWM tracts, and if the outcomes of both imaging modalities would be associated with higher clinical disability. Because previous clinical TSPO PET studies have displayed high interindividual variability (Collste et al., 2016), an additional aim was to study if the individual physiological

properties including age, body mass index (BMI) and sex have influence on the observed variability.

2 Review of the Literature

2.1 Multiple sclerosis

Multiple sclerosis (MS) is an inflammatory autoimmune disease of the central nervous system (CNS), where the immune system attacks the protective myelin sheet surrounding the nerve cell axons. This results in focal sclerotic areas of myelin loss called plaques or lesions, which in addition to the neurodegeneration, i.e., axonal and neuronal loss, are the hallmarks of the disease. The focal inflammatory infiltrates are the pathological substrate for the clinical episodic symptoms (relapses). The neurological dysfunctions related to relapses may recover entirely or partially, leaving residual symptoms. In addition, there may be steady increase of disability also between the relapses, and this is how the patients may experience the disease progression. The disease starts typically at the age of 20-40 years (average 30 years), and due to the axonal degeneration during the disease course most of the patients will develop substantial disability, which will gradually increase after 5-35 years from disease onset. (Compston and Coles, 2008; Hemmer, Kerschensteiner and Korn, 2015; Ransohoff, Hafler and Lucchinetti, 2015).

The cause of MS is still unknown, but it is suggested to be a result of genetic and environmental factors. Both female sex and changes in human leukocyte antigen (HLA) system increase the susceptibility for MS. The disease distribution is also increased in northern geographical regions, whereas near equator the incidence is low. This is suggested to be related to the low sunlight exposure and vitamin D deficiency. Other environmental risk factors include cigarette smoking, Epstein-Barr virus infection and adolescence obesity. (Olsson, Barcellos and Alfredsson, 2016).

2.1.1 Disease course and diagnosis

MS is currently divided in four subtypes (Lublin *et al.*, 2014, 2020). For approximately 80% of MS patients, the disease begins with an acute episode of symptoms, which is called as the clinically isolated syndrome (CIS). For the remaining 20% the disease is progressive from the onset, and it is classified as the primary progressive MS (PPMS). For both of these subtypes, the disease progression starts approximately at the age of 45 (Tutuncu *et al.*, 2013). CIS may convert to

relapsing remitting MS (RRMS), which is defined by new and worse relapses, which recover to some extent, following a period of no signs of disease activity (remission). Symptoms of MS include weakness and fatigue, numbness and tingling, loss of vision, pain, tremor, bladder dysfunction, poor balance, clumsiness, vertigo, and cognitive impairment, depending on the location of the lesions (Compston and Coles, 2002). Each neurological dysfunction recovers only partially and eventually approximately 65% of RRMS patients will convert to secondary progressive MS (SPMS), where the disability becomes irreversible and progressive. The median life expectancy is approximately 30 years from the disease onset, which is 5-10 years lower than normal. (Compston and Coles, 2008).

The current diagnostic criteria of MS (revised McDonald criteria) are based on clinical neurological symptoms and on dissemination of magnetic resonance imaging (MRI)-detectable lesions in space (DIS) and time (DIT). In addition, laboratory cerebrospinal fluid (CSF) analysis can be used to improve diagnostic accuracy (Thompson, Banwell, *et al.*, 2018). Because the disease progression is slow and indefinite, the diagnosis of RRMS to SPMS conversion is difficult. It is usually made retrospectively based on a history of gradual worsening after an initial relapsing disease course (Lublin *et al.*, 2014). Clinical evaluation of the disability progression is often based on the Expanded Disability Status Scale (EDSS) rating system (Kurtzke, 1983). EDSS rating is comprised of a scale ranging from 0 to 10, with a step size of 0.5, where 0 corresponds to no disability and 10 corresponds to a death due to MS. EDSS ratings 1-4.5 relate to MS patients that are able to walk without aid, but who have impairment in some of the eight functional systems: pyramidal (motor functions), cerebellar, brainstem, sensory, bowel and bladder, visual, cerebral or mental, and other functions. Ratings 5–9.5 are differentiated by the severity of walking impairment, where e.g., 7 corresponds to restriction to wheelchair. The progression-related disability is considered to be irreversible when EDSS > 3 (Leray *et al.*, 2010), but it is possible that higher measurement decreases after relapse. Another disability progression rating system is the MS severity score (MSSS), which is based on EDSS, but takes also into account the disease duration (Roxburgh *et al.*, 2005). For example, high MSSS corresponds to MS patients either with moderate EDSS with short disease duration, or patients with high EDSS and longer disease duration (Pachner and Steiner, 2009).

2.1.2 Disease mechanism and treatment

Currently, there are two hypotheses for the initiation of multiple sclerosis. A commonly proposed hypothesis is that the MS is an autoimmune disease, which starts in the peripheral tissues by the adaptive immune response of T- and B-cells and then is mediated in CNS by activated phagocytes of the innate immune system.

In this "outside-in" view, the peripheral T- and B-cells are assumed to be activated via two alternative mechanisms, molecular mimicry, or bystander activation (Geginat *et al.*, 2017). In both scenarios B–cells act as primary antigen presenting cells that drive the pathogenic T-cells (Baecher-Allan, Kaskow and Weiner, 2018). In molecular mimicry the T- and B-cells react against foreign antigen, but incorrectly attack against CNS myelin that shares similar antigen epitopes. In bystander activation, the immune response of pathogen specific cells activates also the bystander cells that are not specific for the particular pathogen. In contrast to the "outside-in" hypothesis, the opposing "inside-out" view suggests that the disease is a primary neurodegenerative process followed by a secondary inflammatory response. In this view, the disease originates intrinsically inside CNS as a consequence of primary infection or neuronal disturbance, and consequently the inflammatory response of adaptive immune system amplifies the disease and tissue damage. (Hemmer, Kerschensteiner and Korn, 2015; Mahad, Trapp and Lassmann, 2015).

Regardless of the underlying disease activation mechanism, the interaction of immune system components and the elements of CNS determine the continuation of disease process (Constantinescu *et al.*, 2011). Briefly, the peripheral T-cells, B-cells, plasma cells and macrophages infiltrate the blood-brain barrier (BBB) into the CNS and through cytotoxicity and demyelinating antibodies they target the oligodendrocytes, which form the CNS myelin. The pro-inflammatory cytokines, secreted by the T-cells, activate microglia cells, which are the resident innate immune cells in the CNS. Microglia, along with blood derived macrophages, cause direct and indirect damage to oligodendrocyte cells through several possible mechanisms, including myelin phagocytosis, secretion of proinflammatory cytokines, chemokines, reactive oxygen species, free radicals, and increased release of glutamate (Thompson, Baranzini, *et al.*, 2018). Microglia cells also promote a proinflammatory reaction by the recruitment of additional peripheral T- and B-cells, causing a cycle reaction that develops the MS lesions. The myelin is eventually destroyed as a consequence of repeated injury, which then leads to axonal degeneration. However, despite contributing to many harmful processes, microglia have also a neuroprotective phenotype, which participates to the lesion repair by removing myelin debris and promotes the remyelination. In addition to microglia, glial astrocyte cells in CNS contribute to the lesion formation by regulating the BBB permeability and thus promoting the lymphocyte recruitment in early lesions (Pitt and Ponath, 2019). Later in active lesions, these cells induce damage to oligodendrocytes and neurons by adopting a neurotoxic phenotype, which is suggested to be induced by activated microglia (Liddelow *et al.*, 2017). Astrocytes contribute also to later stages of lesion development by supporting remyelination and by forming a glial scar, which limits the inflammation after the demyelination

process. (Hemmer, Kerschensteiner and Korn, 2015; Ponath, Park and Pitt, 2018; Thompson, Baranzini, *et al.*, 2018).

MS lesions go through different phases during the disease course, which allows the lesions to be classified in four subtypes, based on the presence of myelin degradation products and inflammatory cells (Calvi *et al.*, 2020). These lesion subtypes include early active, chronic active (or slowly expanding), inactive, and remyelinated (or shadow) lesions. Lesions have different levels of activity based on the distribution of microglia and macrophages (Kutzelnigg *et al.*, 2005). Acute lesions in early MS contain a dense infiltration of macrophages throughout the lesion, whereas chronically active lesions of progressive MS show activated microglia and macrophages in a broad rim shape at the lesion edge with only few macrophages in the lesion centre (Frischer *et al.*, 2009, 2015). Chronic lesions remain for decades, while acute lesions can be present for weeks (Mahad, Trapp and Lassmann, 2015). Inactive lesions show a sharp lesion border without macrophages or activated microglia (Frischer *et al.*, 2009).

The characteristic feature of progressive MS is diffuse pathology in the white and the gray matter, which is caused by different mechanisms compared to the more focal inflammatory processes of RRMS. Key factors influencing the persistent disability in progressive disease are diffuse axonal loss and demyelination in the normal appearing white matter (NAWM), largely due to the anterograde (or Wallerian) and retrograde degeneration of axons that are passing thorough focal lesions (Singh *et al.*, 2017). The other pathologic changes include neuronal degeneration and cortical demyelination in the grey matter, meningeal inflammation, brain atrophy and failure of remyelination. Based on current view, the progressive MS is driven by a chronic compartmentalized inflammation behind closed BBB, although it's still unclear if the inflammation is a cause or a result of neurodegeneration. Principal elements associated to the pathologic changes are activated microglia, which maintain the chronic inflammation by inducing oxidative damage to oligodendrocytes and neurons through oxidative burst. Furthermore, the oxidative injury is amplified by increased mitochondrial damage in axons, and age-related iron accumulation in the brain. (Mahad, Trapp and Lassmann, 2015; Baecher-Allan, Kaskow and Weiner, 2018).

At the moment there is no curative treatment for MS. Current anti-inflammatory or immunosuppressive treatments have shown to be effective in patients with RRMS, but not in patients with the progressive MS. The aims of the disease modifying immunomodulatory treatments are to reduce relapse intensity and frequency, prevent fixed disability to the relapses, prevent and treat progression related disability, and provide management of neurological deficits. Early diagnosis and start of treatment is advantageous, as it reduces the sustained disability progression. (Compston and

Coles, 2002; Mahad, Trapp and Lassmann, 2015; Thompson, Baranzini, *et al.*, 2018).

2.2 Imaging techniques in MS

2.2.1 Structural magnetic resonance imaging

Structural magnetic resonance imaging (MRI) is a non-invasive imaging technique, which is used to acquire and functional anatomical images. Most common application of MRI method employs a strong magnetic field affecting to the hydrogen atoms in water molecules and fat, which are found in different amounts in all body tissues. A hydrogen atom consists of a highly magnetic nucleus with one proton and one electron orbiting the nucleus. In normal conditions, the hydrogen nuclei protons in the human body are unaligned in relation to one another, but the strong static magnetic field of MRI scanner causes the magnetic moments of the protons to align either parallel or antiparallel to the field. However, more protons align with the parallel alignment, producing a net magnetization, which is the source of the MR signal. (Carr and Grey, 2002; Jensen, 2014).

When a rapid series of magnetic oscillations at radio frequencies (Larmor frequency) is transmitted to the examined area, the energy of the pulses excites the hydrogen nuclei protons and causes them to resonate. When the pulse is switched on, the protons absorb energy and reverse their orientation to the static magnetic field so that the net magnetization is rotated to transverse plane; after a switch off the protons release energy and return to alignment with the static magnetic field. A receiver coil is used to measure the released energy and the relaxation time required to the protons to return to their initial state in the static magnetic field. The relaxation time is different for protons in different tissues, which creates the tissue dependent contrast in the MR images. Moreover, two different relaxation times are used to characterize the imaged tissues. T1 relaxation time determines the rate of the protons to realign with the static magnetic field, whereas T2 relaxation time describes the rate of decay of the magnetization in transverse plane perpendicular to the static magnetic field. T1-weighted images show high intensities (bright) in fat-based tissues such as white matter and low intensities in water-based tissues such as cerebrospinal fluid (dark). Gray matter has an intermediate T1 relaxation rate showing pixels in shades of gray. Fat is bright also on T2-weighted images, but the most important feature of these images is that water is bright. This allows that tissue edema (excess water) can be evaluated as bright signal, especially when high signal from fat is saturated. (Carr and Grey, 2002; Jensen, 2014).

MRI is currently the most commonly used biomarker of MS disease activity and it plays an important role in MS diagnosis, where it is used to evaluate the DIS and

DIT criteria (Sahraian and Radue, 2008; Baecher-Allan, Kaskow and Weiner, 2018). In MS studies, T1-weighted images are applicable in assessing the structures of fatty tissue, such as the WM, whereas T2-weighted images are particularly used in identifying focal white matter lesions, which are visible as hyperintense areas in the image. Lesions can be also detected with improved contrast using Fluid Attenuated Inversion Recovery (FLAIR) images, which are modified T2-weighted images, where the CSF signal is attenuated and shows dark. Therefore FLAIR images are more sensitive in detecting MS lesions next to cortex and ventricles, but lesions in the brainstem and cerebellum may be underestimated. (Carr and Grey, 2002; Sahraian and Radue, 2008; Jensen, 2014).

T1-weighted imaging can be also performed with administration of gadolinium contrast agent, which shortens the T1 relaxation time and results in increased signal intensity. Therefore, gadolinium enhanced images are especially useful in defining vascular structures and BBB breakdown, which allows visualizing new MS lesions after few days from the lesion onset. In most of the new lesions, the gadolinium enhancement lasts 2-6 weeks. Only a small number of lesions demonstrate enhancement for 3-4 months and very rarely the lesions enhance more than 6 months. After the enhancement, lesions remain visible in the T2-weighted image as a hyperintense bright areas and may appear as hypointense “black hole” areas in the T1-weighted image, which indicates increased water content and a loss of structural components as a result of demyelination. (Sahraian and Radue, 2008).

The most important MS disease course biomarker assessed with T1-weighted images is brain atrophy, as resulted by enlargement of the ventricles and sulci. The WM atrophy is presumably a result from myelin and axonal loss in the neuronal pathways, whereas the GM atrophy is demonstrated to be independent of demyelination (Klaver *et al.*, 2015). Atrophy is displayed especially in the progressive MS patients and particularly a longitudinal evaluation of the GM atrophy can be used to predict the long term outcome of the patients and also to differentiate clinically and cognitively declining patients (Sahraian and Radue, 2008; Rocca *et al.*, 2017). However, after atrophy is quantifiable with conventional MRI it is already too late for therapeutic intervention to prevent cognitive and ambulatory decline, and thus better methods are needed for evaluating neuroinflammation and microstructural changes.

2.2.2 Diffusion tensor imaging

Diffusion tensor imaging (DTI) is an MRI based method, which allows the quantification of natural movement of water molecules within brain tissues as a result of physical diffusion process. During the diffusion, water molecules explore tissue structures at a microscopic scale, which provides means to study the tissue

microstructural architecture in high resolution. Water diffusion is caused by random thermal fluctuations, and it is hindered by cellular structures. In CNS, water mobility is free in all directions (isotropic) in CSF. Conversely, in fibrous tissues such as the WM, the diffusion varies with direction (is anisotropic) and is least constrained in the parallel direction to the myelinated axonal fibers, compared to the constrained perpendicular direction. (Le Bihan, 2003; Alexander *et al.*, 2007)

The magnitude and direction of water diffusion anisotropy can be modelled by using a symmetric, positive definite 3x3 matrix called a tensor:

$$D = \begin{pmatrix} D_{xx} & D_{xy} & D_{xz} \\ D_{xy} & D_{yy} & D_{yz} \\ D_{xz} & D_{yz} & D_{zz} \end{pmatrix}.$$

Precisely, *D* is the covariance matrix of a three-dimensional Gaussian distribution that is used to model the displacements of the water molecules (O'Donnell and Westin, 2011). The eigenvalues $\lambda_1, \lambda_2, \lambda_3$ of *D* define the diffusivity in the direction of each eigenvector. The principal eigenvector of *D* corresponding to the highest eigenvalue describes the direction of the fastest diffusion, which considering the WM is parallel to the WM tracts. The diffusion tensor *D* can be visualized using an ellipsoid, where the eigenvectors of diffusion tensor matrix *D* define the directions of principal axes and the eigenvalues of *D* define the ellipsoidal radii (Figure 1). Diffusion is isotropic, when the eigenvalues are nearly equal. In this case the diffusion ellipsoid appears as a sphere. Conversely, eigenvalues with unequal magnitude yield a cigar-shaped diffusion ellipsoid, which depicts anisotropic diffusion. The damaged tracts alter the water diffusivity, and therefore the eigenvalues can be utilized in investigation of abnormal WM tissue structure. (Le Bihan, 2003; Alexander *et al.*, 2007)

The precise theory of DTI acquisition goes beyond the scope of this thesis, but the overview of the process is described briefly as follows. Diffusion acquisition using MRI employs magnetic field gradients to create an image corresponding to diffusion in a particular direction. Repeating this process of diffusion weighted imaging (DWI) in multiple directions allows the estimation of the diffusion tensor model. DWI is carried out commonly with a MRI sequence, which is called as a pulse-gradient spin echo (PGSE) with a single-shot echo planar imaging (EPI) readout. In this sequence, the static magnetic field is altered by separate pulses of field gradients in different directions with respect to the static magnetic field. For each direction, a pair of pulses is applied, where the first pulse dephases the hydrogen protons and another gradient pulse that has a same magnitude but with opposite direction, rephrases the protons. The net magnetization returns to its original level, if no proton movement has occurred. However, in case of proton movement due to

diffusion, the measured signal is attenuated. The amount of attenuation is in a given direction is proportional to the amount of diffusion in a given direction. In the WM, this means that the fiber tracts parallel to the gradient direction appear dark in the diffusion weighted image (Alexander *et al.*, 2007; O'Donnell and Westin, 2011).

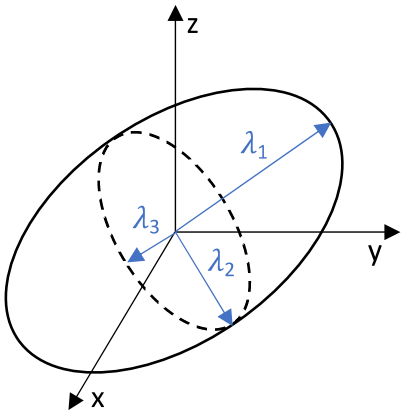

Figure 1. Diffusion tensor ellipsoid. Eigenvalues λ_1, λ_2, λ_3 define the diffusivity in the direction of each eigenvector. Modified from (Mori and Zhang, 2006).

Assuming a simple isotropic Gaussian diffusion, the measured signal attenuation S_k in a given gradient direction $\hat{g}_k$ can be described by the following Stejskal-Tanner equation

(1) $$S_k = S_0 e^{-b\hat{g}_k^T D \hat{g}_k},$$

where S_0 is the signal without diffusion gradients, $\hat{g}_k^T D \hat{g}_k$ represents the diffusion coefficient D in a given gradient direction $\hat{g}_k$, and b is a fixed diffusion weighting constant defined as

$$b = (\gamma G \delta)^2 \left(\Delta - \frac{\delta}{3}\right),$$

where γ is the gyromagnetic ratio, G is the strength of the diffusion sensitizing gradient pulses, δ is the gradient duration and Δ is the time between diffusion gradient pulses. A minimum of six different gradient directions, as well as baseline signal S_0, are required to be measured, in order to estimate the six elements of the diffusion tensor matrix D. However, more gradient directions improve the accuracy. Subsequently, the diffusion matrix D elements for each voxel can be estimated from equation (1) with least squares method (O'Donnell and Westin, 2011).

Interpretation of diffusion anisotropy and magnitude from the diffusion matrix *D* elements is difficult and therefore macroparameters are used to compress the diffusivity information into simpler form. One of such macroparameters is the mean diffusivity (MD), which describes the average magnitude of diffusion and is defined as an average of the diffusion tensor matrix eigenvalues:

$$MD = (\lambda_1 + \lambda_2 + \lambda_3)/3.$$

Currently the most widely used measure of anisotropy is the fractional anisotropy (FA), which is defined as

$$FA = \sqrt{\frac{3}{2}}\sqrt{\frac{(\lambda_1 - MD)^2 + (\lambda_2 - MD)^2 + (\lambda_3 - MD)^2}{\lambda_1^2 + \lambda_2^2 + \lambda_3^2}}.$$

FA range is bounded between 0 and 1, where value 1 corresponds to tensor that appears as a sphere. Additional eigenvalue-based measures are axial diffusivity (AD) and radial diffusivity (RD)

$$AD = \lambda_1, \qquad RD = (\lambda_1 + \lambda_2)/3.$$

Consequently, AD describes the diffusivity in the principal direction of the tensor parallel to the fibers, whereas RD describes the diffusivity perpendicular to the fibers. (Alexander *et al.*, 2007).

The macroparameters are typically investigated in regions of interest (ROI), where analysis is carried out with regional average values or with regional macroparameter histograms. Additionally, a voxel-level statistical analysis can be performed with macroparameter images, which are projected to a same pre-defined template image in a standard space. (Sbardella *et al.*, 2013).

The tensor model has also limitations. There is a large-scale difference between the DTI resolution and the size of individual axons, which have a diameter of approximately 0.2 to 20 μm. As the typical voxel size in DTI is approximately 2 mm, the estimated tensor represents only the average diffusion in a given voxel. Also, the tensor model is able to present only one principal direction in a given voxel. Therefore multiple factors, such as axonal density, cell death, alterations in myelination and in the levels of intracellular and extracellular water may contribute to changes in DTI macroparameters and therefore cannot be differentiated. (Wheeler-Kingshott and Cercignani, 2009; O'Donnell and Westin, 2011).

Also, DTI data processing steps may have influence on the variability of the results. Single-shot EPI readout related distortions, which originate from magnetic field inhomogeneities and eddy currents, can induce misalignments, warping and artifacts in the DW images and consequently cause errors in the DTI macroparameter images. Therefore, before the tensor estimation the raw images need to be visually examined for correcting or excluding the corrupted data. (Alexander *et al.*, 2007).

Despite the limitations DTI is a sensitive marker of neuropathology and it is applied in many neurologic applications (e.g., in ischemic stroke diagnosis and in neurosurgical planning), as well as in various neuroscientific studies including patients with schizophrenia, traumatic brain injury and multiple sclerosis. Particularly in MS, structural damage increases water content in parenchymal tissues, which results in increased MD and decreased FA (Tommasin *et al.*, 2019). (Alexander *et al.*, 2007; O'Donnell and Westin, 2011).

2.2.2.1 DTI in previous MS studies

Previous MS studies have demonstrated altered DTI macroparameters in the NAWM in all MS subtypes compared to healthy control subjects (Filippi *et al.*, 2000; Ceccarelli *et al.*, 2007; Roosendaal *et al.*, 2009; Onu *et al.*, 2012; Welton *et al.*, 2015; Pokryszko-Dragan *et al.*, 2018; Kolasa *et al.*, 2019). Assuming no WM fiber crossing, higher MD and lower FA have been suggested to associate with axonal and myelin loss, increased AD withs axonal degeneration and increased RD with WM demyelination (Sbardella *et al.*, 2013). However, various tissue characteristics including neuroinflammation, demyelination, axonal loss, and Wallerian/retrograde degeneration of axons traversing the focal lesions may have similar effect on the DTI macroparameters, which can complicate the interpretation of these parameters, particularly in normal appearing brain tissue (Ceccarelli *et al.*, 2007; Wheeler-Kingshott and Cercignani, 2009; Inglese and Bester, 2010). Typically in MS, increased RD and MD, and decreased FA are observed, where the degree of abnormality of the diffusion metrics depends on the severity of the disease (Inglese and Bester, 2010). AD is typically decreased at the early stages of MS, but as the disease progresses to the chronic state, AD may increase as a consequence of reparative processes, such as gliosis and cellular infiltration (Aung, Mar and Benzinger, 2013). Generally, as the disease progresses, the structural damage becomes more detectable with DTI (Inglese and Bester, 2010).

Progressive MS patients demonstrate more pronounced diffusivity changes in the normal appearing gray matter (NAGM) compared to other phenotypes (Preziosa *et al.*, 2011). However, increased FA is observed in the NAGM (Calabrese *et al.*, 2011), and in the GM lesions (Poonawalla *et al.*, 2008; Calabrese *et al.*, 2011), which is thought to originate due to different histological characteristics including lower degree of inflammation, higher level of activated microglia, and greater loss of dendrites and axons, compared to the WM lesions (Sbardella *et al.*, 2013).

The diffusivity changes are more pronounced in the T2 lesions compared to the NAWM and NAGM, whereas the most severe alterations are detected in the T1 hypointense lesions, resulting from the irreversible pathological damage (Sbardella *et al.*, 2013). An overlap between increased MD, decreased FA and the T2 lesion

maps has been demonstrated in all MS subtypes other than PPMS, which suggests that in this subtype the axonal damage and the T2 lesion development could be independent processes (Preziosa *et al.*, 2011).

DTI macroparameters have been shown to be associated with cognitive impairment (Rovaris *et al.*, 2002) and clinical disability measured with EDSS (Liu *et al.*, 2012; Onu *et al.*, 2012). DTI has been also utilized in longitudinal MS studies, where for example disease progression in NAWM (Kolasa *et al.*, 2019) and cortical structural changes (Calabrese *et al.*, 2011) have been evaluated. However, no longitudinal differences were detected in CIS (Raz *et al.*, 2010) and RRMS (Rashid *et al.*, 2008) patients suggesting slow progression of the WM damage (Sbardella *et al.*, 2013).

2.2.3 Positron emission tomography

Positron emission tomography (PET) is a molecular imaging method, which is used for investigating different biochemical processes *in vivo.* This is achieved by measuring the activity concentration of a radioactively labelled compound, called radioligand, in a target ROI. Most common radioactive labels are short lived radioisotopes ^{11}C, ^{15}O or ^{18}F, which are the radioactive forms of the natural constituents found in biomolecules and drugs. This allows the syntheses of various radioligands that are chemically identical with their nonradioactive counterparts. The radioligand is administered in very low mass in order to prevent it from perturbing the investigated system, and only a small fraction of radioligand molecules contain the radioactive isotope. (Phelps and Mazziotta, 1985).

The radioligand is typically administered intravenously, after which it is delivered to a target region via blood flow. As the radioisotope decays by the emission of positrons, the emitted positron travels approximately 1 mm and eventually collides with an electron in the body. Then both particles annihilate, and as a result two photons, each with energy of 511 keV, are emitted in the opposite directions. These photons travelling along a line of response (LOR) in the speed of light are detected almost simultaneously by two opposing coincidence detectors arranged adjacently in rings inside PET scanner (Figure 2).

Although the exact location of the annihilations is unknown, many detected coincidence events along all LORs allow the spatial distribution of radioligand to be reconstructed in a 3D image. Additional corrections for scattering and attenuation of the detected photons are included in the image reconstruction. PET scan can be divided into multiple time frames, which provides the radioligand spatial distribution as a function of time. However, because of the decaying radioisotope, the frame lengths are required to be longer in the latter part of the scan to ensure an adequate amount of detected coincidence events. Along with the image reconstruction, the

measured radioactivity concentration in blood is corrected for radioactive metabolites, radioactivity in blood cells and platelets, and plasma protein factions to obtain the radioactivity concentration of free radioligand in plasma. (Phelps and Mazziotta, 1985; Van Den Hoff, 2005; Turkheimer *et al.*, 2015).

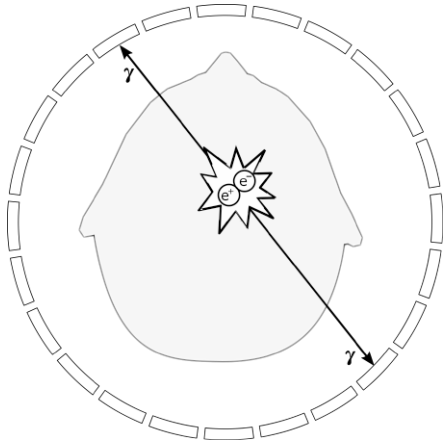

Figure 2. Illustration of positron emission inside PET scanner. As a result of annihilation of positron (e^+) and electron (e^-), two photons (γ) emit in the opposite directions.

PET images have relatively poor spatial resolution and therefore the reconstructed images are overlaid with MR images in order to relate the radioligand kinetics to the anatomical structures. The consequence of the limited spatial resolution is that a single voxel can represent a combination of different structures, each having different radioligand distribution. This source of error is called as the partial volume effect (PVE) and it becomes important when the investigated target is less than two times the spatial resolution of the PET scanner (Hoffman, Huang and Phelps, 1979; Carson, 2006). Different partial volume correction methods have been developed for removing PVE. These methods are either included in the image reconstruction, or applied to the reconstructed images (Erlandsson *et al.*, 2012).

The underlying physiology of regional radioligand measurement in a given voxel, or larger ROI, is commonly quantified using compartment models. Each compartment defines one possible physical location or chemical state of the radioligand from the administration to the binding to its target. Sometimes a number of different radioligand states are lumped together in a single compartment. Figure 3A illustrates a two-tissue compartment model, which is used in studies investigating receptor binding. It consists of three compartments, where C_P is the measured activity concentration of free radioligand in arterial plasma, C_{ND} is the concentration of so called non-displaceable radioligand, which represents the lumped concentrations of free radioligand and non-specifically bound radioligand in tissue,

and C_B is the concentration of specifically bound radioligand. The rate constants K_1-k_4 define the proportion of radioligand molecules that are moving between compartments in a specified time.

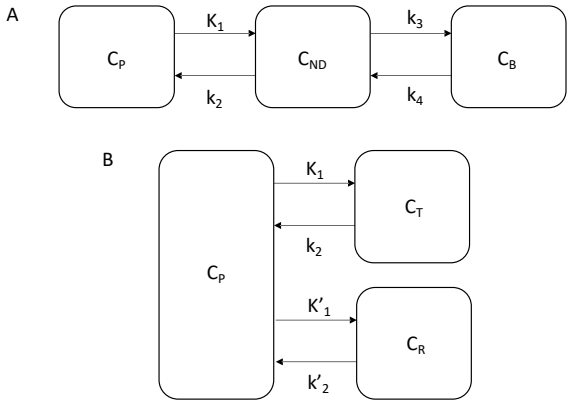

Figure 3. Two-tissue compartment model (A) and the simplified reference tissue model (B).

Another model depicted in Figure 3B is titled as the simplified reference tissue model (SRTM). It is comprised of two parallel one tissue compartment models, one for the target region and one for the reference region, which is devoid of specific radioligand binding. The target region model is based on the two-tissue compartment model in Figure 3A, but it is assumed that the radioligand kinetics are fast between non-displaceable and specific compartments C_{ND} and C_B, compared to the exchange between compartments C_p and C_{ND}. Hence, C_{ND} and C_B can be lumped together, and the kinetics of the target ROI can be described by a single compartment C_T. It is also assumed that the rate of exchange between C_p and C_T, and between C_p and C_R is similar, which implies $K_1/k_2 = K'_1/k'_2$. (Lammertsma and Hume, 1996; Carson, 2006).

Compartment models are based on assumption that the compartments are well mixed and therefore all radioligand molecules have the same probability to move between compartments. The underlying physiological processes are also assumed to be in steady state, which means that the rate constants do not change with time. These assumptions allow the compartment model to be described using linear differential equations. For example, the model in Figure 3A is described by following equations (2) and (3)

(2) $$\frac{dC_{ND}}{dt} = K_1 C_p - (k_2 + k_3) C_{ND} + k_4 C_B$$

(3) $$\frac{dC_B}{dt} = k_3 C_{ND} - k_4 C_B,$$

which have following closed form solutions (Phelps *et al.*, 1979)

(4) $$C_{\mathrm{ND}}(t) = \frac{K_1}{\alpha_2 - \alpha_1}[(k_4 - \alpha_1)e^{-\alpha_1 t} + (\alpha_2 - k_4)e^{-\alpha_1 t}] * C_{\mathrm{p}}(t)$$

(5) $$C_{\mathrm{B}}(t) = \frac{K_1 k_3}{\alpha_2 - \alpha_1}(e^{-\alpha_1 t} - e^{-\alpha_1 t}] * C_{\mathrm{p}}(t),$$

where $*$ denotes the convolution operation, and (α_1, α_2) are

$$\alpha_1 = ((k_2 + k_3 + k_4) - \sqrt{(k_2 + k_3 + k_4)^2 - 4k_2k_4})/2,$$
$$\alpha_2 = ((\mathrm{k}_2 + \mathrm{k}_3 + \mathrm{k}_4) + \sqrt{(\mathrm{k}_2 + \mathrm{k}_3 + \mathrm{k}_4)^2 - 4\mathrm{k}_2\mathrm{k}_4})/2.$$

PET measurement is not able to differentiate the compartments C_{ND} or C_{B}, or the blood in the tissue vasculature. Therefore, the measurement corresponds to

(6) $$C_{PET}(t) = V_{\mathrm{B}}C_{\mathrm{B}}(t) + (1 - V_{\mathrm{B}})C_{\mathrm{T}}(t),$$

where V_{B} is the vascular volume fraction, C_{B}(t) is the radioactivity concentration in the blood and$d$ $C_{\mathrm{T}}(t) = C_{\mathrm{ND}}(t) + C_{\mathrm{B}}(t)$. (Morris *et al.*, 2004).

Estimates of model rate constants are obtained by fitting the model equation (6) to the measured time activity curve (TAC). Consequently, macroparameters which are calculated from the estimated rate constants, are used to quantify radioligand binding. A macroparameter which is called a volume of distribution (V_{T}), is defined as a tissue to plasma activity concentration ratio at equilibrium state. For example, V_{T} = 2 means that 2 ml of plasma has the same quantity of radioactivity as 1 cm^3 of tissue. (Morris *et al.*, 2004).

V_{T} is derived for the two tissue compartment model, as follows (Innis *et al.*, 2007). Equation (3) provides a ratio of specifically bound and non-displaceable radioligand:

(7) $$\frac{C_{\mathrm{B}}}{C_{\mathrm{ND}}} = \frac{k_3}{k_4}.$$

Consequently, equations (2) and (7) yield the volumes of distribution for specifically bound and non-displaceable radioligand:

$$V_{\mathrm{S}} = \frac{C_{\mathrm{B}}}{C_{\mathrm{p}}} = \frac{K_1 k_3}{k_2 k_4} \text{ and } V_{\mathrm{ND}} = \frac{C_{\mathrm{ND}}}{C_{\mathrm{p}}} = \frac{K_1}{k_2},$$

from where the total volume of distribution V_{T} can be obtained as a sum of non-displaceable and specifically bound components:

$$V_{\mathrm{T}} = V_{\mathrm{ND}} + V_{\mathrm{S}} = \frac{K_1}{k_2}\left(1 + \frac{k_3}{k_4}\right).$$

Besides compartment models, V_{T} can be estimated with linearized methods that are not dependent on a particular model structure. These techniques are computationally efficient and allow the modelling to be performed in the voxel-level. One example of linearized methods is titled as the Logan plot, where the measured activity

concentrations from target ROI (C_T) and arterial plasma (C_p) are arranged to an equation of a straight line:

(8) $$\frac{\int_0^t C_T(s)ds}{C_T(t)} = V_T \frac{\int_0^t C_p(s)ds}{C_T(t)} + b.$$

The intercept b is linear after t^* from the radioligand administration, which allows the estimation of slope parameter V_T (Logan *et al.*, 1990). However, equation (8) contains a noisy term C_T(t) as a denominator in the independent variable, and the dependent and independent variables have correlated noise, which leads to biased V_T estimate (Ichise *et al.*, 2002). Alternatively, equation (8) can be rearranged to form the Ichise's multilinear analysis 1 (ma1) model:

(9) $$C_T(t) = -\frac{V_T}{b}\int_0^t C_p(s)ds + \frac{1}{b}\int_0^t C_T(s)ds,$$

where the bias in the V_T estimate is reduced (Ichise *et al.*, 2002).

Another macroparameter used for quantifying particularly the specific radioligand binding is called as the non-displaceable binding potential (BP_{ND}). It is defined as a ratio of specifically bound radioligand and nondisplaceable radioligand at equilibrium. BP_{ND} is a combined measure of fraction of free radioligand in non-displaceable compartment f_{ND}, available receptors B_{avail} and the receptor affinity $1/K_D$:

$$BP_{ND} = f_{ND}\frac{B_{avail}}{K_d},$$

and by its definition, it is related to the volumes of distribution of the specifically bound and non-displaceable radioligand, as follows:

$$BP_{ND} = \frac{V_S}{V_{ND}} = \frac{V_T - V_{ND}}{V_{ND}} = \frac{V_T}{V_{ND}} - 1 = \mathrm{DVR} - 1.$$

The term $\mathrm{DVR} = \frac{V_T}{V_{ND}}$ is called as the distribution volume ratio and it can be obtained indirectly with compartment models by calculating a ratio of V_T estimates from the target and the reference region. However, usually DVR or BP_{ND} is estimated directly using methods that are not requiring the arterial input function. (Innis *et al.*, 2007).

The arterial input function C_p is obtained with expensive and often error-sensitive procedures in blood sample analysis. It also requires an arterial catheterization, which is an invasive procedure and causes discomfort to the patient. Therefore, simplified modelling methods are derived from the compartment models for estimating the macroparameters directly, without using the arterial input. These

simplified methods are based on utilizing the reference region as a model input function. This step requires two assumptions:

1. The reference ROI doesn't contain specific radioligand binding.
2. The non-specific radioligand binding and V_{ND} is assumed to be similar in reference and target ROIs.

If these assumptions are met, then for example DVR can be estimated using a following Logan plot variant

$$\frac{\int_0^t C_T(s)ds}{C_T(t)} = \mathrm{DVR}\frac{\int_0^t C_R(s)ds + C_R(t)/k_2'}{C_T(t)} + b,$$

where $C_T(t)$ and $C_R(t)$ are the measured activity concentrations in the target and reference ROIs, and k_2' is the reference ROI tissue to plasma clearance rate constant. If individual k_2' is unavailable, then a population average is sufficient (Logan *et al.*, 1996).

On the other hand, BP_{ND} can be estimated directly using SRTM, which is depicted in Figure 3B. SRTM has a following solution:

$$C_T(t) = R_1 C_R(t) + \left(k_2 - \frac{R_1 k_2}{1+BP_{ND}}\right) C_R(t) * e^{\frac{-k_2 t}{1+BP_{ND}}}, \quad (10)$$

where $*$ denotes the convolution operation, and $R_1 = \frac{K_1}{K_1'}$ (Lammertsma and Hume, 1996). Equation (10) can be rewritten as a linear equation:

$$C_T(t) = \theta_1 C_R(t) + \theta_2 B_i(t),$$

where $\theta_1 = R_1$, $\theta_2 = k_2 - \frac{R_1 k_2}{1+BP_{ND}}$ and $B_i(t) = C_R(t) * e^{-\theta_3 t}$ are the predefined basis functions, in which $\theta_3 = \frac{k_2}{1+BP_{ND}}$ (Gunn et al., 1997). This reformulation allows the SRTM to be applied at voxel-level.

The preceding simplified methods all require a reference region in order to estimate the DVR or BP_{ND}. When an anatomically defined reference region doesn't exist, it is possible to apply a supervised clustering method to extract a pseudo-reference region, which has negligible specific radioligand binding. The aim of supervised clustering is to partition the PET voxel data so that the voxel-level TACs within a cluster are similar to each other but different compared to the TACs of other clusters. In supervised clustering, voxel-wise TACs inside brain tissue are partitioned in such a way that each TAC is a linear combination of four predefined average TACs representing radioligand binding in gray matter, white matter, vasculature and in ROIs with specific radioligand binding. The reference region is calculated as a weighted average over all brain TACs, where the estimated gray matter coefficients of the linear combination are used as the weighting factors. (Turkheimer *et al.*, 2007; Yaqub *et al.*, 2012).

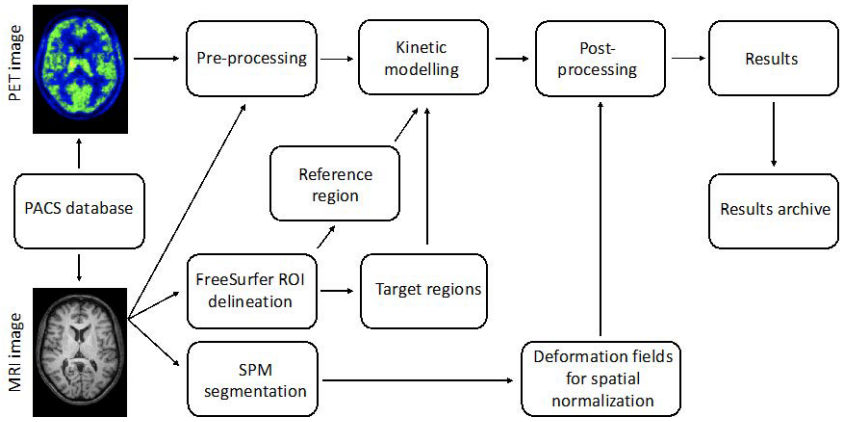

Figure 4. Flowchart illustrating the PET and MRI data processing. Modified from (Karjalainen *et al.*, 2020).

The basic preprocessing steps needed to run the PET data analysis are typically carried out by using an automated image analysis pipeline, in order to perform efficient data analysis and reduce the inter operator variance, which mainly results from the manual ROI delineation. Multiple different non-commercial analysis pipelines, such as MIAKAT (Gunn *et al.*, 2016), BioImage Suite (Papademetris *et al.*, 2006) or kinfitR (Tjerkaski *et al.*, 2020) are available and in use at different institutes. At Turku PET centre, a similar MAGIA pipeline (Karjalainen *et al.*, 2020) is currently used in the brain data processing and analysis (Figure 4). In MAGIA pipeline, the preprocessing starts with downloading the PET and MRI data from the Picture Archiving and Communication Systems (PACS) database, where the images are stored in Digital Imaging and Communications in Medicine (DICOM) format.

DICOM data is consequently converted to Neuroimaging Informatics Technology Initiative (NIfTI) format, which is commonly used in neuroimaging software packages such as SPM (Wellcome Trust Centre for Neuroimaging, London, UK), or FreeSurfer software (Laboratory for Computational Neuroimaging, Athinoula A. Martinos Center for Biomedical Imaging, Charlestown, MA, United States). Subsequently, PET data motion correction is carried out in SPM with PET frame realignment, after which MR image is co-registrated with PET image. Next, the ROIs are delineated automatically with FreeSurfer. In order to run the voxel level statistical analysis, the image data is required to be transformed into same 3D space. This step is called as a spatial normalization, and it utilizes SPM tissue segmentation in the normalization parameter calculation. Consequently, both regional and voxel level kinetic modelling is performed. The resulting 3D images of parameter estimates are then spatially normalized and smoothed to compensate the normalization errors and to ensure the data normality, which is required in the voxel level statistical analysis. Finally, the modelling results and visual quality control

metrics of the preprocessing steps are stored in the centralized archive in a standardized format.

The PET quantification contains several limitations. Due to the ethical reasons of the radiation exposure, the number of participants in the PET studies is limited. Additionally, the financial cost of single PET study is high, which restricts the sample sizes and may lead to studies that are underpowered and results that cannot be replicated. Similar to DTI, the PET quantification is relied on models that are only approximations of the underlying processes. Additionally, these models are based on a number of assumptions that may not be entirely fulfilled. PET kinetic modelling is based on the compartmentalization, which may not completely correspond to the observed system and for the practical computability reasons, models may also be oversimplified. The V_T estimate is a composite of specific and non-specific or non-displaceable components, whereas DVR with respect to reference region may be biased estimate due to specific binding in the reference region. There are also several different models, which can be used to estimate V_T or BP_{ND}, but the outcome estimates may depend on the used model. The PET radioligand may have limited specificity and the specific target may be located in the multiple different cell types. The patient movement may induce artifacts and false effects in the imaging data, the PET and MRI image co-registration may not be perfect, and the arterial data processing may contain errors. The parameter estimates may depend on the ROI delineation accuracy and as PET and MRI likely have different spatial resolution, the results may be different if MRI is resampled to PET resolution as compared to vice versa. PVE degrades the quantitative accuracy, whereas commonly used partial volume correction methods are based on assumptions of homogenic activity concentration within the corrected regions. All of the aforementioned sources of error are attempted to be minimized, or corrected but need to be taken into account when interpreting the results. (Knudsen *et al.*, 2020).

2.2.3.1 PET imaging of microglial activation in MS

Substantial amount of recent research in PET imaging of MS has focused in identifying the activated microglia, because of its central role in the disease pathophysiology. Microglia cells occupy approximately 10% of the total cell population of human brain and they form the first line in the CNS immune defense (Kreutzberg, 1996). In the healthy brain, microglia remain in the ramified surveying state promoting synaptogenesis, neurotransmitter release, maintenance of synapses, and participate in regulating the blood brain barrier (Schwarz, Sholar and Bilbo, 2012). When activated in response to CNS injury, microglia cells are responsible of attacking the invading cells, removing previously damaged cells, and promoting neural tissue repair (Hanisch and Kettenmann, 2007).

Activated microglia cells and macrophages express a translocator protein (TSPO), which is an 18 kDa protein structure located on the outer mitochondrial cell membrane. Although the precise function of TSPO remains unclear, it is involved in regulating cell death, cytokine production, and microglial proliferation (Notter *et al.*, 2018). TSPO is also proposed to participate in cholesterol transport and steroid hormone synthesis, although the role of TSPO in steroidogenesis is currently a matter of debate (Gut, 2015). Besides microglia, TSPO is expressed in the brain in astrocytes, endothelial and smooth muscle cells and in neurons (Cosenza-Nashat *et al.*, 2009), even though its presence in the brain is only negligible compared to other tissues, which are essential for steroid production or lipid storage and metabolism (Notter *et al.*, 2018). While TSPO is expressed in low levels in healthy brain (Doble *et al.*, 1987; Owen *et al.*, 2014a; Kobayashi *et al.*, 2018a), it is increased in the activated microglia and reactive astrocytes as a response to immune activation and therefore it is considered a putative marker of neuroinflammation (Lavisse *et al.*, 2012).

The upregulation of TSPO can be detected in vivo by using PET and TSPO-binding radioligands. In MS, the majority of cells expressing TSPO in active lesions or chronic active rims are microglia and macrophages (Kaunzner *et al.*, 2019; Nutma *et al.*, 2019). Therefore, in MS, TSPO PET signal is currently interpreted to reflect mainly microglial density, irrespective of the pro-inflammatory or anti-inflammatory phenotype, but the phenotype may still depend on the ROI. For example, at the edge of chronic active lesions the phenotype is likely pro-inflammatory (Kaunzner *et al.*, 2019; Pitt and Ponath, 2019). However, reactive astrocytes and endothelial cells may also present a significant contribution to the TSPO expression, indicating again that the interpretation of PET results depends on the context. In a neuropathological study, astrocytic TSPO accounted for 25% of the binding in the active WM lesions and in the chronic active lesion rims, and for 65% in the centres of chronic active and inactive lesions (Nutma *et al.*, 2019). On the other hand, the contribution of endothelial cells is demonstrated to vary from 5% in the WM (Nutma *et al.*, 2019) to 20-30% in the frontal GM and WM (Veronese *et al.*, 2018; Wimberley *et al.*, 2018).

The most widely used TSPO radioligand [^{11}C](*R*)-PK11195 has been available since late 1980s and during the recent 20 years it is used in several previous MS studies (Cumming *et al.*, 2018). These studies have demonstrated e.g. increased TSPO availability in Gadolinium-enhancing active WM lesions (Vowinckel *et al.*, 1997; Banati *et al.*, 2000; J. C. Debruyne *et al.*, 2003) and in focal pathology areas identified by T1-weighted and T2-weighted MRI, as well as in the thalamus and brainstem of RRMS patients, compared to healthy volunteers (Banati *et al.*, 2000). Higher [^{11}C](*R*)-PK11195 uptake has been also observed in NAWM of CIS and SPMS patients (Rissanen *et al.*, 2014; Giannetti *et al.*, 2015), in the thalamus of

SPMS patients (Rissanen *et al.*, 2014), and in NAGM of SPMS and RRMS patients (Politis *et al.*, 2012) compared to healthy control subjects. In addition, increased TSPO uptake in the NAWM has been suggested to be associated to disease duration (J. C. Debruyne *et al.*, 2003), brain atrophy (Versijpt *et al.*, 2005) and clinical disability progression, measured with EDSS (Politis *et al.*, 2012; Giannetti *et al.*, 2014, 2015). [^{11}C](*R*)-PK11195 TSPO PET has been also utilized in several longitudinal studies evaluating the effect of disease modifying MS therapies (Ratchford *et al.*, 2012; Kaunzner *et al.*, 2017; M. Sucksdorff *et al.*, 2017, 2019).

The 1st generation TSPO radioligand [^{11}C](*R*)-PK11195 has several limitations, such as the short half-life (20.1 min) of ^{11}C isotope, a low brain bioavailability, and a poor signal-to-noise ratio due to high nonspecific binding, particularly originating from binding to endothelial cells. TSPO is also present in blood in platelets, monocytes and in the plasma proteins and therefore the free radioligand fraction in plasma f_p is very low (< 5%). This may add variation in the radioligand quantification using arterial input function and may lead to biased results because of the differences between free fractions of the healthy volunteers and MS patients (Lockhart *et al.*, 2003). To overcome the difficulties with arterial plasma data, the input function required for kinetic modelling can be derived from a TAC of an appropriate reference region. Although the cerebellum and the white matter both have relatively low TSPO density, an anatomically defined reference region doesn't exist for TSPO radioligands, because of the ubiquitous TSPO distribution in the brain. Therefore, all reference regions will underestimate the true BP_{ND} in TSPO PET imaging (Cumming *et al.*, 2018). Nevertheless, supervised clustering of pseudo-reference region, including likely a lesser amount of specific binding, is applied particularly in the recent PET studies using [^{11}C](*R*)-PK11195. (Turkheimer *et al.*, 2015).

To improve the poor signal to noise properties of [^{11}C](R)-PK11195, many improved high affinity TSPO radioligands, such as [^{11}C]DAA1106, [^{11}C]DPA713, [^{18}F]DPA714, [^{18}F]PBR06, [^{11}C]PBR28, [^{18}F]GE-180, [^{11}C]ER176, and [^{18}F]PBR111, have been designed possessing better features compared to the 1st generation radioligand [^{11}C](R)-PK11195. However, as a consequence of nucleotide polymorphism of rs6971 gene, three different patterns of binding affinity were found (Owen *et al.*, 2012) affecting all novel TSPO radioligands. Conversely, in vitro and in vivo studies have suggested no allelic dependence of brain TSPO binding for [^{11}C](R)-PK11195, but due to low signal to noise ratio this insensitivity of genotype is difficult to detect (Owen *et al.*, 2010; Kobayashi *et al.*, 2018b). In Caucasians, 49% of subjects are high affinity binders (HABs), 42% mixed affinity binders (MABs) and 9% low affinity binders (LABs) (Janssen *et al.*, 2016). The binding differences between HABs, MABs and LABs depend on the radioligand binding affinity, and for example [^{11}C]PBR28 HABs have twofold higher specific binding compared to MABs (Owen *et al.*, 2014b)**.** Currently, imaging LABs is possible only

by using high affinity radioligand [^{11}C]ER176 (Ikawa *et al.*, 2017). (Turkheimer *et al.*, 2015).

Among the 2nd generation TSPO-radioligands, [^{18}F]GE-180, [^{18}F]PBR06, [^{11}C]PBR28, [^{18}F]PBR111 have been utilized in the recent MS studies. Similarly to previous [^{11}C](R)-PK11195 studies, increased [^{11}C]PBR28 and [^{18}F]GE-180 uptake is displayed in Gadolinium enhanced active WM lesions (Oh *et al.*, 2011; Park, J.-D. Gallezot, *et al.*, 2015; Unterrainer *et al.*, 2018). Higher [^{18}F]PBR111 uptake has been also demonstrated in T2 hyperintense WM lesions, and perilesional regions of MS patients compared to WM of healthy controls (Colasanti *et al.*, 2014, 2016). Additionally, higher [^{11}C]PBR28 and [^{18}F]GE-180 uptake has been observed in NAWM (Herranz *et al.*, 2016; Datta, Colasanti, Kalk, *et al.*, 2017; Vomacka *et al.*, 2017), increased [^{11}C]PBR28 uptake in cortex, cortical lesions, and subcortical regions, and higher [^{18}F]PBR06 uptake in cerebral gray matter of MS subjects, as compared to healthy volunteers (Herranz *et al.*, 2016; Singhal *et al.*, 2019). Increased [^{11}C]PBR28 uptake in cortex, deep GM and NAWM has been demonstrated to be positively associated with clinical disability (EDSS) and impaired cognitive performance (Herranz *et al.*, 2016). Also, [^{11}C]PBR28 uptake in T2 hyperintense lesions and [^{18}F]PBR06 uptake in subcortical gray matter have been positively associated with grey matter atrophy (Datta, Violante, *et al.*, 2017; Singhal *et al.*, 2019).

In addition to the TSPO-radioligands, new alternative targets are developed in order to differentiate the pro-inflammatory and the anti-inflammatory phenotypes of activated microglia. For instance, cannabinoid type 2 receptors, cyclooxygenase-2 (COX-2), and purinergic P2X7 receptors are all expressed in the activated microglia and are specific for the pro-inflammatory phenotype (Janssen *et al.*, 2018). However, currently only one of these new radioligands binding to P2X7 receptors, [^{11}C]SMW139, has been utilized in a proof of concept MS patient study (Hagens *et al.*, 2020).

2.2.3.2 Variability in the TSPO PET uptake

To date, there have been only few test-retest TSPO PET studies. In stable MS patients, a moderate mean absolute test-retest variability for [^{11}C]PBR28 V_T ranging from 7% to 9% has been observed in GM, NAWM and MS lesions (Park, J. D. Gallezot, *et al.*, 2015), but in contrast higher variability was detected in GM (18%) and WM (48%) of healthy control subjects (Collste *et al.*, 2016). Similarly for [^{11}C](*R*)-PK11195 DVR, high variability was seen in GM (16% to 27%), WM (44%) and thalamus (8% to 22%) of healthy volunteers, where the uptake was quantified with respect to pseudo-reference region obtained with supervised clustering (Kaunzner *et al.*, 2017; Plavén-Sigray *et al.*, 2018). However, the observed high

variability presumably reflects the low TSPO expression in young healthy controls, as lower test-retest variability in GM (averagely 11%) was recognized in Alzheimer's disease patients (Turkheimer *et al.*, 2007).

Unfortunately, the 2nd generation TSPO radioligands offer no improvements to overcome the difficulties with arterial input data. Consequently, the quantification methods for TSPO PET imaging have not yet been standardized. To reduce the variability in distribution volume estimates of 2nd generation TSPO radioligands, a corrected estimate with the free fraction in plasma V_T/f_p has been used (Oh *et al.*, 2011), but the low value of f_p including potential measurement errors may increase the variance of the V_T/f_p ratio (Park, J.-D. Gallezot, *et al.*, 2015). The high variation in TSPO PET V_T has been attempted to be minimized also by using pseudo-reference regions from cortical gray matter (Turkheimer *et al.*, 2015), cerebellum (Lyoo *et al.*, 2015) and occipital cortex (Albrecht *et al.*, 2018), but the validity of the pseudo-reference region depends considerably on the study sample. For instance, cerebellum may be usable reference region in Alzheimer's disease patients (Lyoo *et al.*, 2015), but may not be such for MS patients because of scattered pathology. Particularly in the recent MS studies, pseudo-reference regions of clustered NAWM (Herranz *et al.*, 2016), global brain (Singhal *et al.*, 2019), gray matter (Oh *et al.*, 2011), frontal non-affected cortex (Unterrainer *et al.*, 2018), and caudate (Datta, Colasanti, Rabiner, *et al.*, 2017) have been utilized. The results of applying supervised clustering with 2nd generation TSPO radioligands have also remained elusive, where recent studies have succeeded in utilizing the method with [^{18}F]DPA714 and [^{11}C]PBR28 (García-Lorenzo *et al.*, 2018; Zanotti-Fregonara *et al.*, 2019), but in contrast negative results have also been described with [^{11}C]PBR28 (Rizzo *et al.*, 2019). As a consequence of the increased radioligand binding affinities of the 2nd generation TSPO radioligands, the increased non-specific endothelial binding hinders the accurate identification of signal from gray, white and inflamed tissue, which may lead to pitfalls in extracting the pseudo-reference region with supervised clustering. (Turkheimer *et al.*, 2015; Cumming *et al.*, 2018).

Although the main source of variance in TSPO PET uptake is caused by the TSPO genotype, also biological factors may have influence to the variation (Collste *et al.*, 2016). For example, ageing may affect to the TSPO uptake. With increasing age, microglia exhibit less "surveying" morphology and activate slower in response to injury (Damani *et al.*, 2011). However, previous TSPO brain PET studies related to age have been inconclusive, where studies have showed either higher TSPO levels with increased age (Cagnin *et al.*, 2001; Schuitemaker, Thalia F van der Doef, *et al.*, 2012; Paul *et al.*, 2018), or no observed effect (J. C. Debruyne *et al.*, 2003; Yasuno *et al.*, 2008; I Suridjan *et al.*, 2014). Except activated microglia, the other physiological processes that require TSPO in vivo, are still unclear (Gut, 2015). Several endogenous ligands, such as cholesterol, endozepines and porphyrins are

able to displace TSPO radioligands, indicating a possibility of competitive endogenous binding (Gut, 2015). Moreover, stimulants and drugs such as tobacco, cannabis, alcohol and methamphetamine are indicated to alter TSPO levels measured with PET (Sekine *et al.*, 2008; Brody *et al.*, 2017; Hillmer *et al.*, 2017; Da Silva *et al.*, 2019). Recently, TSPO has been also suggested to participate in mitochondrial energy production, and for instance, neuronal activity was demonstrated to increase TSPO levels presumably due to the increased energy demands (Notter *et al.*, 2020). In conclusion, many factors may affect to the TSPO uptake, which can complicate the PET imaging findings.

3 Aims

This thesis was set out to investigate the usability of TSPO PET and DTI for assessment of neuroinflammation and diffuse neuroaxonal damage in MS brain. Additionally, the aim was to study the biological factors influencing the variability of TSPO PET uptake.

The specific objectives of this thesis are:

I. To evaluate the association between TSPO PET uptake and microstructural changes observed with DTI in NAWM of MS patients, and to evaluate the association of the imaging macroparameters of both modalities in NAWM with the measured clinical disability.

II. To evaluate how well TSPO PET imaging and DTI coincide in ability to capture the disseminated NAWM pathology related to MS disease progression.

III. To study the effects of ageing, BMI and sex on the TSPO availability.

4 Methods

4.1 Subjects

All studies were conducted according to the principles of the Declaration of Helsinki. Ethical approvals were obtained from the Hospital District of Southwest Finland for studies I-III, from the Greater Manchester East Research Ethics Committee, and the Administration of Radioactive Substances Advisory Committee in the United Kingdom for study I, and from the Stockholm Regional Ethical Board and the Yale Human Investigation Committee for study III. Informed consent was obtained from all individual participants included in the studies.

The inclusion criteria used for SPMS and RRMS/CIS patients are listed below.

SPMS:

- Age between 18 – 75 years
- Definite MS diagnosis (Poser *et al.*, 1983; Polman *et al.*, 2005) for more than 5 years prior to enrolment
- A progressive course of MS for a minimum of two years
- Moderate to heavy lesion load (> 9 T2 hyperintense MS-lesions) in brain MRI.

RRMS/CIS:

- Definite diagnosis of RRMS according to the revised McDonald criteria or CIS with no evidence of dissemination in time
- Typical demyelinating lesions fulfilling the Barkhof criteria in brain MRI (Barkhof *et al.*, 1997).

The following exclusion criteria were used for both groups of MS patients:

- Corticosteroid treatment within 30 days of evaluation
- EDSS score > 8
- Active neurological or autoimmune disease other than MS, or some other comorbidity that was considered significant

- Inability to tolerate PET or MRI, and a current or desired pregnancy following study enrollment

The control subjects for studies I and II were healthy individuals with no known neurological symptoms or diseases. The healthy subjects were included in the study III, if they had no previous major psychiatric illness (e.g., schizophrenia or major depression), alcohol or drug dependence, or history of a serious somatic or neurological illness. The additional details about the study subjects and sample sizes of studies I-III are described in the following subsections.

Study I

Study I included data from 10 RRMS/CIS and 10 SPMS patients, who were recruited at Turku PET centre (TPC). All SPMS patients hadn't had immunomodulatory treatment within 3 months, and all CIS/ RRMS patients hadn't yet initiated a disease-modifying therapy. Additionally, altogether 17 healthy control subjects were enrolled at TPC and Wolfson Molecular Imaging Centre (WMIC), University of Manchester, United Kingdom. The TPC older healthy control subjects (n=8) were age- and sex matched with the SPMS group, whereas the WMIC younger healthy control subjects (n=9) were included as part of previous PET studies (Su *et al.*, 2013; Hunter *et al.*, 2016) were age- and sex-matched with RRMS/CIS group.

Study II

Study II included a cohort of 40 RRMS and 15 SPMS patients, as well as 15 age- and sex-matched healthy control subjects, but for five healthy participants, only conventional MRI and DTI data were available. 10 RRMS patients were enrolled in previous study (Marcus Sucksdorff *et al.*, 2017), whereas 5 RRMS and all 15 SPMS patients were included in other earlier study (Marcus Sucksdorff *et al.*, 2019). The remaining 25 RRMS patients were selected so that their age would be close to the average age (45 ± 10 years) of the disease progression onset (Tutuncu *et al.*, 2013).

20 RRMS and 15 SPMS patients had no immunomodulatory treatment at the time of imaging, while other 20 RRMS patients were using disease modifying treatments (DMTs) (three patients were taking dimethyl fumarate, five patients were on fingolimod treatment, six patients had interferon beta 1-a treatment, four patients were receiving glatiramer acetate and two were on teriflunomide). All patients with DMT were clinically stable and free from relapses at the time of imaging.

Study III

Study III included data from 140 healthy volunteers that had previously been enrolled at three centres: Karolinska Institutet (KI), n = 53, TPC, n = 62 and Yale University PET Center (Yale), n = 25. Prior to imaging with [^{11}C]PBR28, all participants were genotyped for the rs6971 polymorphism of the TSPO gene and categorized as MABs or HABs utilizing methods described previously (Owen *et al.*, 2012; Hannestad *et al.*, 2013). Low-affinity binders were excluded from this study.

4.2 MR imaging

Brain MRI was performed to exclude individuals with anatomical abnormalities, for acquiring an anatomical reference for the PET data analysis, and in DTI data acquisition.

In study I, the MRI for MS patients and older healthy control subjects was carried out with Philips Gyroscan Intera 1.5T Nova Dual scanner (Philips, Best, the Netherlands) with spatial resolution of 1x1x1 mm at TPC. The MRI sequences included axial T1 and T2 weighted, coronal FLAIR, DTI and axial gadolinium-enhanced 3DT1 weighted series. The structural T1 MRI for younger healthy controls at the WMIC was performed with a 1.5T scanner (Philips Achieva; Philips Medical Systems, Best, The Netherlands). DTI data was not available for the younger control subjects.

In study II, MRI was performed with 3T MRI Phillips Ingenuity (Philips Healthcare, Cleveland, OH) scanner with spatial resolution of 1x1x1 mm. The MRI protocol included T1-, T2-weighted, FLAIR, and DTI sequences.

DTI was acquired using 16 gradient directions in study I. In study II, 33 gradient directions were used for imaging of 20 patients with MS (15 SPMS and 5 RRMS), whereas DTI with 64 gradient directions was applied for the rest of the subjects.

Because of the data pooling in study II, the differences between the gradient directions (33 vs. 64) were assessed by investigating the impacts to DTI scalar indices and deemed to be insignificant.

In study III, T1-weighted MRI scans were acquired using a 3T scanner at each Centre (Discovery MR750 system (GE, Milwaukee, WI, at KI; Philips Ingenuity TF PET/MR, Philips Medical Systems, Cleveland, OH, USA, at TPC; Trio system, Siemens Medical Solutions, Malvern, Pennsylvania, at Yale).

4.3 PET imaging

All PET examinations in studies I-III were performed on a HRRT scanner (Siemens/CTI, Knoxville, TN, USA), which acquired 207 slices separated by 1.28 mm with a reconstructed image resolution of approximately 2.5 mm (Jong *et al.*,

2007). A transmission scan using ^{137}Cs point source was obtained for attenuation correction of the PET emission data prior to intravenous bolus injection of tracer. A head fixation system with a thermoplastic mask was used to minimize subject movement artefacts.

[^{11}C](*R*)-PK11195 imaging in studies I and II

The production of [^{11}C](*R*)-PK11195 at TPC is described in detail in (Rissanen *et al.*, 2014). The mean (sd) administered radioactivity in the scans in TPC was 474 (29) MBq with no significant differences between the groups. Mean (sd) for older healthy control, SPMS and RRMS groups were 479 (19), 482 (19) and 463 (42). The mean administered radioactivity for the WMIC younger control group was significantly higher 590 (108) MBq, compared to the other groups. In study II, the mean (sd) of injected activity was 473.6 (59.5) MBq for patients with MS and 498.8 (7.9) MBq for HCs, with no significant differences between groups.

Total [^{11}C](*R*)-PK11195 scanning time was 60 min. List–mode data were reconstructed in 17 time frames (2 × 15 s, 3 × 30 s, 3 × 60 s, 7 × 300 s, and 2 × 600 s) using 3D Ordinary Poisson Ordered Subset Estimation Maximization (OP-OSEM) with 8 iterations and 16 subsets at TPC, and 12 iterations and 16 subsets at WMIC The reconstructed PET data were smoothed with Gaussian 2.5 mm post reconstruction filter for TPC data and 2 mm for WMIC data (Hinz *et al.*, 2008).

[^{11}C]PBR28 imaging in study III

The production of [^{11}C]PBR28 at TPC is described in detail in the original article. In KI and Yale the [11C]PBR28 was prepared as previously described (Hannestad *et al.*, 2013; Jucaite *et al.*, 2015). The injection dose was administered as a rapid intravenous bolus, where the mean (sd) of injected activity at each centre was 413.5 (53.4) MBq at KI, 494.3 (18.9) MBq at TPC and 575.3 (151.6) MBq at Yale.

[^{11}C]PBR28 Data were acquired while participants were at rest over 70, 75 or 90 minutes, respectively at TPC, KI and Yale. A head fixation system with a thermoplastic mask was used at KI and TPC, to minimize subject movement artefacts. At Yale, an optical motion detector (Vicra, NDI Systems, Waterloo, Ontario, Canada) was utilized for motion correction during image reconstruction.

List–mode data were reconstructed using 3D OP-OSEM with 10 iterations and 16 subsets at KI, 8 iterations and 16 subsets at TPC, and 2 iterations and 30 subsets at Yale. At KI and Yale the reconstruction included additional modeling of the point-spread function (Carson *et al.*, 2003; Varrone *et al.*, 2009), and at Yale the subject motion was corrected within reconstruction employing the MOLAR algorithm (Carson *et al.*, 2003). The analysis was restricted to 70 minutes at TPC, and 75

minutes at KI and Yale, with frame lengths of 9 x 10 s, 2 x 15 s, 3 x 20 s, 4 x 30 s, 4 x 60 s, 4 x 180 s and 9 x 360 s at KI; 6 x 30 s, 3 x 60 s, 2 x 120s and 12 x 300s at TPC and 6 x 30 s, 3 x 60 s, 2 x 120s and 13 x 300s at Yale.

Arterial blood sampling were carried out as described previously (Jucaite *et al.*, 2015; Sandiego *et al.*, 2015) in order to obtain an arterial input function. An automated blood sampling system (ABSS, Allogg AB, Mariefred, Sweden) was used during the first 5 min of each PET measurement. Arterial blood samples were also drawn manually at 1, 3, 5, 7, 9, 10.5, 20, 30, 40, 50, 60, 70 min at KI; at 4, 6, 8,10, 15, 20, 25, 30, 40, 50 and 70 at TPC, and at 8, 12, 15, 20, 25, 30, 40, 50, 60, 75 at Yale, to allow for radioactivity sampling and metabolite analysis.

Metabolite analysis was carried out in KI and Yale as described previously (Hannestad *et al.*, 2013; Collste *et al.*, 2016), whereas the procedure used at TPC is described in detail in the original article. A metabolite corrected arterial input curve was created by first merging the ABSS blood curve with the manually drawn blood samples. The blood samples were centrifuged, and radioactivity in plasma was measured. Following this, a plasma-to-blood ratio curve was established and multiplied with the whole blood curve, to create the plasma curve over the entire examination. At KI and Yale, individual plasma-to-blood ratio data was used in the conversion, whereas at TPC, Hill type population-based plasma-to-blood ratio curves corresponding to both genotypes were utilized. Next, for all centers a Hill type function was fitted to each individual's parent fraction measurements, after which the metabolite corrected plasma time-activity curves were calculated by multiplying the uncorrected plasma curves with the estimated model curves. The differences in appearance times of radioactivity between PET and arterial plasma TACs were corrected by first estimating the delay of the arterial plasma TAC, which produced the best fit of two tissue compartment model to whole brain TAC and then shifting the arterial plasma TAC accordingly.

4.4 Image processing and analysis

In all studies, all 4D PET data were preprocessed in a similar manner, in which PET images were first realigned for motion correction and then coregistered to anatomical T1 MR images using SPM software running in MATLAB (The Mathworks, Natick, MA). The study specific image processing and analysis steps are described below.

Study I

At first, the T2 hyperintense WM MS lesions were obtained by the lesion growth algorithm (Schmidt *et al.*, 2012) implemented in the lesion segmentation toolbox (LST, version 1.2.3 for SPM8, after which they were manually corrected slice by

slice. T1 hypointense lesion mask images were then obtained by comparing the segmented WM, GM and CSF of the original T1 image to the segmented T1 images obtained from LST's T1 lesion filling feature. Thereafter, the T1 hypointense lesion masks were visually checked and manually corrected, if needed. T1 hypointense and T2 hyperintense lesion load volumes were derived from the respective lesion mask volumes. T1 hypointense masks were separated into two groups for gadolinium negative (Gd-) and gadolinium positive (Gd+) T1 hypointense lesions, which were used for the evaluation of the intralesional WM, and as a core for the perilesional WM. For each T1 hypointense lesion mask, perilesional mask images with distances of 0-3 mm and 3-6 mm to the lesion mask border were created by dilating the lesion mask image 3 and 6 voxels and then removing the cores from the resulting images. Overlapping regions surrounding both Gd- and Gd+ masks were removed.

In addition to lesional and perilesional regions, ROI parcellation for cerebellum, striatum, thalamus, WM and cortical GM were performed with Freesurfer software (v5.3.0) The thalamus ROI was further eroded 4 mm from its borders to match it visually with the specific thalamic [^{11}C](*R*)-PK11195 uptake. Finally, NAWM ROI was created by subtracting all lesional and perilesional T1 hypointense mask images from the segmented WM. The cortical GM, whole cerebral WM and total brain volumes were derived from the respective Freesurfer segments.

All ROIs were used to extract the TACs from the [^{11}C](*R*)-PK11195 PET images. In order to correct for the partial volume effect caused by differences in [^{11}C](*R*)-PK11195 binding between adjacent ROIs and by increased radioligand binding in the meningeal, vascular, bone and soft tissue next to cortical ROIs, a regional partial volume correction using the Geometric transfer Matrix method (Rousset, Ma and Evans, 1998) was performed for all time activity curves. A Gaussian function with 2.5 mm FWHM was used to approximate the HRRT scanner point spread function and for each cortical ROI a corresponding background ROI was used to correct for the background activity.

Regional [^{11}C](*R*)-PK11195 binding was evaluated as DVR with respect to a clustered gray matter reference region, which was obtained using the supervised cluster algorithm (SCA) approach (Turkheimer *et al.*, 2007; Yaqub *et al.*, 2012) with the SuperPK software package. The clustered GM map was further cleaned from contribution of positive blood and high specific binding coefficients. The reference tissue-input Logan method, within 20–60 minute time interval, was applied to the regional TACs, where the median reference region k_2 value 0.16 minute^{-1} for Logan's method was derived from the parameter estimates of simplified reference tissue model (Lammertsma and Hume, 1996) fitted to thalamus TACs.

DTI data preprocessing was carried out by using the FSL toolbox (Smith *et al.*, 2004) (FMRIB Software Library, Version 4.1.8; FMRIB, Oxford, UK). The raw diffusion data were first corrected for head motion and the effects of gradient coil

eddy currents. After this step, the FA and MD images were created by using FDT (FMRIB's diffusion toolbox), and the extracranial tissue was extracted from the FA and MD images with BET (FMRIB's Brain Extraction Tool). Finally, FA and MD images were linearly coregistered to the corresponding T2 images with FLIRT (FMRIB's Linear Image Registration Tool).

Study II

The T2 hyperintense lesions were first identified from the FLAIR images with the lesion prediction algorithm (Schmidt, 2017) as implemented in the LST toolbox version 2.0.15 for SPM, and then manually corrected. Subsequently, T1 hypointense lesion masks were manually defined slice by slice. The T1 images were filled with the manually corrected lesion masks, following a region of interest (ROI) parcellation with FreeSurfer software (v6.0). NAWM ROI was created by excluding T2 hyperintense lesions from cerebellar WM ROI. Next, NAWM subregions (deep, cingulate, frontal, temporal, occipital, and parietal NAWM) were derived from Freesurfer WM parcellation (Salat *et al.*, 2009). Finally, all ROIs were used to extract the TACs from the [^{11}C](*R*)-PK11195 PET images

In a similar manner to study I, regional [^{11}C](*R*)-PK11195 binding was evaluated as DVR with respect to a reference region extracted with the SCA (SuperPK software). The reference tissue-input Logan method was applied to the regional TACs, within 20–60 minutes of time interval. In addition, parametric BP_{ND} images were calculated at voxel-level using a basis function implementation of simplified reference tissue model (Gunn *et al.*, 1997) with 250 basis functions, lower θ_3 bound of 0.06 min^{-1}, and upper θ_3 bound of 0.8 min^{-1}. The resulting parametric BP_{ND} maps were further transformed to DVR and normalized into MNI152 space in SPM12.

DTI data were preprocessed with ExploreDTI software package (Leemans and Jones, 2009) for motion, eddy current, and EPI/susceptibility induced distortion correction. The diffusion tensor estimation method was set to RESTORE (robust estimation of tensors by outlier rejection) approach (Chang, Jones and Pierpaoli, 2005). After DTI data preprocessing, four maps of interest (FA, MD, AD, and RD) were reconstructed from the diffusion tensor map and coregistered in SPM12 to corresponding T1-weighted image. Finally, all images were spatially normalized into the MNI152 space in SPM12.

Study III

Regions of interest were defined in the following manner. The MR images were segmented into tissue classes using SPM. The grey matter segment was thresholded (GM>0.5) and then used as the main region of interest for the statistical analysis.

Additionally, six automated ROIs (frontal, temporal, occipital and parietal cortices, hippocampus and thalamus) were generated by using the Automated Anatomical Labeling (AAL) template (Tzourio-Mazoyer *et al.*, 2002). These AAL ROIs were first coregistered to summed PET images via the deformation fields obtained from the MRI segmentation and then multiplied with the thresholded GM segment, before the ROI extraction.

Regional [^{11}C]PBR28 uptake was evaluated as V_T, which was estimated at each centre using ma1 model (Ichise et al., 2002) (t^* = 30 min) with the metabolite and the delay corrected arterial plasma curves as an input function. Uniform weights were used in the ma1 analysis at KI and TPC, whereas at Yale the weights were based on the noise equivalent counts in each frame.

4.5 Statistics

Demographic comparisons in the beginning of the results section are reported as means and standard deviations, or as medians and ranges. Sample differences between studies I and II are examined with Student's t-test for continuous variables and with Pearson's Chi-squared test for categorical variables. In study III, the differences between centres are determined with one-way analysis of variance (ANOVA) for continuous variables and with pairwise Pearson's Chi-squared test for categorical variables.

The normality of the regional [^{11}C](R)-PK11195 and [^{11}C]PBR28 binding estimates were inspected with Shapiro-Wilk test of normality and the Q-Q plot. The group differences in the results section are illustrated using box-plots with asterisks indicating statistical differences. The raw data is presented using scatterplots with Spearman correlation coefficients. The unstandardized regression effect estimates and their estimated standard errors, or 95% confidence intervals, are presented in the original articles of studies I and III. The study specific statistical methods are described below.

Study I

Based on previously published regional [^{11}C](R)-PK11195 DVR values ranging from 1.2 (sd 0.08) to 1.4 (sd 0.10), with respect to clustered reference region (Turkheimer *et al.*, 2007; Politis *et al.*, 2012), it was estimated that control and MS study groups consisting ten subjects per group would be sufficient to reveal 15% difference in [^{11}C](R)-PK11195 binding with 90% power at $p < 0.05$.

The comparisons of the MRI and DTI parameters between MS patient groups and age matched controls were performed using ANOVA, and between RRMS and SPMS groups using analysis of covariance (ANCOVA) controlled for age.

For the groupwise comparison of regional [^{11}C](R)PK11195 binding, the younger and older control subjects were pooled into one group (n=17) after checking that there were no statistically significant differences in radioligand binding between the control groups. The statistical testing was performed with ANCOVA controlled for age and with Tukey-Kramer post hoc test for multiple comparisons.

The interaction between regional [^{11}C](R)PK11195 DVR and clinical, or MRI variables were examined using the pooled data of all MS patients (n=20) with repeated measures ANCOVA (rmANCOVA), adjusted for age. Regional DVRs or volumes were considered as repeated measures, where an unstructured covariance structure was used to model the correlation between the repeated measurements. The effect of age on DVR estimates was compared between pooled healthy controls and MS patients using ANCOVA, where the interaction between group and age variables provided an age coefficient for each group. For all analyses, post-hoc tests were carried out with Tukey-Kramer method for correcting multiple comparisons with significance level of $p<0.05$. All statistical analyses of the clinical, MRI and PET measurements were performed with SAS (SAS, version 9.4, SAS Institute Inc.

Study II

All ROI-level statistical analyses of DTI, [^{11}C](R)PK11195 DVR and clinical parameters were performed with R software (version 3.5.2 “Eggshell Igloo”). The nonparametric Mann–Whitney U test was used for the evaluation of the group differences of non-normally distributed data and in groups with a low number of participants. Multiple comparisons were corrected using the Holm method. Due to significantly different age distribution between MS subgroups and HC, evaluated with Student’s t-test, the regional PET data were analyzed with ANCOVA controlled for age and with Tukey’s honestly significant difference (HSD) test for the adjustment for the multiple comparisons. The correlational analyses between variables of interest were analyzed with Spearman’s nonparametric correlation test, where p-values were adjusted using the Holm method for the number of ROI’s (n=6) in brain. Correlational analyses were not adjusted for age, as diffusion parameters and DVR values did not show a significant correlation with age.

Pearson’s correlation coefficients between PET, DTI were calculated at voxel level in the NAWM between normalized FA and DVR images of 54 MS patients. One patient was excluded from analysis due to DTI image data artefacts. The ROI-level ANCOVA analysis, as well as the correlation analysis between clinical parameters and PET, or DTI are complemented in this thesis with an additional voxel-level analysis, which was carried out in SPM. Before the voxel-level analysis, all parametric images were smoothed with Gaussian 8mm FWHM filter to compensate for anatomical variability in image normalization and to improve signal-

to-noise ratio. The cluster level correction for multiple comparisons in all voxel-level analyses was performed using false discovery rate (FDR) with significance level of $p<0.05$.

Study III

A signed and dated memorandum of understanding containing the main research questions, outcome measures and overall statistical approach, was determined before sharing and analyzing the data. The associations between [^{11}C]PBR28 V_T and age, sex as well as BMI were examined using a linear mixed effects model, with TSPO genotype and PET centre specified as random effects, allowing their intercepts to vary freely. Previously, high correlations ($r>0.96$) between [^{11}C]PBR28 V_T estimates in different ROIs were shown (Matheson *et al.*, 2017). Therefore, the separate ROI analyses were considered to be highly dependent comparisons and the alpha threshold was set to 0.05 (two-tailed). All statistical analyses were conducted using lme4 and lmerTest packages in R (version 3.5.0 “Joy in Playing”).

5 Results

5.1 Demographic data (Studies I-III)

The main demographic features of the studies I and II, including the differences of the study subjects between these two studies, are presented in the Table 1. In both studies, the SPMS patients had advanced disease, which was associated with higher age, longer disease duration, higher T2 hyperintense and T1 hypointense lesion loads, and higher EDSS and MSSS scores compared to the RRMS/CIS and RRMS patients in studies I and II.

In study I, the RRMS/CIS patients were significantly younger than the SPMS patients, whereas in study II, there were no differences between the groups. The RRMS patients in study II had also significantly longer disease duration and higher EDSS, compared to the RRMS/CIS patients in study I. Additionally the SPMS patients in study I had higher EDSS and MSSS and higher GM atrophy, compared to SPMS patients in study II.

Descriptive statistics of study III subjects are presented in Table 2. There were significant differences in the age and BMI between centres, where TPC subjects had higher age, and KI subjects had lower BMI compared to the other centres. However, there were no significant differences in these variables between males and females, or between MAB and HAB genotype subjects.

Table 1. Demographics of studies I and II. Differences of study subjects between study I and study II are indicated with asterisks. Modified from the original publications I and II.

	Study I				Study II			
	HC	**RRMS**	**SPMS**	**SPMS vs. RRMS**	**HC**	**RRMS**	**SPMS**	**SPMS vs. RRMS**
n	17	10	10	-	15	40	15	-
Sex M/F	8/9	3/7	4/6	n.s.	6/9	8/32	7/8	0.05
Age y, median (range)	47.5 (22.0-61.6)	27.6 (20.3-37.6)	50.4 (32.9-66.8)	<0.001	45.7 (21.4-58.9)	47.3*** (28.4-54.1)	54.4 (37.3-64.1)	n.s.
BMI, median (range)	24.4 (21.5-30.1)	24.6 (17.7-43.2)	23.6 (19.3-34.7)	n.s.	24.3 (19.3-30.5)	25.6 (19.3-38.4)	21.7 (16.8-31.9)	0.01
Disease duration y	-	2.1 (3.1)	13.3 (5.8)	<0.001	-	11.7** (6.73)	15.2 (7.50)	n.s.
EDSS, median (range)	-	1.5 (0-2.5)	6.5 (4.0-8.0)	<0.001	-	2.5** (1.0-6.0)	5.0*** (3.0-6.5)	<0.001
MSSS, median (range)	-	4.12 (0.33-7.76)	7.57 (3.8-9.7)	0.001	-	3.9 (0.77-6.81)	5.6* (2.19-8.91)	0.03
Cerebral WM volume, cm^3	496.0 (52.9)	506.8 (52.0)	500.4 (81.8)	n.s.	573.3** (54.7)	502.2 (53.0)	504.5 (48.1)	n.s.
Cortical GM volume, cm^3	470.8 (62.5)	475.3 (31.4)	378.5 (59.2)	n.s.	490.3 (58.6)	434.6** (38.1)	429.0* (41.1)	n.s.
Total brain volume, cm^3	1188.3 (116.8)	1212.5 (95.9)	1068.8 (94.7)	n.s.	1242.0 (101.4)	1141.1 (109.3)	1124.0 (112.5)	n.s.
T2 hyperintense lesion load, cm^3	-	1.9 (1.4)	18.7 (18.2)	0.04	-	10.9* (10.9)	26.7 (21.4)	0.002
T1 hypointense lesion load, cm^3	-	1.5 (1.3)	12.4 (12.4)	0.02	-	6.1* (6.7)	13.9 (14.4)	<0.001

The demographics are reported as mean (SD), unless described otherwise. *P<0.05, **P<0.01, ***P<0.001. P-values indicating difference between study I and study II are determined with Student's t-test for continuous variables and with Pearson's Chi-squared test for categorical variables. Age was used as a covariate in between group volumetric analyses in study I.

Table 2. Demographics of study III.

	KI	TPC	Yale	Total	*p*
n	53	62	25	140	-
Genotype MAB/HAB	22/31	28/34	12/13	62/78	n.s.
Sex M/F	30 / 23	26 / 36	16/9	72 / 68	n.s.
Age, median (range)	46.9 (20 - 72)	70.3 (42 - 80)	31.0 (19 - 55)	58.7 (19 - 80)	p<0.001
BMI median (range)	23.0 (17.6 - 30.5)	25.7 (19.1 - 35.2)	25.7 (20.4 - 36.9)	24.8 (17.6 - 36.9)	p<0.001

P-values indicating difference between centres are determined with one-way ANOVA for continuous variables and with pairwise Pearson's Chi-squared test for categorical variables. Modified from the original publication III.

5.2 Study I: Increased TSPO uptake is associated with advanced clinical disability, higher age and reduced structural integrity in NAWM of SPMS patients

Higher [^{11}C](R)-PK11195 uptake was observed in the NAWM and thalami of SPMS patients compared with RRMS/CIS patients and HC, and in the Gd- T1 hypointense perilesional area in SPMS patients compared to RRMS/CIS patients (Figure 5). Due to low number of subjects (n=3+4 for RRMS+SPMS), no differences between group or within group differences were found in the Gd+ T1-hypointense lesions, nor in their perilesional areas. Perilesional uptake was greater compared to the Gd- T1 hypointense lesion core uptake. SPMS patients had also lower FA in the NAWM compared to RRMS/CIS patients and HC, whereas MD was higher only in SPMS patients compared to HC (Figure 5).

Higher [^{11}C](R)-PK11195 uptake in the NAWM was associated with higher clinical disability and reduced structural integrity, as demonstrated by lower FA, higher MD and increased WM lesion load (Figure 6). Additionally, higher [^{11}C](R)-PK11195 uptake was associated with lower FA and higher MD in thalamus, and higher [^{11}C](R)-PK11195 uptake in a Gd- T1 hypointense perilesional 3-6 mm ROI was associated with higher clinical disability, measured with EDSS (Figure 7).

Increasing age was associated with higher [^{11}C](R)-PK11195 binding in NAWM and thalamus of MS patients, but not in healthy controls. In contrast, increasing age was associated with significantly higher cortical gray matter [^{11}C](R)-PK11195

binding in healthy controls, whereas similar effect was not present in the MS group (Figure 8).

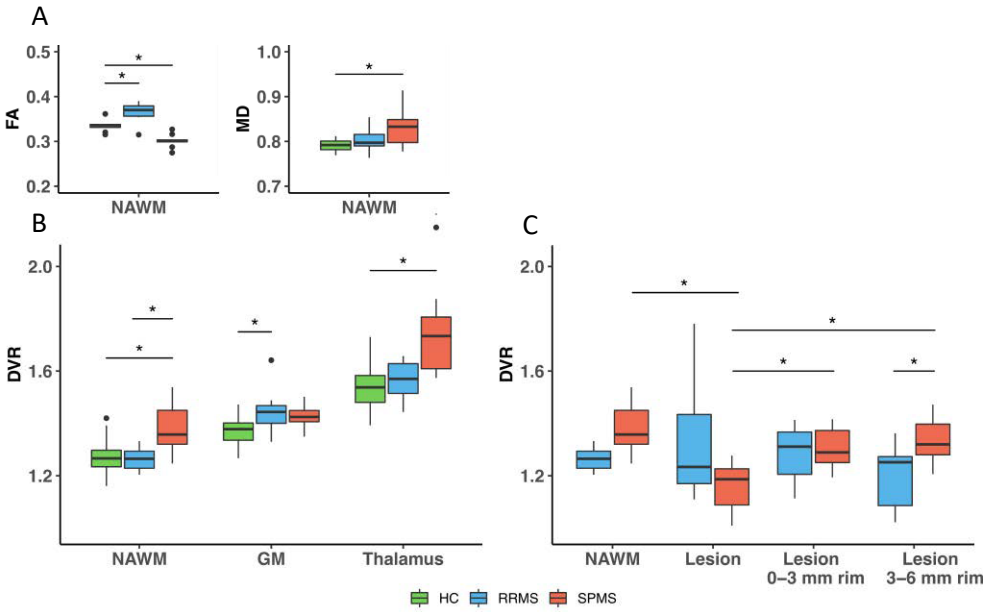

Figure 5. (A) Fractional anisotropy (FA) and mean diffusivity (MD) in normal appearing white matter of relapsing remitting multiple sclerosis/clinically isolated syndrome (RRMS/CIS, n=10) patients, secondary progressive multiple sclerosis (SPMS, n=10) patients and healthy control subjects (HC, n=8). (B) Regional [^{11}C](R)-PK11195 distribution volume ratios (DVR) in non-lesion associated ROIs and (C) Gd- T1 hypointense lesions and their perilesional areas of RRMS/CIS (n=10) patients, SPMS (n=10) patients and HC (n=17). *p < 0.05. Modified from the original publication I.

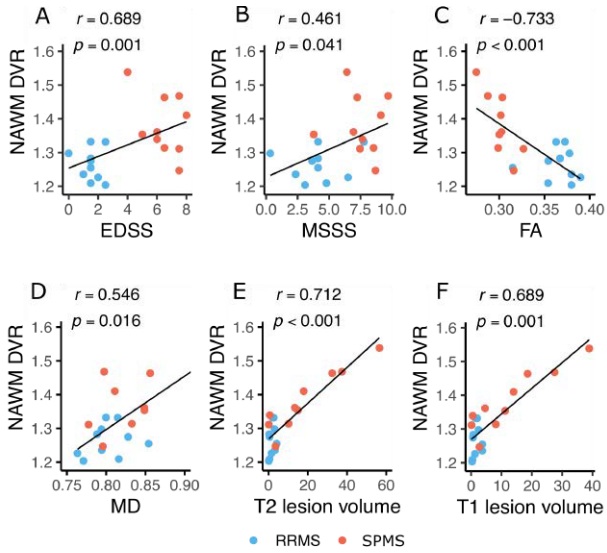

Figure 6. Scatterplots illustrating the association between normal appearing white matter (NAWM) [^{11}C](R)-PK11195 distribution volume ratios (DVR) and (A) Expanded Disability Status Scale (EDSS), (B) MS severity score (MSSS), (C) fractional anisotropy (FA), (D) mean diffusivity (MD), (E) T2 lesion volume, and (F) T1 lesion volume of RRMS/CIS (n=10) and SPMS (n=10) patients. MD unit is scaled with constant 10^3. Modified from the original publication I.

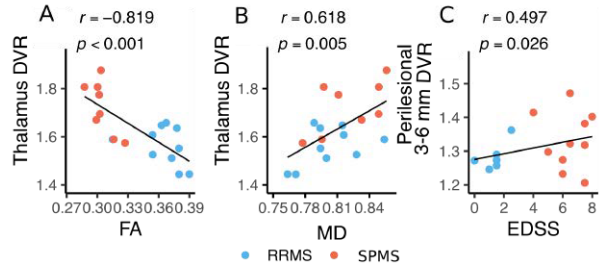

Figure 7. Scatterplots illustrating the association between thalamus [^{11}C](R)-PK11195 distribution volume ratios (DVR) and (A) fractional anisotropy (FA) and (B) mean diffusivity (MD) of RRMS (n=10) and SPMS (n=10) patients. Panel (C) shows the correlation between Expanded Disability Status Scale (EDSS) and [11C](R)-PK11195 DVR in Gd- T1 hypointense perilesional 3-6 mm ROI. Modified from the original publication I.

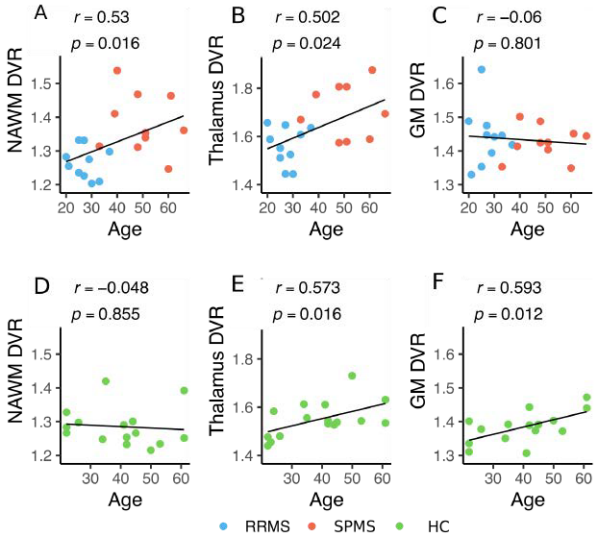

Figure 8. Scatterplots illustrating the association between age and [^{11}C](R)-PK11195 distribution volume ratios (DVR) in normal appearing white matter (NAWM), thalamus and gray matter (GM) of RRMS (n=10) and SPMS (n=10) patients, as well as healthy control subjects (HC, n=17). Modified from the original publication I.

5.3 Study II: Increased TSPO uptake coincides with structural NAWM damage and they both associate with MS clinical disability

Higher [^{11}C](R)-PK11195 binding was observed in the whole normal NAWM, as well as in the frontal, cingulate and deep subregions of NAWM of SPMS patients compared with RRMS patients and healthy controls (Figure 9A). SPMS and RRMS patients had also reduced FA in cingulate and occipital NAWM compared to HC, whereas increases in MD and RD were observed in the same regions between the groups (Figure 9B-D). Moreover, the DVR difference between RRMS and HC was located in frontal NAWM, whereas the differences in DTI macroparameters between these groups were detected in cingulate and occipital NAWM. There were no significant differences in AD between groups. Voxel-based between group analysis revealed several significant overlapping clusters in the NAWM between DVR, FA and MD results (Figure 10).

Increased [^{11}C](R)-PK11195 DVR in the whole NAWM, was associated with the reduced NAWM tract integrity, as demonstrated by reduced FA and increased MD, AD and RD. The associations were widespread, but most notable in the frontal, temporal, occipital and deep subregions of NAWM (Figure 11). The association between DVR and FA was less extensive compared to the association between DVR and the other DTI macroparameters.

Several significant correlations between the DTI macroparameters in the NAWM and disease severity were observed: decreased NAWM FA correlated to higher EDSS and MSSS, whereas increased NAWM MD, AD and RD were associated positively with EDSS and MSSS (Figure 12). Additionally, increased [^{11}C](R)-PK11195 binding in the NAWM was associated with higher EDSS, but regarding the MSSS the association was not significant (Figure 12). Although all EDSS related associations were observed in frontal, cingulate and deep NAWM, there was only a minor overlap in the voxel-based results.

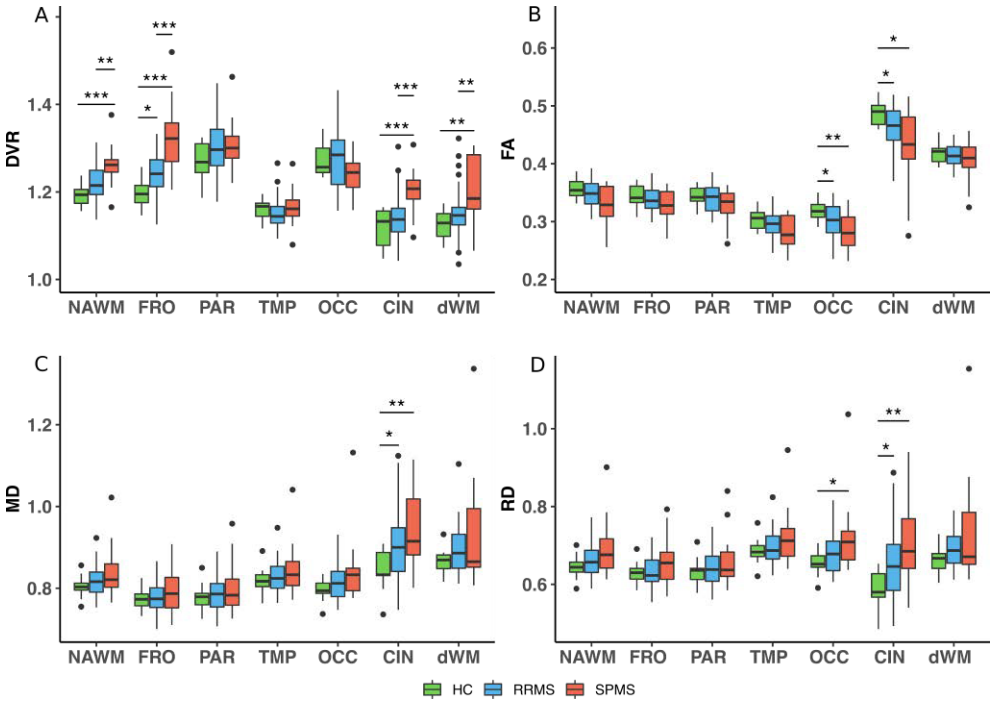

Figure 9. (A) Regional differences of [^{11}C](R)-PK11195 binding in the whole NAWM and in the NAWM subregions of MS patients compared to healthy controls. (B-D) The corresponding regional structural NAWM changes of MS patients compared to healthy controls. MD and RD units are scaled with constant 10^3. *p<0.05; **p< 0.01; ***p< 0.001. Modified from the original publication II.

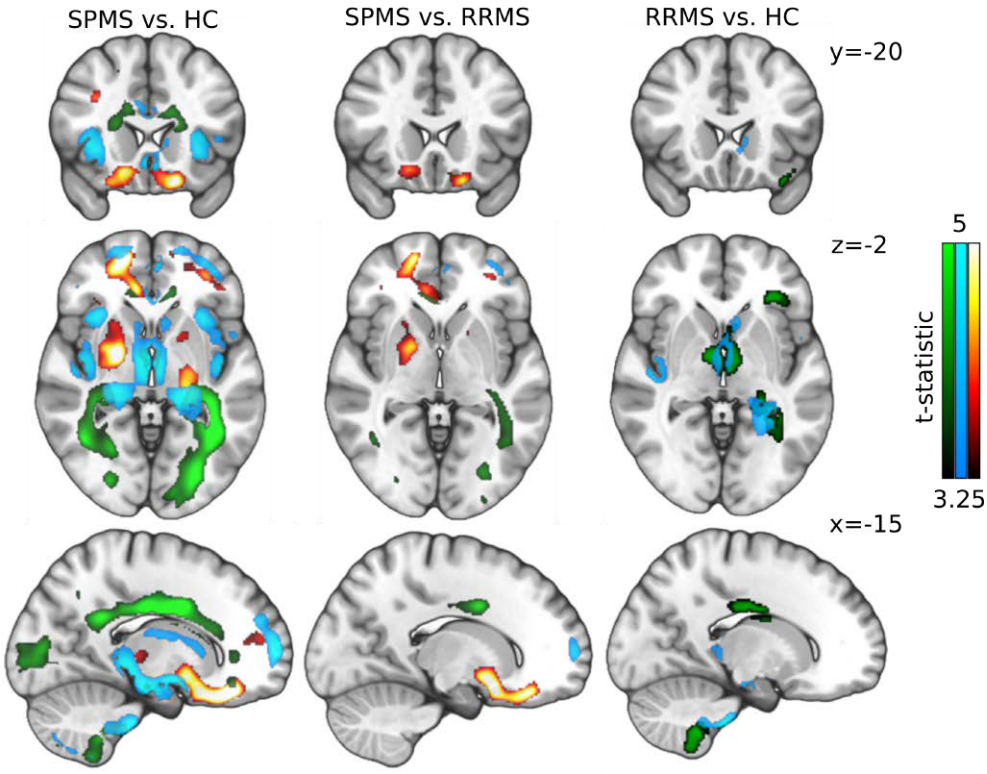

Figure 10. Voxel based paired ANCOVA post-hoc test results between SPMS and RRMS patients, and healthy control subjects (HC). Red color indicates differences in of [11C](R)-PK11195 DVR, blue color indicates differences in MD, and green color indicates differences in FA. The cluster level correction for multiple comparisons was performed using FDR with significance level of $p<0.05$ (t-statistic > 3.25).

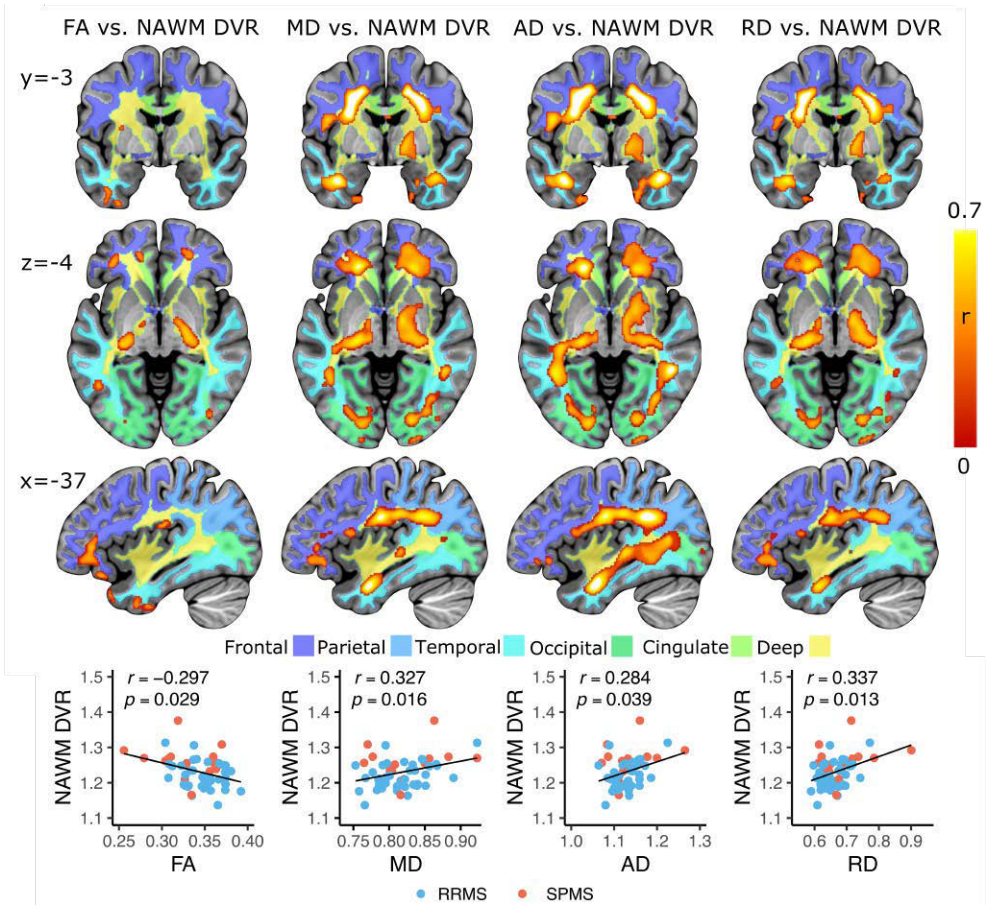

Figure 11. Regional and voxel-level associations of decreased tract integrity to increased [^{11}C](R)-PK11195 DVR in normal appearing white matter (NAWM). Statistically significant voxel-level Pearson correlation coefficients are illustrated on top of each regional scatterplot. The regional correlations are visualized with linear regression lines and Spearman correlation coefficient, significant at the level of $p<0.05$. The correction for multiple comparisons at voxel-level was performed using FDR with significance level of $p<0.05$. NAWM subregions in voxel-level analysis are highlighted in different colors. AD, MD and RD units in regional scatterplots are scaled with constant 10^3. Modified from the original publication II.

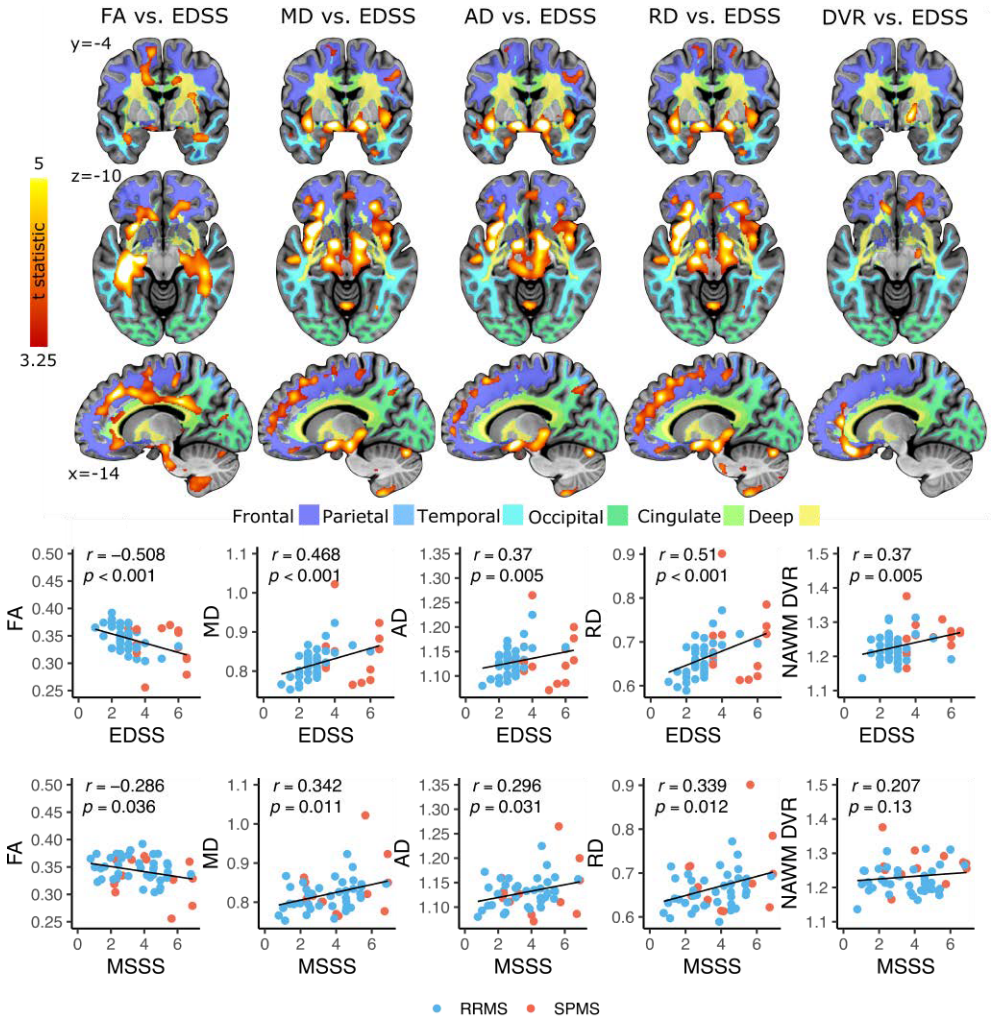

Figure 12. Regional and voxel-level associations between decreased tract integrity and clinical disability evaluated with expanded disability status scale (EDSS) and multiple sclerosis severity score (MSSS). Statistically significant voxel-level Pearson correlation coefficients between DTI and EDSS are illustrated on top of each regional scatterplot. The regional correlations between DTI and EDSS, and between DTI and MSSS are visualized with linear regression lines and Spearman correlation coefficient, significant at the level of $p<0.05$. The cluster level correction for multiple comparisons was performed using FDR with significance level of $p<0.05$ (t-statistic > 3.25). NAWM subregions in voxel-level analysis are highlighted in different colors. AD, MD and RD units in regional scatterplots are scaled with constant 10^3. Modified from the original publication II.

5.4 Study III: Brain TSPO levels are associated with age, BMI and sex

The results showed that higher age was associated with higher [^{11}C]PBR28 V_T in all regions (Figure 13A). Moreover, higher [^{11}C]PBR28 V_T was associated in all investigated regions with lower BMI and that females had higher [^{11}C]PBR28 V_T compared to males in all investigated regions (Figure 13C-F). The magnitude of the estimates was similar between the regions, and e.g., an increase of one BMI unit predicted a 2.2% decrease in GM V_T, whereas the GM V_T was 16.8% higher in females compared to males. Because of sex differences in V_T, the data were divided into sex-specific subgroups. This post-hoc analysis revealed that the age effect was present only in male subjects, where an increase of one year of age predicted a 0.6% increase in GM V_T (Figure 14). For BMI, the effect was stronger in males, where an increase of one BMI unit predicted 2.6% decreases in GM V_T, as compared to females, where an increase of one BMI unit predicted 1.7% decreases in GM V_T.

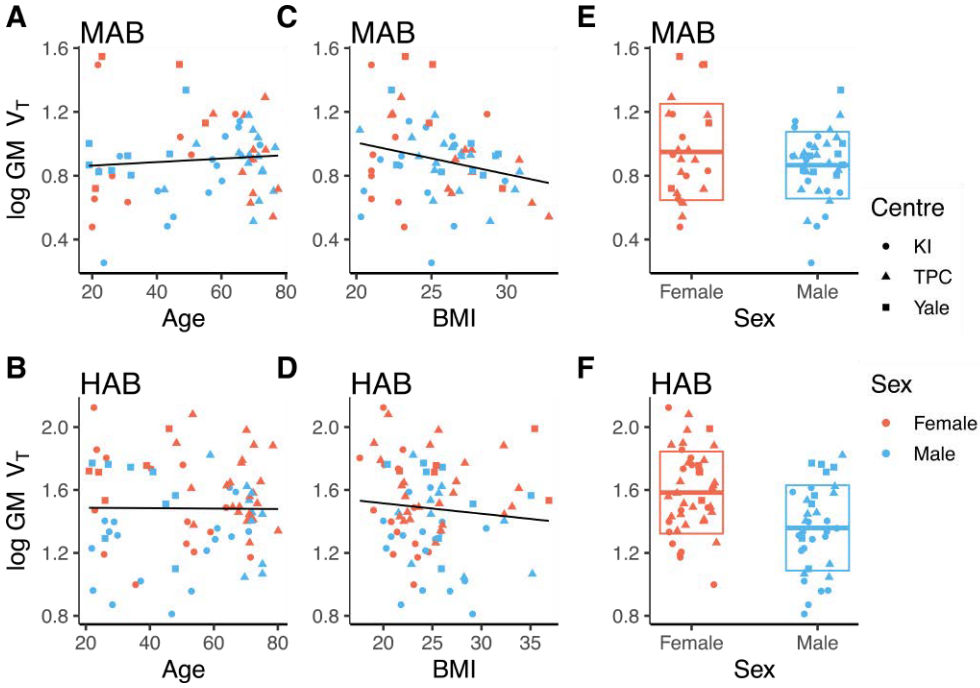

Figure 13. The relationships of age, BMI and sex to log-transformed grey matter (GM) [^{11}C]PBR28 V_T. Age vs. log-transformed [^{11}C]PBR28 GM V_T in MAB genotype (A) and HAB genotype (B). BMI vs. log-transformed [^{11}C]PBR28 GM V_T in MAB genotype subjects (C) and HAB genotype subjects (D). Sex vs. log-transformed [^{11}C]PBR28 GM V_T in MAB genotype subjects (E) and HAB genotype subjects (F). Box-plots in (E) and (F) represent the data means and standard deviations for both sexes. Modified from the original publication III.

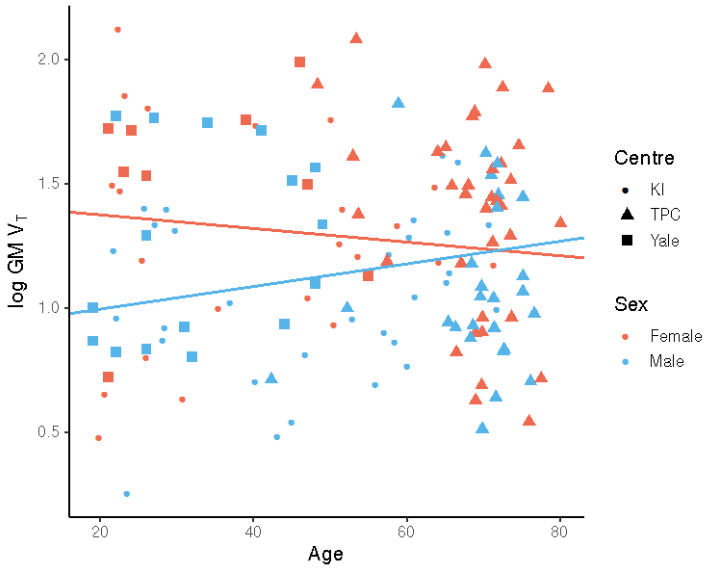

Figure 14. The relationship between log-transformed gray matter (GM) [^{11}C]PBR28 V_T and age for males and females. The regression lines denote the fixed effects from two linear mixed effects models including either females or males, with TSPO genotype and PET center specified as random intercepts. Modified from the original publication III.

6 Discussion

6.1 Association between increased TSPO uptake, altered DTI macroparameters, and clinical disability

Studies I and II demonstrated increased TSPO uptake in the NAWM and in surrounding regions of T1 hypointense lesions of SPMS patients, compared to RRMS and healthy control subjects. Based on evidence from neuropathological studies (Brück *et al.*, 1995; Allen *et al.*, 2001; Kutzelnigg *et al.*, 2005; Cosenza-Nashat *et al.*, 2009; Frischer *et al.*, 2009; Moll *et al.*, 2011; Nutma *et al.*, 2019), the group specific results in studies I and II are likely attributed to diffuse microglial activity in the NAWM, as well as to higher numbers of activated microglia in the edge of chronically active and slowly expanding lesions. Furthermore, these results suggest that in progressive MS, neuroinflammation becomes compartmentalized behind repaired BBB (Frischer *et al.*, 2009).

As a consequence of pro-inflammatory cytokines and reactive oxygen and nitrogen species produced by the activated microglial cells, the diffuse microglial activation likely contributes to demyelination and axonal injury in NAWM (Witte *et al.*, 2014). This hypothesis is supported by the results of studies I and II, which displayed that increased TSPO uptake in the NAWM of MS patients was positively associated with altered DTI macroparameters (decreased FA, and increased RD and MD) in the NAWM. However, both regional and voxel-based results displayed heterogeneous NAWM TSPO uptake, yielding significant differences between groups in the frontal, cingulate and deep subregions, whereas no differences were observed in the temporal, occipital, and parietal NAWM. In a similar manner, the groupwise differences in DTI macroparameters were concentrated only in cingulate and occipital NAWM. Despite these regional discrepancies in ROI-based group analysis of TSPO uptake and DTI macroparameters, voxel-based group analysis and between modality correlation analysis revealed significant overlapping and neighboring clusters, indicating that neuroinflammation and neurodegeneration are closely associated processes in MS disease progression.

Clinical disability, measured with EDSS, was positively associated with both NAWM TSPO uptake and changes in DTI macroparameters, suggesting that both

imaging modalities could be used to monitor the disability progression. Compared to the EDSS, associations with MSSS were lower for DTI macroparameters and not significant for NAWM TSPO uptake. Despite the differences of the study samples, the similarity of NAWM results between studies I and II suggests that the MS-imaging results are replicable with both TSPO PET and DTI. However, larger significant clusters and better agreement was observed between DTI and EDSS, which may indicate that the DTI macroparameters are more sensitive to the physical disability, which EDSS is mainly measuring (Horakova *et al.*, 2012). On the other hand, association of TSPO uptake and EDSS hints that the TSPO uptake could reflect more the pro-inflammatory M1 microglia phenotype, rather than the anti-inflammatory M2 phenotype.

The results of studies I and II are in line with previous *in vivo* TSPO PET studies showing similar differences between groups in the NAWM (Politis *et al.*, 2012; Giannetti *et al.*, 2015; Herranz *et al.*, 2016; Datta, Colasanti, Rabiner, *et al.*, 2017), and in the thalamus (Banati *et al.*, 2000). Although increased NAWM TSPO uptake was observed between RRMS and healthy volunteers in study II, this difference did not reach statistical significance either in study I or study II. This is in contrast with previous NAWM results of CIS patients (Giannetti *et al.*, 2015). However, in study I the small sample size and age difference between HC and RRMS/CIS patients possibly explains this discrepancy. Significant differences in cortical GM were neither detected in study I, opposite to previous in vivo TSPO PET studies, where significant cortical differences in TSPO uptake were displayed between HC and mixed RRMS/SPMS patients (Herranz *et al.*, 2016; Singhal *et al.*, 2019), and between HC and SPMS patients (Politis *et al.*, 2012). Previous post-mortem studies have also observed cortical microglial activation associated to MS progression (Kutzelnigg *et al.*, 2005), but endothelial TSPO binding may also have influence on the cortical results due to increased vascularity in GM, as compared to WM (Hase *et al.*, 2019). These differences in results could potentially result from low sensitivity of 1st generation TSPO radioligand [^{11}C](R)-PK11195, or because SCA pseudo-reference region contains signal from cortical regions, which may lead to underestimation of the true uptake.

Earlier studies have also demonstrated that higher degree of clinical disability is associated with increased TSPO PET uptake in the thalamus (Singhal *et al.*, 2019), in the T1 hypointense lesions (Giannetti *et al.*, 2014) and in the NAWM (Giannetti *et al.*, 2015; Herranz *et al.*, 2016). Similarly, DTI macroparametres in several WM subregions have been shown to be associated with clinical disability (Liu *et al.*, 2012; Onu *et al.*, 2012), although also controversial results exist (Rovaris *et al.*, 2002; Fink *et al.*, 2010) particularly in RRMS cohorts, possibly because EDSS is mainly affected by the motor system and might not be altered in the early disease stage (Sbardella *et al.*, 2013). Despite of EDSS disadvantages, both altered NAWM DTI

macroparameters and increased NAWM TSPO PET uptake have been shown to predict later EDSS change (Bodini *et al.*, 2013; Sucksdorff *et al.*, 2020).

Previous neuropathological studies have shown positive association between the extent of axonal damage and macrophage/microglia levels in NAWM and in cortical GM (Kuhlmann *et al.*, 2002; Kutzelnigg *et al.*, 2005; Frischer *et al.*, 2009). Moreover, previous post-mortem imaging study demonstrated that reduced FA and AD in the perilesional WM and NAWM of SPMS patients was associated with increased density of activated microglia cells, whereas astrocytic cell levels in these ROIs remained constant (Moll *et al.*, 2011). Supported by these previous findings, Studies I and II are the first *in vivo* studies reporting the association between NAWM TSPO uptake and DTI macroparameters in MS. Furthermore, both studies I and II illustrated that increased TSPO uptake was also associated with altered DTI macroparameters in the thalamus and in the thalamocortical radiations. These results indicating thalamic involvement in MS are supported by previous findings showing that FA reduction in thalamus predicts disease evolution in PPMS patients (Mesaros *et al.*, 2011) and contributes to cognitive decline and disability in MS (Minagar *et al.*, 2013). Moreover, previous studies have argued that thalamic injury, observed with DTI, is either a consequence of focal lesions in thalamocortical radiations (Henry *et al.*, 2009), or WM-independent microstructural pathological processes within the thalamus (Deppe *et al.*, 2016). Whatever the exact mechanism is, our results support the notion that thalamus is an important structure in the MS pathology warranting further research.

Altogether, based on our results and previous research, TSPO PET and DTI could be used as complementary imaging modalities to improve the understanding of the association between neuroinflammation and neurodegeneration in MS progression. These results suggest also that longitudinal multimodal DTI and TSPO PET studies could be applied in observing the effects of new treatments, particularly because an effective treatment is currently still missing for the progressive MS.

6.2 The effects of ageing, body mass index and sex on the TSPO availability

Studies I and III demonstrated the effect of ageing on TSPO uptake. In study I, increased age was associated with higher [^{11}C](R)-PK11195 DVR in the NAWM and in the thalamus of MS patients, whereas in healthy control subjects, higher age was associated with higher cortical [^{11}C](R)-PK11195 DVR. In study III, the multicenter data of healthy subjects demonstrated that higher age was associated with higher cortical and subcortical [^{11}C]PBR28 V_T, but a post-hoc analysis yielded that the effect was present only in male subjects. Additionally, higher [^{11}C]PBR28 V_T was associated with lower BMI, and females showed higher [^{11}C]PBR28 V_T

compared to males. In study I, age likely explains also the higher mean FA in the NAWM of RRMS subjects compared to healthy control subjects, because normal ageing causes alterations in WM, which in turn is displayed by reduced FA.

Based on preclinical findings of retinal microglia, it has been suggested that microglia activate slower and exhibit less "surveying" morphology a consequence of ageing (Damani *et al.*, 2011). Several previous neuropathological human studies have also demonstrated age-related alterations in microglia morphology and function and increases in total number of activated pro-inflammatory M1 microglia phenotype due to ageing (DiPatre and Gelman, 1997; Sheng, Mrak and Griffin, 1998; Miller and Streit, 2007; Michell-Robinson *et al.*, 2015). These findings are likely related to two phenomenons called immunosenescence and inflamm-aging, where the former refers to the weakening in integrity and efficiency of the adaptive and innate immune system and latter refers to the low-grade inflammation which is suggested to develop with advanced age (Fulop *et al.*, 2018).

Inflamm-aging is also considered as a significant factor associated to the clinical course of MS (Musella *et al.*, 2018). This view is supported by our results that demonstrate different regional patterns in the association between increased TSPO uptake and increasing age, among age-matched healthy controls and MS subjects. Particularly, these results indicate that subtle microglial activation would be initially related to normal ageing, but as previously suggested it may amplify in MS as a consequence of neuroinflammation (Musella *et al.*, 2018). However, previous TSPO PET studies of normal ageing have been inconclusive, where either positive correlations between age and TSPO binding in thalamus (Cagnin *et al.*, 2001), in several cortical and subcortical areas (Schuitemaker, Thalia F. van der Doef, *et al.*, 2012; Paul *et al.*, 2018), or no observed age effect (Jan C. Debruyne *et al.*, 2003; Yasuno *et al.*, 2008; I. Suridjan *et al.*, 2014) have been demonstrated. Interestingly, the study III results were driven solely by the male subjects, which could explain these previous conflicting results, where study samples had small size and included both male and female subjects.

Based on merely the PET uptake estimates, it is impossible to find reason for the observed sex difference in the study III [^{11}C]PBR28 V_T results. However, our results are supported by previously preclinical studies demonstrating sex-related differences in microglial function. Particularly, female rats had more microglia cells with an activated morphology as juveniles and adults compared to male rats (Schwarz, Sholar and Bilbo, 2012), whereas adult male mice microglia cells showed a tendency to adopt more inflammatory phenotype compared to female counterpart (Villa *et al.*, 2018).

On the other hand, recent preclinical results have showed higher TSPO levels in cerebellum of male rats compared to females (Giatti *et al.*, 2019), which would support the possibility that the role of TSPO in steroidogenesis could contribute to

our observed sex differences in TSPO uptake. Particularly, glial cells express receptors for estrogens and androgens, which suggests an interaction between sex steroid hormones and the innate immune function response (Puy *et al.*, 1995; Barreto *et al.*, 2007; Uchoa, Moser and Pike, 2016). Consequently, as both androgens and female sex hormone levels decline with age, this could explain our observed age-sex interaction in [^{11}C]PBR28 V_T, where male TSPO levels increase with age, eventually reaching the higher TSPO level of females. Our result of age-related sex difference in TSPO uptake may also connect to the observed sex-specific differences of neuroinflammatory autoimmune diseases such as MS and Alzheimer's disease, where the incidence is higher in females compared to males (Villa *et al.*, 2016; Nissen, 2017).

Increasing evidence implicates that obesity is associated with low-grade systemic inflammation (Hotamisligil, 2006), which is hypothesized to induce neuroinflammation in several brain regions including hypothalamus, hippocampus, and cerebellum (Guillemot-Legris and Muccioli, 2017). Findings from preclinical models of obesity have showed that high-fat diet induced obesity increases proinflammatory cytokines in the hypothalamus and hippocampus (Erion *et al.*, 2014; Sobesky *et al.*, 2014) and promotes hippocampal synaptic stripping, induced by microglia (Hao *et al.*, 2016). Rodent models have also indicated that astrocytes are activated after high-fat diet (Buckman *et al.*, 2015), and as observed with [^{18}F]FDG PET, astrocytes drive the increased glucose uptake in the obese rodents (Zimmer *et al.*, 2017), which would implicate that astrocytes could contribute to the human brain [^{18}F]FDG PET findings of obesity (Iozzo and Guzzardi, 2019). Previous human studies have shown also that obesity is associated with reduced white matter atrophy and integrity (Karlsson *et al.*, 2013; Samara *et al.*, 2020), as well as with cognitive decline (Miller and Spencer, 2014) and late-life brain amyloid deposition (Gottesman *et al.*, 2017), which could be related to increased neuroinflammation. However, contrary to these previous results, study III demonstrated that decreased [^{11}C]PBR28 V_T, was associated with higher BMI. One explanation for this unexpected finding could be that due to the low-grade systemic inflammation, the peripheral TSPO expression is dysregulated in obese subjects, which is reflected also in the brain. An example of such periphery-to-brain immune interaction is a previously demonstrated high correlation between TSPO levels in brain and peripheral blood cells (Kanegawa *et al.*, 2016), suggesting that the CNS immune system may be affected by alterations in the peripheral immune system. As recently suggested, the peripheral inflammatory status may also affect the volume of distribution thorough decreased perfusion (Turkheimer *et al.*, 2020).

Study III results indicate that the negative BMI effect is global in all brain regions, and hence if reference tissue input methodology is applied, the effect may disappear. This may explain the results of recent study (Schubert *et al.*, 2020), where

[^{11}C](R)-PK11195 BP_{ND} in anterior cingulate, prefrontal cortex and insula, with respect to clustered pseudo-reference region, were not associated with changes in BMI. On the other hand, recently a positive associations were found between BMI and [^{11}C]PBR28 standardized uptake value (SUV)-ratio in parietal cortex and precuneus with respect to cerebellum reference region (Toppala *et al.*, 2021), which would suggest that either different TSPO radioligand, different target ROIs and reference regions explain the difference compared to results in (Schubert *et al.*, 2020).

Another explanation of our results between BMI and [^{11}C]PBR28 V_T could be related to competition for available TSPO binding sites between TSPO radioligand and endogenous ligands, such as cholesterol and porphyrins, which have high affinity for TSPO (Guo *et al.*, 2015). Obese subjects often have higher levels of serum cholesterol (Després *et al.*, 1990), which could induce such competition. Also, correlation between higher plasma cholesterol levels and lower whole brain [^{11}C]PBR28 V_T was recently demonstrated in healthy control subjects and alcohol use disorder patients (Kim *et al.*, 2018). However, while our results support an involvement of TSPO in obesity, further studies are warranted to address the specific role of TSPO on this topic. In any case, it can be concluded that TSPO levels may be associated with age, BMI and sex, suggesting that they can be confounding factors in clinical designs.

6.3 Methodological considerations

In studies I and II, a strength is the combination of imaging modalities, which allowed to study the association of microglial activation, demyelination and axonal damage in MS disease progression. As a continuation, a longitudinal study would be required to examine the temporal relation of DTI and TSPO PET in disability progression, which we could not evaluate in these cross-sectional studies. In study III, the main advantage is the large amount of TSPO data from healthy subjects (N=140), which provided adequate statistical power to conclusively study the effects of ageing, sex and BMI on TSPO availability. However, in addition to the general methodological limitations described in subsections 2.2.2 and 2.2.3, there are number of limitations and potential confounding effects in the studies I-III which can have influence on the results.

6.3.1 Participants

While in the Study I none of the patients were on immunomodulatory treatments, in Study II the patients had several different disease modifying treatments. Therefore, study I offers a view into the natural course of the disease, whereas study II resembles

the normal clinical setting. Although the variety of treatments may further increase the variability of the findings, the results are in agreement with study I and demonstrate that the association between microglial activity and WM tract damage is present regardless of the variable treatments.

In study III, although all subjects were initially categorized as healthy controls, there were several older subjects who were using statins (n=11; three males and eight females) to control cholesterol levels, which could theoretically affect TSPO availability, either by interfering with TSPOs role in the cholesterol transport or modulating the peripheral inflammation process. Also, two subjects were on hormonal replacement medication and three subjects were smoking regularly, and for several subjects the current smoking status was unknown (n = 10). However, the main analysis results remained the same after excluding the subjects who were using cholesterol lowering or hormonal replacement medication, or whose current smoking status was positive. Thus, it is less likely that these subjects had significant effect on the study III results.

6.3.2 Methods

All studies I-III contain data either from different institutes or different subprojects, which may have influence on the results: the image acquisition parameters may have differences, different data preprocessing methods in different analysis pipelines might have effect on the results, non-overlapping age distributions between institutes cannot be separated with the other institute related effects. In study II, the DTI acquisition parameter differences were tested with a subset of subjects, and no significant differences were observed between the 33 and 64 gradient directions. In study III, the possible PET centre differences were attempted to control within a linear mixed effects model by including a random intercept for each PET centre.

Age may be considered as biomarker for MS disease progression, as the onset of the progressive disease phase appears to depend on age rather than disease duration (Tutuncu *et al.*, 2013). Therefore, it is probable that statistical controlling for the age weakens the statistical differences in microglia activation and DTI macroparameters between RRMS and SPMS. Also, although RRMS had significantly lower BMI compared to HC and SPMS patients, it was not used as a control variable in statistical analysis. However, based on the study III results, the association between BMI and V_T is global and thus by using pseudo-reference tissue input this effect would likely be canceled out.

In studies I and II, clinical disability of patients with MS was evaluated with EDSS. However, EDSS contains bias because of the inter-rater variability and also because cognition, attention and fatigue are disregarded from the score (Horakova *et al.*, 2012). More detailed scale, such as Multiple Sclerosis Functional Composite

(MSFC) could possibly have described the disease characteristics and progression more accurately, although it has also limitations due to practice effects, variations in reference populations, omission of visual assessment and lack of accepted definition of a clinically meaningful change (Polman and Rudick, 2010).

In Study II, a voxel-level comparison between TSPO PET and DTI was performed with 3D images, which were normalized to MNI 152 space. Recently, in patients with dementia with Lewy bodies, similar TSPO PET and DTI association analysis was performed by first running a tract based spatial statistic (TBSS) analysis for DTI and then using multiple regression to explain DTI macroparameters with regional PET binding estimates (Nicastro *et al.*, 2020). However, using this method, TSPO PET measurements are treated as regional average values and therefore TSPO PET is missing the true voxel-level signal location.

In study III, [^{11}C]PBR28 V_T was not corrected for free radioligand fraction in plasma, because these fractions were not measured at TPC. Endothelial binding was not accounted in the modelling in studies I-III, although endothelial TSPO binding may change due to ageing (Veronese *et al.*, 2018). Accounting for endothelial binding could have improved the model fits and reduced the variability of [^{11}C]PBR28 V_T estimates, as previously reported (Veronese *et al.*, 2018; Wimberley *et al.*, 2018).

7 Conclusions

In this thesis, the connection between microglial activation, demyelination and axonal loss was investigated in the NAWM of MS patients with TSPO PET radioligand [^{11}C](R)-PK11195 and DTI. Additionally, the associations of clinical disability with imaging macroparameters of both imaging modalities were evaluated. The effect of aging on the TSPO levels of MS patients and healthy control subjects was studied with [^{11}C](R)-PK11195 and [^{11}C]PBR28 TSPO radioligands. Furthermore, the effect of age, BMI and sex to the variability of [^{11}C]PBR28 V_T was assessed in large multicenter data of healthy volunteers.

The results revealed that [^{11}C](R)-PK11195 DVR in the NAWM, in surrounding regions of T1 hypointense lesions and in thalamus was increased in SPMS patients compared to RRMS and CIS patients and healthy volunteers. Increased NAWM [^{11}C](R)-PK11195 DVR was associated with altered NAWM DTI macroparameters, their regional correspondence was consistent, and they both were associated with advanced clinical disability. Moreover, these results could be replicated with a separate data. Increased age was associated with higher [^{11}C](R)-PK11195 DVR in NAWM and in thalamus of MS patients, whereas in healthy control subjects, higher age was associated with higher cortical [^{11}C](R)-PK11195 DVR. However, larger multicenter data of healthy volunteers revealed that higher age was associated with higher cortical and subcortical [^{11}C]PBR28 V_T only in male subjects. Additionally, higher [^{11}C]PBR28 V_T was associated with lower BMI, and females showed higher [^{11}C]PBR28 V_T compared to males.

In summary, the following conclusions can be drawn based on the results of this thesis:

1. A tight interrelation between [^{11}C](R)-PK11195 DVR and DTI macroparameters in between group analysis, between modality correlation analysis, and in correlation analysis with respect to clinical disability scores suggests that PET and DTI can be used as complementary imaging modalities in clinical MS studies, and that neuroinflammation and neurodegeneration are closely associated processes in the progressive MS.

2. TSPO levels may be associated with age, BMI and sex suggesting that they can be confounding factors in clinical designs. Subtle microglial activation may be initially related to normal ageing but is accentuated following neuroinflammation
3. A multicentre collaboration provides increased power to detect clinically relevant effects, mitigating the problem of small sample sizes in PET research.

Acknowledgements

This thesis project was supported financially by the drug research doctoral programme (DRDP), Alfred Kordelin foundation, the Finnish Brain Foundation, the Instrumentarium science foundation, the Orion research foundation, the Paulo foundation, the Päivikki and Sakari Sohlberg foundation and the Turku University Hospital Foundation.

I wish to sincerely thank several people for their contribution to this thesis project. Without their advice and assistance this project would not have been completed.

First, I would like to thank all my supervisors, Professor Laura Airas, Professor Juha Rinne and Docent Jussi Hirvonen for the encouraging guidance. Particularly, Laura's expertise in neuroinflammation and enthusiasm for improving the MS research methods, as well as Juha's and Jussi's broad knowledge of neuroscience and PET imaging have helped me to carry out this project. I would like to thank all of you also for the help with the numerous grant applications, which made this project possible to accomplish.

I would like to thank the follow-up committee members Professor Jarmo Hietala and Professor Mika Scheinin for the suggestions and encouragements during the annual steering group meetings. Also, I would like to acknowledge the pre-examiners of this thesis, Professor Olli Gröhn and Assistant Professor Yeona Kang for the comments and suggestions, which improved the thesis.

I am particularly grateful to my co-authors Jarkko Johansson and Eero Rissanen for all of the guidance you have given to me in PET imaging and MS. I would also like to express my gratitude for all my other co-authors, particularly Svetlana Bezukladova, Laura Ekblad, Rainer Hinz, Noora Lindgren, Markus Matilainen, Päivi Marjamäki and Pontus Plavén-Sigray for the assistance, helpful comments and suggestions. I would like to thank all members of the [11C]PBR28 study group, and particularly Professor Simon Cervenka and Assistant Professor David Matuskey for giving me the opportunity to join the multi-center collaboration. I would also like express my thanks to all participants of the studies.

It has been a privilege to conduct research at Turku PET Centre, and I would like to thank the director Professor Juhani Knuuti for providing the excellent facilities

and working environment. Also, I would like to thank the Turku PET Centre radiographers, laboratory technicians and the IT personnel for your kind help and sharing your expertise.

I would like to give special thanks to Tomi Karjalainen and Lauri Nummenmaa for sharing the same office during my thesis project. I appreciate your valuable advice and comments, as well as the inspiring research atmosphere you have created. I am also very thankful to Vesa Oikonen for the patience in answering all my questions related to PET modelling.

I wish to thank all current and former members of neuroimmunology, neurology and human emotion systems research groups, Kati Alakurtti, Anna Brück, Marco Bucci, Janne Isojärvi, Tatu Kantonen, Sini Laaksonen, Heikki Laurikainen, Lasse Lukkarinen, Tuulia Malen, Mehrbod Mohammadian, Sanaz Nazari-Farsani, Marjo Nylund, Vesa Putkinen, Eleni Rebelos, Tiina Saanijoki, Severi Santavirta, Kerttu Seppälä, Anniina Snellman, Marcus Sucksdorff, Lihua Sun, Jarmo Teuho, Sini Toppala, Anna Vuorimaa, Imran Waggan and all the rest, who I probably forgot to add, for all the cheerful moments at the group meetings and during the lunch breaks. I would also like to thank all my friends and bandmates for the good times outside the office.

I would like to thank my dear parents Leena and Antero, my sister Salla, and my dear parents-in-law Päivi and Jarmo for all of your love, encouragement and support through the years.

Finally, I would like to thank my dearests Maiju and Niilo for the lovely moments and all the joy you have brought in my life, which have helped me to get my thoughts out of this project.

Turku, May 2021

Jouni Tuisku

References

Albrecht, D. S. *et al.* (2018) 'Pseudoreference regions for glial imaging with 11 C-PBR28: Investigation in 2 clinical cohorts', *Journal of Nuclear Medicine*. Society of Nuclear Medicine Inc., 59(1), pp. 107–114. doi: 10.2967/jnumed.116.178335.

Alexander, A. L. *et al.* (2007) 'Diffusion Tensor Imaging of the Brain', *Neurotherapeutics*. Neurotherapeutics, 4(3), pp. 316–329. doi: 10.1016/j.nurt.2007.05.011.

Allen, I. V. *et al.* (2001) 'Pathological abnormalities in the normal-appearing white matter in multiple sclerosis', *Neurological Sciences*. Springer Milan, 22(2), pp. 141–144. doi: 10.1007/s100720170012.

Aung, W. Y., Mar, S. and Benzinger, T. L. (2013) 'Diffusion tensor MRI as a biomarker in axonal and myelin damage', *Imaging in Medicine*. Imaging Med, pp. 427–440. doi: 10.2217/iim.13.49.

Baecher-Allan, C., Kaskow, B. J. and Weiner, H. L. (2018) 'Multiple Sclerosis: Mechanisms and Immunotherapy', *Neuron*. Cell Press, pp. 742–768. doi: 10.1016/j.neuron.2018.01.021.

Banati, R. B. *et al.* (2000) 'The peripheral benzodiazepine binding site in the brain in multiple sclerosis. Quantitative in vivo imaging of microglia as a measure of disease activity', *Brain*. Oxford University Press, 123(11), pp. 2321–2337. doi: 10.1093/brain/123.11.2321.

Barkhof, F. *et al.* (1997) *Comparison of MRI criteria at first presentation to predict conversion to clinically definite multiple sclerosis*, *Brain*.

Barreto, G. *et al.* (2007) 'Testosterone decreases reactive astroglia and reactive microglia after brain injury in male rats: role of its metabolites, oestradiol and dihydrotestosterone', *European Journal of Neuroscience*. John Wiley & Sons, Ltd (10.1111), 25(10), pp. 3039–3046. doi: 10.1111/j.1460-9568.2007.05563.x.

Le Bihan, D. (2003) 'Looking into the functional architecture of the brain with diffusion MRI', *Nature Reviews Neuroscience*. Nature Publishing Group, 4(6), pp. 469–480. doi: 10.1038/nrn1119.

Bodini, B. *et al.* (2013) 'Corpus callosum damage predicts disability progression and cognitive dysfunction in primary-progressive MS after five years', *Human Brain Mapping*. Hum Brain Mapp, 34(5), pp. 1163–1172. doi: 10.1002/hbm.21499.

Brody, A. L. *et al.* (2017) 'Effect of Cigarette Smoking on a Marker for Neuroinflammation: A [11C]DAA1106 Positron Emission Tomography Study.', *Neuropsychopharmacology : official publication of the American College of Neuropsychopharmacology*. Nature Publishing Group, 42(8), pp. 1630–1639. doi: 10.1038/npp.2017.48.

Brück, W. *et al.* (1995) 'Monocyte/macrophage differentiation in early multiple sclerosis lesions', *Annals of Neurology*. Ann Neurol, 38(5), pp. 788–796. doi: 10.1002/ana.410380514.

Buckman, L. B. *et al.* (2015) 'Evidence for a novel functional role of astrocytes in the acute homeostatic response to high-fat diet intake in mice.', *Molecular metabolism*. Elsevier, 4(1), pp. 58–63. doi: 10.1016/j.molmet.2014.10.001.

Cagnin, A. *et al.* (2001) 'In-vivo measurement of activated microglia in dementia', *The Lancet*. Elsevier, 358(9280), pp. 461–467. doi: 10.1016/S0140-6736(01)05625-2.

Calabrese, M. *et al.* (2011) 'Cortical diffusion-tensor imaging abnormalities in multiple sclerosis: A 3-year longitudinal study', *Radiology*. Radiology, 261(3), pp. 891–898. doi: 10.1148/radiol.11110195.

Calvi, A. *et al.* (2020) 'In vivo imaging of chronic active lesions in multiple sclerosis', *Multiple Sclerosis Journal*. SAGE Publications Ltd, p. 135245852095858. doi: 10.1177/1352458520958589.

Carr, M. W. and Grey, M. L. (2002) 'Magnetic resonance imaging: Overview, risks, and safety measures', *American Journal of Nursing*. Lippincott Williams and Wilkins, pp. 26–33. doi: 10.1097/00000446-200212000-00012.

Carson, R. E. *et al.* (2003) 'Design of a motion-compensation OSEM list-mode algorithm for resolution-recovery reconstruction for the HRRT', in *2003 IEEE Nuclear Science Symposium. Conference Record (IEEE Cat. No.03CH37515)*. IEEE, pp. 3281–3285. doi: 10.1109/NSSMIC.2003.1352597.

Carson, R. E. (2006) 'Tracer Kinetic Modeling in PET', in *Positron Emission Tomography*. Springer-Verlag, pp. 127–159. doi: 10.1007/1-84628-007-9_6.

Ceccarelli, A. *et al.* (2007) 'Normal-appearing white and grey matter damage in MS: A volumetric and diffusion tensor MRI study at 3.0 Tesla', *Journal of Neurology*. Springer, 254(4), pp. 513–518. doi: 10.1007/s00415-006-0408-4.

Chang, L. C., Jones, D. K. and Pierpaoli, C. (2005) 'RESTORE: Robust estimation of tensors by outlier rejection', *Magnetic Resonance in Medicine*. Magn Reson Med, 53(5), pp. 1088–1095. doi: 10.1002/mrm.20426.

Colasanti, A. *et al.* (2014) 'In vivo assessment of brain white matter inflammation in multiple sclerosis with 18F-PBR111 PET', *Journal of Nuclear Medicine*. Society of Nuclear Medicine Inc., 55(7), pp. 1112–1118. doi: 10.2967/jnumed.113.135129.

Colasanti, A. *et al.* (2016) 'Hippocampal neuroinflammation, functional connectivity, and depressive symptoms in multiple sclerosis', *Biological Psychiatry*. Elsevier USA, 80(1), pp. 62–72. doi: 10.1016/j.biopsych.2015.11.022.

Collste, K. *et al.* (2016) 'Test–retest reproducibility of [11C]PBR28 binding to TSPO in healthy control subjects', *European Journal of Nuclear Medicine and Molecular Imaging*. Springer Berlin Heidelberg, 43(1), pp. 173–183. doi: 10.1007/s00259-015-3149-8.

Compston, A. and Coles, A. (2002) 'Multiple sclerosis', in *Lancet*. Elsevier Limited, pp. 1221–1231. doi: 10.1016/S0140-6736(02)08220-X.

Compston, A. and Coles, A. (2008) 'Multiple sclerosis', *The Lancet*. Elsevier, pp. 1502–1517. doi: 10.1016/S0140-6736(08)61620-7.

Constantinescu, C. S. *et al.* (2011) 'Experimental autoimmune encephalomyelitis (EAE) as a model for multiple sclerosis (MS)', *British Journal of Pharmacology*. Wiley-Blackwell, pp. 1079–1106. doi: 10.1111/j.1476-5381.2011.01302.x.

Cosenza-Nashat, M. *et al.* (2009) 'Expression of the translocator protein of 18 kDa by microglia, macrophages and astrocytes based on immunohistochemical localization in abnormal human brain', *Neuropathology and Applied Neurobiology*. NIH Public Access, 35(3), pp. 306–328. doi: 10.1111/j.1365-2990.2008.01006.x.

Cumming, P. *et al.* (2018) 'Sifting through the surfeit of neuroinflammation tracers', *Journal of Cerebral Blood Flow & Metabolism*. SAGE PublicationsSage UK: London, England, 38(2), pp. 204–224. doi: 10.1177/0271678X17748786.

Damani, M. R. *et al.* (2011) 'Age-related alterations in the dynamic behavior of microglia.', *Aging cell*. NIH Public Access, 10(2), pp. 263–76. doi: 10.1111/j.1474-9726.2010.00660.x.

Datta, G., Colasanti, A., Kalk, N., *et al.* (2017) '11C-PBR28 and 18F-PBR111 detect white matter inflammatory heterogeneity in multiple sclerosis', *Journal of Nuclear Medicine*. Society of Nuclear Medicine Inc., 58(9), pp. 1477–1482. doi: 10.2967/jnumed.116.187161.

Datta, G., Colasanti, A., Rabiner, E. A., *et al.* (2017) 'Neuroinflammation and its relationship to changes in brain volume and white matter lesions in multiple sclerosis', *Brain*. Oxford University Press, 140(11), pp. 2927–2938. doi: 10.1093/brain/awx228.

Datta, G., Violante, I. R., *et al.* (2017) 'Translocator positron-emission tomography and magnetic resonance spectroscopic imaging of brain glial cell activation in multiple sclerosis', *Multiple Sclerosis*. SAGE Publications Ltd, 23(11), pp. 1469–1478. doi: 10.1177/1352458516681504.

Debruyne, Jan C. *et al.* (2003) 'Pet visualization of microglia in multiple sclerosis patients using [11C]PK11195', *European Journal of Neurology*, 10(3), pp. 257–264. doi: 10.1046/j.1468-1331.2003.00571.x.

Debruyne, J. C. *et al.* (2003) 'PET visualization of microglia in multiple sclerosis patients using [11C]PK11195', *European Journal of Neurology*. Wiley/Blackwell (10.1111), 10(3), pp. 257–264. doi: 10.1046/j.1468-1331.2003.00571.x.

Deppe, M. *et al.* (2016) 'Early silent microstructural degeneration and atrophy of the thalamocortical network in multiple sclerosis', *Human Brain Mapping*, 37(5), pp. 1866–1879. doi: 10.1002/hbm.23144.

Després, J. P. *et al.* (1990) 'Regional distribution of body fat, plasma lipoproteins, and cardiovascular disease.', *Arteriosclerosis (Dallas, Tex.)*, 10(4), pp. 497–511. Available at: http://www.ncbi.nlm.nih.gov/pubmed/2196040 (Accessed: 27 November 2018).

DiPatre, P. L. and Gelman, B. B. (1997) 'Microglial cell activation in aging and Alzheimer disease: partial linkage with neurofibrillary tangle burden in the hippocampus.', *Journal of neuropathology and experimental neurology*, 56(2), pp. 143–9. Available at: http://www.ncbi.nlm.nih.gov/pubmed/9034367 (Accessed: 18 June 2018).

Doble, A. *et al.* (1987) 'Labelling of peripheral-type benzodiazepine binding sites in human brain with [3H]PK 11195: Anatomical and subcellular distribution', *Brain Research Bulletin*. Elsevier, 18(1), pp. 49–61. doi: 10.1016/0361-9230(87)90033-5.

Erion, J. R. *et al.* (2014) 'Obesity elicits interleukin 1-mediated deficits in hippocampal synaptic plasticity.', *The Journal of neuroscience : the official journal of the Society for Neuroscience*. Society for Neuroscience, 34(7), pp. 2618–31. doi: 10.1523/JNEUROSCI.4200-13.2014.

Erlandsson, K. *et al.* (2012) 'A review of partial volume correction techniques for emission tomography and their applications in neurology, cardiology and oncology', *PHYSICS IN MEDICINE AND BIOLOGY Phys. Med. Biol*, 57, pp. 119–159. doi: 10.1088/0031-9155/57/21/R119.

Filippi, M. *et al.* (2000) 'A quantitative study of water diffusion in multiple sclerosis lesions and normal-appearing white matter using echo- planar imaging', *Archives of Neurology*. American Medical Association, 57(7), pp. 1017–1021. doi: 10.1001/archneur.57.7.1017.

Fink, F. *et al.* (2010) 'Comparison of Diffusion Tensor-Based Tractography and Quantified Brain Atrophy for Analyzing Demyelination and Axonal Loss in MS', *Journal of Neuroimaging*. John Wiley & Sons, Ltd, 20(4), pp. 334–344. doi: 10.1111/j.1552-6569.2009.00377.x.

Frischer, J. M. *et al.* (2009) 'The relation between inflammation and neurodegeneration in multiple sclerosis brains.', *Brain : a journal of neurology*. Oxford University Press, 132(Pt 5), pp. 1175–89. doi: 10.1093/brain/awp070.

Frischer, J. M. *et al.* (2015) 'Clinical and pathological insights into the dynamic nature of the white matter multiple sclerosis plaque', *Annals of Neurology*. John Wiley and Sons Inc., 78(5), pp. 710–721. doi: 10.1002/ana.24497.

Fulop, T. *et al.* (2018) 'Immunosenescence and inflamm-aging as two sides of the same coin: Friends or Foes?', *Frontiers in Immunology*. Frontiers Media S.A., p. 1. doi: 10.3389/fimmu.2017.01960.

García-Lorenzo, D. *et al.* (2018) 'Validation of an automatic reference region extraction for the quantification of [18 F]DPA-714 in dynamic brain PET studies', *Journal of Cerebral Blood Flow and Metabolism*. SAGE Publications Ltd, 38(2), pp. 333–346. doi: 10.1177/0271678X17692599.

Geginat, J. *et al.* (2017) 'The Enigmatic Role of Viruses in Multiple Sclerosis: Molecular Mimicry or Disturbed Immune Surveillance?', *Trends in Immunology*. Elsevier Ltd, pp. 498–512. doi: 10.1016/j.it.2017.04.006.

Giannetti, P. *et al.* (2014) 'Microglia activation in multiple sclerosis black holes predicts outcome in progressive patients: An in vivo [(11)C](R)-PK11195-PET pilot study', *Neurobiology of Disease*. Academic Press Inc., 65, pp. 203–210. doi: 10.1016/j.nbd.2014.01.018.

Giannetti, P. *et al.* (2015) 'Increased PK11195-PET binding in normal-appearing white matter in clinically isolated syndrome', *Brain : a journal of neurology*. Oxford University Press, 138(1), pp. 110–119. doi: 10.1093/brain/awu331.

Giatti, S. *et al.* (2019) 'Sex differences in steroid levels and steroidogenesis in the nervous system: Physiopathological role', *Frontiers in Neuroendocrinology*, p. 100804. doi: 10.1016/j.yfrne.2019.100804.

Gottesman, R. F. *et al.* (2017) 'Association between midlife vascular risk factors and estimated brain amyloid deposition', *JAMA - Journal of the American Medical Association*. American Medical Association, 317(14), pp. 1443–1450. doi: 10.1001/jama.2017.3090.

Guillemot-Legris, O. and Muccioli, G. G. (2017) 'Obesity-Induced Neuroinflammation: Beyond the Hypothalamus', *Trends in Neurosciences*. Elsevier Ltd, pp. 237–253. doi: 10.1016/j.tins.2017.02.005.

Gunn, R. *et al.* (2016) 'Molecular imaging and kinetic analysis toolbox (MIAKAT)-a quantitative software package for the analysis of PET neuroimaging data', *Journal of Nuclear Medicine*, 57, p. 1928. Available at: http://jnm.snmjournals.org/content/57/supplement_2/1928.short (Accessed: 14 December 2020).

Gunn, R. N. *et al.* (1997) 'Parametric Imaging of Ligand-Receptor Binding in PET Using a Simplified Reference Region Model', *NeuroImage*. Academic Press, 6(4), pp. 279–287. doi: 10.1006/NIMG.1997.0303.

Guo, Y. *et al.* (2015) 'Protein structure. Structure and activity of tryptophan-rich TSPO proteins.', *Science (New York, N.Y.)*. American Association for the Advancement of Science, 347(6221), pp. 551–5. doi: 10.1126/science.aaa1534.

Gut, P. (2015) 'Targeting mitochondrial energy metabolism with TSPO ligands', *Biochemical Society Transactions*. Portland Press Ltd, 43(4), pp. 537–542. doi: 10.1042/BST20150019.

Hagens, M. H. J. *et al.* (2020) 'The P2X7 receptor tracer [11C]SMW139 as an in vivo marker of neuroinflammation in multiple sclerosis: a first-in man study', *European Journal of Nuclear Medicine and Molecular Imaging*. Springer, 47(2), pp. 379–389. doi: 10.1007/s00259-019-04550-x.

Hanisch, U.-K. and Kettenmann, H. (2007) 'Microglia: active sensor and versatile effector cells in the normal and pathologic brain', *Nature Neuroscience*. Nature Publishing Group, 10(11), pp. 1387–1394. doi: 10.1038/nn1997.

Hannestad, J. *et al.* (2013) 'The neuroinflammation marker translocator protein is not elevated in individuals with mild-to-moderate depression: a [^{11}C]PBR28 PET study.', *Brain, behavior, and immunity*. NIH Public Access, 33, pp. 131–8. doi: 10.1016/j.bbi.2013.06.010.

Hao, S. *et al.* (2016) 'Dietary obesity reversibly induces synaptic stripping by microglia and impairs hippocampal plasticity.', *Brain, behavior, and immunity*. NIH Public Access, 51, pp. 230–9. doi: 10.1016/j.bbi.2015.08.023.

Hase, Y. *et al.* (2019) 'White matter capillaries in vascular and neurodegenerative dementias', *Acta neuropathologica communications*. Acta Neuropathol Commun, 7(1). doi: 10.1186/S40478-019-0666-X.

Hemmer, B., Kerschensteiner, M. and Korn, T. (2015) 'Role of the innate and adaptive immune responses in the course of multiple sclerosis', *The Lancet Neurology*. Lancet Publishing Group, pp. 406–419. doi: 10.1016/S1474-4422(14)70305-9.

Henry, R. G. *et al.* (2009) 'Connecting white matter injury and thalamic atrophy in clinically isolated syndromes', *Journal of the Neurological Sciences*. J Neurol Sci, 282(1–2), pp. 61–66. doi: 10.1016/j.jns.2009.02.379.

Herranz, E. *et al.* (2016) 'Neuroinflammatory component of gray matter pathology in multiple sclerosis.', *Annals of neurology*. John Wiley and Sons Inc., 80(5), pp. 776–790. doi: 10.1002/ana.24791.

Hillmer, A. T. *et al.* (2017) 'In vivo imaging of translocator protein, a marker of activated microglia, in alcohol dependence.', *Molecular psychiatry*. NIH Public Access, 22(12), pp. 1759–1766. doi: 10.1038/mp.2017.10.

Hinz, R. *et al.* (2008) 'Reference tissue kinetics extraction from [11C]-(R)-PK11195 scans on the high resolution research tomograph (HRRT)', *NeuroImage*. Elsevier BV, 41, p. T65. doi: 10.1016/j.neuroimage.2008.04.035.

Van Den Hoff, J. (2005) 'Principles of quantitative positron emission tomography', in *Amino Acids*. Springer, pp. 341–353. doi: 10.1007/s00726-005-0215-8.

Hoffman, E. J., Huang, S. C. and Phelps, M. E. (1979) 'Quantitation in positron emission computed tomography: 1. effect of object size', *Journal of Computer Assisted Tomography*. J Comput Assist Tomogr, 3(3), pp. 299–308. doi: 10.1097/00004728-197906000-00001.

Horakova, D. *et al.* (2012) 'Clinical correlates of grey matter pathology in multiple sclerosis', *BMC Neurology*. BioMed Central, p. 10. doi: 10.1186/1471-2377-12-10.

Hotamisligil, G. S. (2006) 'Inflammation and metabolic disorders', *Nature*. Nature Publishing Group, pp. 860–867. doi: 10.1038/nature05485.

Hunter, H. J. A. *et al.* (2016) 'Brain inflammation and psoriasis: a [11C]-(R)-PK11195 positron emission tomography study', *British Journal of Dermatology*. Blackwell Publishing Ltd, pp. 1082–1084. doi: 10.1111/bjd.13788.

Ichise, M. *et al.* (2002) 'Strategies to Improve Neuroreceptor Parameter Estimation by Linear Regression Analysis'. doi: 10.1097/01.WCB.0000038000.34930.4E.

Ikawa, M. *et al.* (2017) '11C-ER176, a radioligand for 18-kDa translocator protein, has adequate sensitivity to robustly image all three affinity genotypes in human brain', *Journal of Nuclear Medicine*. Society of Nuclear Medicine Inc., 58(2), pp. 320–325. doi: 10.2967/jnumed.116.178996.

Inglese, M. and Bester, M. (2010) 'Diffusion imaging in multiple sclerosis: Research and clinical implications', *NMR in Biomedicine*. NIH Public Access, pp. 865–872. doi: 10.1002/nbm.1515.

Innis, R. B. *et al.* (2007) 'Consensus Nomenclature for *in vivo* Imaging of Reversibly Binding Radioligands', *Journal of Cerebral Blood Flow & Metabolism*. SAGE PublicationsSage UK: London, England, 27(9), pp. 1533–1539. doi: 10.1038/sj.jcbfm.9600493.

Iozzo, P. and Guzzardi, M. A. (2019) 'Imaging of brain glucose uptake by PET in obesity and cognitive dysfunction: Life-course perspective', *Endocrine Connections*. BioScientifica Ltd., pp. R169–R183. doi: 10.1530/EC-19-0348.

Janssen, B. *et al.* (2016) 'Imaging of neuroinflammation in Alzheimer's disease, multiple sclerosis and stroke: Recent developments in positron emission tomography', *Biochimica et Biophysica Acta - Molecular Basis of Disease*. Elsevier B.V., 1862(3), pp. 425–441. doi: 10.1016/j.bbadis.2015.11.011.

Janssen, B. *et al.* (2018) 'PET Imaging of Microglial Activation-Beyond Targeting TSPO.', *Molecules (Basel, Switzerland)*. Multidisciplinary Digital Publishing Institute (MDPI), 23(3). doi: 10.3390/molecules23030607.

Jensen, E. C. (2014) 'Technical Review, Types of Imaging, Part 4-Magnetic Resonance Imaging', *The Anatomical Record*. John Wiley and Sons Inc., 297(6), pp. 973–978. doi: 10.1002/ar.22927.

Jong, H. W. A. M. de *et al.* (2007) 'Performance evaluation of the ECAT HRRT: an LSO-LYSO double layer high resolution, high sensitivity scanner', *Physics in Medicine and Biology*, 52(5), pp. 1505–1526. doi: 10.1088/0031-9155/52/5/019.

Jucaite, A. *et al.* (2015) 'Effect of the myeloperoxidase inhibitor AZD3241 on microglia: a PET study in Parkinson's disease', *Brain*. Oxford University Press, 138(9), pp. 2687–2700. doi: 10.1093/brain/awv184.

Kanegawa, N. *et al.* (2016) 'In vivo evidence of a functional association between immune cells in blood and brain in healthy human subjects', *Brain, Behavior, and Immunity*. Academic Press, 54, pp. 149–157. doi: 10.1016/J.BBI.2016.01.019.

Karjalainen, T. *et al.* (2020) 'Magia: Robust Automated Image Processing and Kinetic Modeling Toolbox for PET Neuroinformatics', *Frontiers in Neuroinformatics*, 14. doi: 10.3389/fninf.2020.00003.

Karlsson, H. K. *et al.* (2013) 'Obesity is associated with white matter atrophy: A combined diffusion tensor imaging and voxel-based morphometric study', *Obesity*, 21(12), pp. 2530–2537. doi: 10.1002/oby.20386.

Kaunzner, U. W. *et al.* (2017) 'Reduction of PK11195 uptake observed in multiple sclerosis lesions after natalizumab initiation', *Multiple Sclerosis and Related Disorders*. Elsevier B.V., 15, pp. 27–33. doi: 10.1016/j.msard.2017.04.008.

Kaunzner, U. W. *et al.* (2019) 'Quantitative susceptibility mapping identifies inflammation in a subset of chronic multiple sclerosis lesions', *Brain*. Oxford University Press, 142(1), pp. 133–145. doi: 10.1093/brain/awy296.

Kim, S. W. *et al.* (2018) 'Influence of alcoholism and cholesterol on TSPO binding in brain: PET [11 C]PBR28 studies in humans and rodents', *Neuropsychopharmacology*. Nature Publishing Group, 43(9), pp. 1832–1839. doi: 10.1038/s41386-018-0085-x.

Klaver, R. *et al.* (2015) 'Neuronal and Axonal Loss in Normal-Appearing Gray Matter and Subpial Lesions in Multiple Sclerosis', *Journal of Neuropathology and Experimental Neurology*. Lippincott Williams and Wilkins, 74(5), pp. 453–458. doi: 10.1097/NEN.0000000000000189.

Knudsen, G. M. *et al.* (2020) 'Guidelines for the content and format of PET brain data in publications and archives: A consensus paper', *Journal of Cerebral Blood Flow & Metabolism*. SAGE PublicationsSage UK: London, England, 40(8), pp. 1576–1585. doi: 10.1177/0271678X20905433.

Kobayashi, M. *et al.* (2018a) '^{11} C-DPA-713 has much greater specific binding to translocator protein 18 kDa (TSPO) in human brain than ^{11} C-(*R*)-PK11195', *Journal of Cerebral Blood Flow & Metabolism*. SAGE PublicationsSage UK: London, England, 38(3), pp. 393–403. doi: 10.1177/0271678X17699223.

Kobayashi, M. *et al.* (2018b) '^{11} C-DPA-713 has much greater specific binding to translocator protein 18 kDa (TSPO) in human brain than ^{11} C-(*R*)-PK11195', *Journal of Cerebral Blood Flow & Metabolism*. SAGE PublicationsSage UK: London, England, 38(3), pp. 393–403. doi: 10.1177/0271678X17699223.

Kolasa, M. *et al.* (2019) 'Diffusion tensor imaging and disability progression in multiple sclerosis: A 4-year follow-up study', *Brain and Behavior*. John Wiley and Sons Ltd, 9(1). doi: 10.1002/brb3.1194.

Kreutzberg, G. W. (1996) 'Microglia: A sensor for pathological events in the CNS', *Trends in Neurosciences*. Elsevier Ltd, pp. 312–318. doi: 10.1016/0166-2236(96)10049-7.

Kuhlmann, T. *et al.* (2002) 'Acute axonal damage in multiple sclerosis is most extensive in early disease stages and decreases over time', *Brain*. Oxford University Press, 125(10), pp. 2202–2212. doi: 10.1093/brain/awf235.

Kurtzke, J. F. (1983) 'Rating neurologic impairment in multiple sclerosis: An expanded disability status scale (EDSS)', *Neurology*. Neurology, 33(11), pp. 1444–1452. doi: 10.1212/wnl.33.11.1444.

Kutzelnigg, A. *et al.* (2005) 'Cortical demyelination and diffuse white matter injury in multiple sclerosis', *Brain*, 128, pp. 2705–2712. doi: 10.1093/brain/awh641.

Lammertsma, A. A. and Hume, S. P. (1996) 'Simplified Reference Tissue Model for PET Receptor Studies', *NeuroImage*, 4(3), pp. 153–158. doi: 10.1006/nimg.1996.0066.

Lavisse, S. *et al.* (2012) 'Reactive astrocytes overexpress TSPO and are detected by TSPO positron emission tomography imaging', *Journal of Neuroscience*. Society for Neuroscience, 32(32), pp. 10809–10818. doi: 10.1523/JNEUROSCI.1487-12.2012.

Leemans, A. and Jones, D. K. (2009) 'The B-matrix must be rotated when correcting for subject motion in DTI data', *Magnetic Resonance in Medicine*. Magn Reson Med, 61(6), pp. 1336–1349. doi: 10.1002/mrm.21890.

Leray, E. *et al.* (2010) 'Evidence for a two-stage disability progression in multiple sclerosis', *A JOURNAL OF NEUROLOGY*, 133, pp. 1900–1913. doi: 10.1093/brain/awq076.

Liddelow, S. *et al.* (2017) 'Neurotoxic reactive astrocytes are induced by activated microglia', *nikhil Panicker*, 10, p. 17. doi: 10.1038/nature21029.

Liu, Y. *et al.* (2012) 'Whole brain white matter changes revealed by multiple diffusion metrics in multiple sclerosis: A TBSS study', *European Journal of Radiology*. Eur J Radiol, 81(10), pp. 2826–2832. doi: 10.1016/j.ejrad.2011.11.022.

Lockhart, A. *et al.* (2003) 'The peripheral benzodiazepine receptor ligand PK11195 binds with high affinity to the acute phase reactant α1-acid glycoprotein: Implications for the use of the ligand as a CNS inflammatory marker', *Nuclear Medicine and Biology*. Elsevier, 30(2), pp. 199–206. doi: 10.1016/S0969-8051(02)00410-9.

Logan, J. *et al.* (1990) 'Graphical analysis of reversible radioligand binding from time-activity measurements applied to [N-11C-methyl]-(-)-cocaine PET studies in human subjects', *Journal of Cerebral Blood Flow and Metabolism*. Lippincott Williams and Wilkins, 10(5), pp. 740–747. doi: 10.1038/jcbfm.1990.127.

Logan, J. *et al.* (1996) 'Distribution volume ratios without blood sampling from graphical analysis of PET data.', *Journal of cerebral blood flow and metabolism : official journal of the International Society of Cerebral Blood Flow and Metabolism*. Nature Publishing Group, 16(5), pp. 834–40. doi: 10.1097/00004647-199609000-00008.

Lublin, F. D. *et al.* (2014) 'Defining the clinical course of multiple sclerosis: The 2013 revisions', *Neurology*. Lippincott Williams and Wilkins, pp. 278–286. doi: 10.1212/WNL.0000000000000560.

Lublin, F. D. *et al.* (2020) 'The 2013 clinical course descriptors for multiple sclerosis: A clarification', *Neurology*. NLM (Medline), pp. 1088–1092. doi: 10.1212/WNL.0000000000009636.

Lyoo, C. H. *et al.* (2015) 'Cerebellum can serve as a pseudo-reference region in Alzheimer disease to detect neuroinflammation measured with PET radioligand binding to translocator protein', *Journal of Nuclear Medicine*. Society of Nuclear Medicine Inc., 56(5), pp. 701–706. doi: 10.2967/jnumed.114.146027.

Mahad, D. H., Trapp, B. D. and Lassmann, H. (2015) 'Pathological mechanisms in progressive multiple sclerosis', *The Lancet Neurology*. Lancet Publishing Group, pp. 183–193. doi: 10.1016/S1474-4422(14)70256-X.

Matheson, G. J. *et al.* (2017) 'Assessment of simplified ratio-based approaches for quantification of PET [11C]PBR28 data.', *EJNMMI research*. Springer, 7(1), p. 58. doi: 10.1186/s13550-017-0304-1.

Mesaros, S. *et al.* (2011) 'Thalamic damage predicts the evolution of primary-progressive multiple sclerosis at 5 years', *American Journal of Neuroradiology*, 32(6), pp. 1016–1020. doi: 10.3174/ajnr.A2430.

Michell-Robinson, M. A. *et al.* (2015) 'Roles of microglia in brain development, tissue maintenance and repair.', *Brain : a journal of neurology*. Oxford University Press, 138(Pt 5), pp. 1138–59. doi: 10.1093/brain/awv066.

Miller, A. A. and Spencer, S. J. (2014) 'Obesity and neuroinflammation: A pathway to cognitive impairment', *Brain, Behavior, and Immunity*. Academic Press, 42, pp. 10–21. doi: 10.1016/J.BBI.2014.04.001.

Miller, K. R. and Streit, W. J. (2007) 'The effects of aging, injury and disease on microglial function: a case for cellular senescence', *Neuron Glia Biology*. Cambridge University Press, 3(03), pp. 245–253. doi: 10.1017/S1740925X08000136.

Minagar, A. *et al.* (2013) 'The thalamus and multiple sclerosis: Modern views on pathologic, imaging, and clinical aspects', *Neurology*, 80(2), pp. 210–219. doi: 10.1212/WNL.0b013e31827b910b.

Moll, N. M. *et al.* (2011) 'Multiple sclerosis normal-appearing white matter: Pathology-imaging correlations', *Annals of Neurology*. Ann Neurol, 70(5), pp. 764–773. doi: 10.1002/ana.22521.

Mori, S. and Zhang, J. (2006) 'Principles of Diffusion Tensor Imaging and Its Applications to Basic Neuroscience Research', *Neuron*. Cell Press, pp. 527–539. doi: 10.1016/j.neuron.2006.08.012.

Morris, E. D. *et al.* (2004) 'Kinetic Modeling in Positron Emission Tomography', in *Emission Tomography: The Fundamentals of PET and SPECT*. Elsevier Inc., pp. 499–540. doi: 10.1016/B978-012744482-6.50026-0.

Musella, A. *et al.* (2018) 'Interplay between age and neuroinflammation in multiple sclerosis: Effects on motor and cognitive functions', *Frontiers in Aging Neuroscience*. Frontiers Media S.A. doi: 10.3389/fnagi.2018.00238.

Nicastro, N. *et al.* (2020) 'Correlation of microglial activation with white matter changes in dementia with Lewy bodies', *NeuroImage: Clinical*. Elsevier Inc., 25, p. 102200. doi: 10.1016/j.nicl.2020.102200.

Nissen, J. C. (2017) 'Microglial Function across the Spectrum of Age and Gender.', *International journal of molecular sciences*. Multidisciplinary Digital Publishing Institute (MDPI), 18(3). doi: 10.3390/ijms18030561.

Notter, T. *et al.* (2018) 'Reconceptualization of translocator protein as a biomarker of neuroinflammation in psychiatry', *Molecular Psychiatry*. Nature Publishing Group, 23(1), pp. 36–47. doi: 10.1038/mp.2017.232.

Notter, T. *et al.* (2020) 'Neuronal activity increases translocator protein (TSPO) levels', *Molecular Psychiatry*. Springer Nature, pp. 1–13. doi: 10.1038/s41380-020-0745-1.

Nutma, E. *et al.* (2019) 'A quantitative neuropathological assessment of translocator protein expression in multiple sclerosis', *Brain*. Oxford University Press, 142(11), pp. 3440–3455. doi: 10.1093/brain/awz287.

O'Donnell, L. J. and Westin, C. F. (2011) 'An introduction to diffusion tensor image analysis', *Neurosurgery Clinics of North America*. NIH Public Access, pp. 185–196. doi: 10.1016/j.nec.2010.12.004.

Oh, U. *et al.* (2011) 'Translocator protein PET imaging for glial activation in multiple sclerosis', *Journal of Neuroimmune Pharmacology*. Springer New York LLC, 6(3), pp. 354–361. doi: 10.1007/s11481-010-9243-6.

Olsson, T., Barcellos, L. F. and Alfredsson, L. (2016) 'Interactions between genetic, lifestyle and environmental risk factors for multiple sclerosis', *Nature Reviews Neurology*. Nature Publishing Group, pp. 26–36. doi: 10.1038/nrneurol.2016.187.

Onu, M. *et al.* (2012) 'Diffusion abnormality maps in demyelinating disease: Correlations with clinical scores', *European Journal of Radiology*. Eur J Radiol, 81(3). doi: 10.1016/j.ejrad.2011.12.014.

Owen, D. R. *et al.* (2010) 'Two binding sites for 3 HPBR28 in human brain: Implications for TSPO PET imaging of neuroinflammation', *Journal of Cerebral Blood Flow and Metabolism*. SAGE Publications, 30(9), pp. 1608–1618. doi: 10.1038/jcbfm.2010.63.

Owen, D. R. *et al.* (2012) 'An 18-kDa Translocator Protein (TSPO) Polymorphism Explains Differences in Binding Affinity of the PET Radioligand PBR28', *Journal of Cerebral Blood Flow & Metabolism*, 32(1), pp. 1–5. doi: 10.1038/jcbfm.2011.147.

Owen, D. R. *et al.* (2014a) 'Determination of [(11)C]PBR28 binding potential in vivo: a first human TSPO blocking study.', *Journal of cerebral blood flow and metabolism : official journal of the International Society of Cerebral Blood Flow and Metabolism*. SAGE Publications, 34(6), pp. 989–94. doi: 10.1038/jcbfm.2014.46.

Owen, D. R. *et al.* (2014b) 'Determination of [(11)C]PBR28 binding potential in vivo: a first human TSPO blocking study.', *Journal of cerebral blood flow and metabolism : official journal of the International Society of Cerebral Blood Flow and Metabolism*. SAGE Publications, 34(6), pp. 989–994. doi: 10.1038/jcbfm.2014.46.

Pachner, A. R. and Steiner, I. (2009) 'The multiple sclerosis severity score (MSSS) predicts disease severity over time', *Journal of the Neurological Sciences*. Elsevier, 278(1–2), pp. 66–70. doi: 10.1016/j.jns.2008.11.020.

Papademetris, X. *et al.* (2006) 'BioImage Suite: An integrated medical image analysis suite: An update.', *The insight journal*. NIH Public Access, 2006, p. 209. Available at: http://www.ncbi.nlm.nih.gov/pubmed/25364771 (Accessed: 14 December 2020).

Park, E., Gallezot, J.-D., *et al.* (2015) '11C-PBR28 imaging in multiple sclerosis patients and healthy controls: test-retest reproducibility and focal visualization of active white matter areas', *European Journal of Nuclear Medicine and Molecular Imaging*. Springer Berlin Heidelberg, 42(7), pp. 1081–1092. doi: 10.1007/s00259-015-3043-4.

Park, E., Gallezot, J. D., *et al.* (2015) '11C-PBR28 imaging in multiple sclerosis patients and healthy controls: test-retest reproducibility and focal visualization of active white matter areas', *European Journal of Nuclear Medicine and Molecular Imaging*. Springer Berlin, 42(7), pp. 1081–1092. doi: 10.1007/s00259-015-3043-4.

Paul, S. *et al.* (2018) 'Building a database for brain 18 kDa translocator protein imaged using [^{11} C]PBR28 in healthy subjects', *Journal of Cerebral Blood Flow & Metabolism*. SAGE PublicationsSage UK: London, England, p. 0271678X1877125. doi: 10.1177/0271678X18771250.

Phelps, M. E. *et al.* (1979) 'Tomographic measurement of local cerebral glucose metabolic rate in humans with (F-18)2-fluoro-2-deoxy-D-glucose: Validation of method', *Annals of Neurology*, 6(5), pp. 371–388. doi: 10.1002/ana.410060502.

Phelps, M. E. and Mazziotta, J. C. (1985) 'Positron emission tomography: Human brain function and biochemistry', *Science*. American Association for the Advancement of Science, 228(4701), pp. 799–809. doi: 10.1126/science.2860723.

Pitt, D. and Ponath, G. (2019) 'Astrocytes play a crucial role in the formation and evolution of MS lesions – Yes', *Multiple Sclerosis Journal*. SAGE PublicationsSage UK: London, England, 25(1), pp. 15–17. doi: 10.1177/1352458518793026.

Plavén-Sigray, P. *et al.* (2018) 'Test-retest reliability and convergent validity of (R)-[11C]PK11195 outcome measures without arterial input function'. doi: 10.1101/298992.

Pokryszko-Dragan, A. *et al.* (2018) 'Diffusion tensor imaging findings in the multiple sclerosis patients and their relationships to various aspects of disability', *Journal of the Neurological Sciences*, 391(June), pp. 127–133. doi: 10.1016/j.jns.2018.06.007.

Politis, M. *et al.* (2012) 'Increased PK11195 PET binding in the cortex of patients with MS correlates with disability', *Neurology*. Lippincott Williams and Wilkins, 79(6), pp. 523–530. doi: 10.1212/WNL.0b013e3182635645.

Polman, C. H. *et al.* (2005) 'Diagnostic criteria for multiple sclerosis: 2005 revisions to the "McDonald Criteria"', *Annals of Neurology*, 58(6), pp. 840–846. doi: 10.1002/ana.20703.

Polman, C. H. and Rudick, R. A. (2010) 'The multiple sclerosis functional composite a clinically meaningful measure of disability', *Neurology*. Lippincott Williams and Wilkins. doi: 10.1212/WNL.0b013e3181dbb571.

Ponath, G., Park, C. and Pitt, D. (2018) 'The role of astrocytes in multiple sclerosis', *Frontiers in Immunology*. Frontiers Media S.A., p. 1. doi: 10.3389/fimmu.2018.00217.

Poonawalla, A. H. *et al.* (2008) 'Diffusion-tensor MR imaging of cortical lesions in multiple sclerosis: Initial findings', *Radiology*. Radiology, 246(3), pp. 880–886. doi: 10.1148/radiol.2463070486.

Poser, C. M. *et al.* (1983) 'New diagnostic criteria for multiple sclerosis: Guidelines for research protocols', *Annals of Neurology*. John Wiley & Sons, Ltd, 13(3), pp. 227–231. doi: 10.1002/ana.410130302.

Preziosa, P. *et al.* (2011) 'Intrinsic Damage to the Major White Matter Tracts in Patients with Different Clinical Phenotypes of Multiple Sclerosis: A Voxelwise Diffusion-Tensor MR Study 1', *Radiology*, 260(2). doi: 10.1148/radiol.11110315/-/DC1.

Puy, L. *et al.* (1995) 'Immunocytochemical detection of androgen receptor in human temporal cortex characterization and application of polyclonal androgen receptor antibodies in frozen and paraffin-embedded tissues.', *The Journal of steroid biochemistry and molecular biology*, 55(2), pp. 197–209. Available at: http://www.ncbi.nlm.nih.gov/pubmed/7495699 (Accessed: 19 December 2018).

Ransohoff, R. M., Hafler, D. A. and Lucchinetti, C. F. (2015) 'Multiple sclerosis - A quiet revolution', *Nature Reviews Neurology*. Nature Publishing Group, pp. 134–142. doi: 10.1038/nrneurol.2015.14.

Rashid, W. *et al.* (2008) 'Longitudinal evaluation of clinically early relapsing-remitting multiple sclerosis with diffusion tensor imaging', *Journal of Neurology*. J Neurol, 255(3), pp. 390–397. doi: 10.1007/s00415-008-0678-0.

Ratchford, J. N. *et al.* (2012) 'Decreased microglial activation in MS patients treated with glatiramer acetate', *Journal of Neurology*. NIH Public Access, 259(6), pp. 1199–1205. doi: 10.1007/s00415-011-6337-x.

Raz, E. *et al.* (2010) 'Gray- and white-matter changes 1 year after first clinical episode of multiple sclerosis: MR imaging', *Radiology*. Radiology, 257(2), pp. 448–454. doi: 10.1148/radiol.10100626.

Rissanen, E. *et al.* (2014) 'In vivo detection of diffuse inflammation in secondary progressive multiple sclerosis using PET imaging and the radioligand11C-PK11195', *Journal of Nuclear Medicine*. Society of Nuclear Medicine Inc., 55(6), pp. 939–944. doi: 10.2967/jnumed.113.131698.

Rizzo, G. *et al.* (2019) 'Generalization of endothelial modelling of TSPO PET imaging: Considerations on tracer affinities', *Journal of Cerebral Blood Flow and Metabolism*. SAGE Publications Ltd, 39(5), pp. 874–885. doi: 10.1177/0271678X17742004.

Rocca, M. A. *et al.* (2017) 'Brain MRI atrophy quantification in MS', *Neurology*. Lippincott Williams and Wilkins, 88(4), pp. 403–413. doi: 10.1212/WNL.0000000000003542.

Roosendaal, S. D. *et al.* (2009) 'Regional DTI differences in multiple sclerosis patients', *NeuroImage*. Academic Press, 44(4), pp. 1397–1403. doi: 10.1016/j.neuroimage.2008.10.026.

Rousset, O. G., Ma, Y. and Evans, A. C. (1998) 'Correction for Partial Volume Effects in PET: Principle and Validation', *Journal of Nuclear Medicine*, 39(5), p. 904-911.

Rovaris, M. *et al.* (2002) 'Cognitive dysfunction in patients with mildly disabling relapsing-remitting multiple sclerosis: An exploratory study with diffusion tensor MR imaging', *Journal of the Neurological Sciences*. Elsevier, 195(2), pp. 103–109. doi: 10.1016/S0022-510X(01)00690-6.

Roxburgh, R. H. S. R. *et al.* (2005) 'Multiple sclerosis severity score: Using disability and disease duration to rate disease severity', *Neurology*. Lippincott Williams and Wilkins, 64(7), pp. 1144–1151. doi: 10.1212/01.WNL.0000156155.19270.F8.

Sahraian, M. A. and Radue, E.-W. (2008) *MRI Atlas of MS Lesions*, *MRI Atlas of MS Lesions*. Springer Berlin Heidelberg. doi: 10.1007/978-3-540-71372-2.

Salat, D. H. *et al.* (2009) 'Regional white matter volume differences in nondemented aging and Alzheimer's disease', *NeuroImage*. Neuroimage, 44(4), pp. 1247–1258. doi: 10.1016/j.neuroimage.2008.10.030.

Samara, A. *et al.* (2020) 'Neuroinflammation and White Matter Alterations in Obesity Assessed by Diffusion Basis Spectrum Imaging', *Frontiers in Human Neuroscience*. Frontiers Media S.A., 13, p. 464. doi: 10.3389/fnhum.2019.00464.

Sandiego, C. M. *et al.* (2015) 'Imaging robust microglial activation after lipopolysaccharide administration in humans with PET.', *Proceedings of the National Academy of Sciences of the United States of America*. National Academy of Sciences, 112(40), pp. 12468–73. doi: 10.1073/pnas.1511003112.

Sbardella, E. *et al.* (2013) 'DTI Measurements in Multiple Sclerosis: Evaluation of Brain Damage and Clinical Implications', *Multiple Sclerosis International*. Hindawi Limited, 2013, pp. 1–11. doi: 10.1155/2013/671730.

Schmidt, P. *et al.* (2012) 'An automated tool for detection of FLAIR-hyperintense white-matter lesions in Multiple Sclerosis', *NeuroImage*. Elsevier Inc., 59(4), pp. 3774–3783. doi: 10.1016/j.neuroimage.2011.11.032.

Schmidt, P. (2017) 'Bayesian inference for structured additive regression models for large-scale problems with applications to medical imaging', (November).

Schubert, J. J. *et al.* (2020) 'A modest increase in 11 C-PK11195-PET TSPO binding in depression is not associated with serum C-reactive protein or body mass index', *medrxiv.org*. doi: 10.1101/2020.06.04.20099556.

Schuitemaker, A., van der Doef, Thalia F, *et al.* (2012) 'Microglial activation in healthy aging', *Neurobiology of Aging*, 33(6), pp. 1067–1072. doi: 10.1016/j.neurobiolaging.2010.09.016.

Schuitemaker, A., van der Doef, Thalia F., *et al.* (2012) 'Microglial activation in healthy aging', *Neurobiology of Aging*. Elsevier, 33(6), pp. 1067–1072. doi: 10.1016/J.NEUROBIOLAGING.2010.09.016.

Schwarz, J. M., Sholar, P. W. and Bilbo, S. D. (2012) 'Sex differences in microglial colonization of the developing rat brain.', *Journal of neurochemistry*. NIH Public Access, 120(6), pp. 948–63. doi: 10.1111/j.1471-4159.2011.07630.x.

Sekine, Y. *et al.* (2008) 'Methamphetamine causes microglial activation in the brains of human abusers', *Journal of Neuroscience*. J Neurosci, 28(22), pp. 5756–5761. doi: 10.1523/JNEUROSCI.1179-08.2008.

Sheng, J. G., Mrak, R. E. and Griffin, W. S. (1998) 'Enlarged and phagocytic, but not primed, interleukin-1 alpha-immunoreactive microglia increase with age in normal human brain.', *Acta neuropathologica*, 95(3), pp. 229–34. Available at: http://www.ncbi.nlm.nih.gov/pubmed/9542587 (Accessed: 18 June 2018).

Da Silva, T. *et al.* (2019) 'In Vivo Imaging of Translocator Protein in Long-term Cannabis Users', *JAMA Psychiatry*. American Medical Association, 76(12), pp. 1305–1313. doi: 10.1001/jamapsychiatry.2019.2516.

Singh, S. *et al.* (2017) 'Relationship of acute axonal damage, Wallerian degeneration, and clinical disability in multiple sclerosis', *Journal of Neuroinflammation*. BioMed Central Ltd., 14(1), p. 57. doi: 10.1186/s12974-017-0831-8.

Singhal, T. *et al.* (2019) 'Gray matter microglial activation in relapsing vs progressive MS: A [F-18]PBR06-PET study', *Neurology: Neuroimmunology and NeuroInflammation*. Lippincott Williams and Wilkins, 6(5), p. 587. doi: 10.1212/NXI.0000000000000587.

Smith, S. M. *et al.* (2004) 'Advances in functional and structural MR image analysis and implementation as FSL', in *NeuroImage*. Academic Press, pp. S208–S219. doi: 10.1016/j.neuroimage.2004.07.051.

Sobesky, J. L. *et al.* (2014) 'High-fat diet consumption disrupts memory and primes elevations in hippocampal IL-1β, an effect that can be prevented with dietary reversal or IL-1 receptor antagonism.', *Brain, behavior, and immunity*. NIH Public Access, 42, pp. 22–32. doi: 10.1016/j.bbi.2014.06.017.

Su, Z. *et al.* (2013) '[11C]-(R)PK11195 tracer kinetics in the brain of glioma patients and a comparison of two referencing approaches', *European Journal of Nuclear Medicine and Molecular Imaging*. Springer, 40(9), pp. 1406–1419. doi: 10.1007/s00259-013-2447-2.

Sucksdorff, Marcus *et al.* (2017) 'Evaluation of the Effect of Fingolimod Treatment on Microglial Activation Using Serial PET Imaging in Multiple Sclerosis.', *Journal of nuclear medicine : official publication, Society of Nuclear Medicine*. Society of Nuclear Medicine, 58(10), pp. 1646–1651. doi: 10.2967/jnumed.116.183020.

Sucksdorff, M. *et al.* (2017) 'Evaluation of the effect of fingolimod treatment on microglial activation using serial PET imaging in multiple sclerosis', *Journal of Nuclear Medicine*, 58(10), pp. 1646–1651. doi: 10.2967/jnumed.116.183020.

Sucksdorff, M. *et al.* (2019) 'Natalizumab treatment reduces microglial activation in the white matter of the MS brain', *Neurology: Neuroimmunology and NeuroInflammation*, 6(4). doi: 10.1212/NXI.0000000000000574.

Sucksdorff, Marcus *et al.* (2019) 'Natalizumab treatment reduces microglial activation in the white matter of the MS brain', *Neurology: Neuroimmunology and NeuroInflammation*. Lippincott Williams and Wilkins, 6(4). doi: 10.1212/NXI.0000000000000574.

Sucksdorff, M. *et al.* (2020) 'Brain TSPO-PET predicts later disease progression independent of relapses in multiple sclerosis', *Brain*. Oxford University Press (OUP), 143(11), pp. 3318–3330. doi: 10.1093/brain/awaa275.

Suridjan, I. *et al.* (2014) 'Neuroinflammation in healthy aging: A PET study using a novel Translocator Protein 18 kDa (TSPO) radioligand, [18F]-FEPPA', *NeuroImage*. Academic Press, 84, pp. 868–875. doi: 10.1016/J.NEUROIMAGE.2013.09.021.

Suridjan, I *et al.* (2014) 'Neuroinflammation in healthy aging: A PET study using a novel Translocator Protein 18kDa (TSPO) radioligand, [18F]-FEPPA', *NeuroImage*, 84, pp. 868–875. doi: 10.1016/j.neuroimage.2013.09.021.

Thompson, A. J., Banwell, B. L., *et al.* (2018) 'Diagnosis of multiple sclerosis: 2017 revisions of the McDonald criteria', *The Lancet Neurology*. Lancet Publishing Group, pp. 162–173. doi: 10.1016/S1474-4422(17)30470-2.

Thompson, A. J., Baranzini, S. E., *et al.* (2018) 'Multiple sclerosis', *The Lancet*. Lancet Publishing Group, pp. 1622–1636. doi: 10.1016/S0140-6736(18)30481-1.

Tjerkaski, J. *et al.* (2020) 'Kinfitr — an open-source tool for reproducible PET modelling: validation and evaluation of test-retest reliability', *EJNMMI Research*. Springer, 10(1). doi: 10.1186/s13550-020-00664-8.

Tommasin, S. *et al.* (2019) 'Neuroimaging Techniques to Assess Inflammation in Multiple Sclerosis', *Neuroscience*. Elsevier Ltd, pp. 4–16. doi: 10.1016/j.neuroscience.2017.07.055.

Toppala, S. *et al.* (2021) 'Association of Early Beta-amyloid Accumulation and Neuroinflammation Measured with [11C]PBR28 in Elderly Individuals Without Dementia.', *Neurology*. Wolters Kluwer Health, Inc. on behalf of the American Academy of Neurology. doi: 10.1212/WNL.0000000000011612.

Turkheimer, F. E. *et al.* (2007) 'Reference and target region modeling of [11C]-(R)-PK11195 brain studies', *Journal of Nuclear Medicine*. Society of Nuclear Medicine, 48(1), pp. 158–167.

Turkheimer, F. E. *et al.* (2015) 'The methodology of TSPO imaging with positron emission tomography', *Biochemical Society Transactions*. Portland Press Ltd, pp. 586–592. doi: 10.1042/BST20150058.

Turkheimer, F. E. *et al.* (2020) 'Increased serum peripheral C-reactive protein is associated with reduced brain barriers permeability of TSPO radioligands in healthy volunteers and depressed patients: implications for inflammation and depression', *Brain, Behavior, and Immunity*. Academic Press Inc. doi: 10.1016/j.bbi.2020.10.025.

Tutuncu, M. *et al.* (2013) 'Onset of progressive phase is an age-dependent clinical milestone in multiple sclerosis', *Multiple Sclerosis Journal*. NIH Public Access, 19(2), pp. 188–198. doi: 10.1177/1352458512451510.

Tzourio-Mazoyer, N. *et al.* (2002) 'Automated Anatomical Labeling of Activations in SPM Using a Macroscopic Anatomical Parcellation of the MNI MRI Single-Subject Brain', *NeuroImage*. Academic Press, 15(1), pp. 273–289. doi: 10.1006/NIMG.2001.0978.

Uchoa, M. F., Moser, V. A. and Pike, C. J. (2016) 'Interactions between inflammation, sex steroids, and Alzheimer's disease risk factors.', *Frontiers in neuroendocrinology*. NIH Public Access, 43, pp. 60–82. doi: 10.1016/j.yfrne.2016.09.001.

Unterrainer, M. *et al.* (2018) 'TSPO PET with [18F]GE-180 sensitively detects focal neuroinflammation in patients with relapsing–remitting multiple sclerosis', *European Journal of Nuclear Medicine and Molecular Imaging*. Springer Berlin Heidelberg, 45(8), pp. 1423–1431. doi: 10.1007/s00259-018-3974-7.

Varrone, A. *et al.* (2009) 'Advancement in PET quantification using 3D-OP-OSEM point spread function reconstruction with the HRRT', *European Journal of Nuclear Medicine and Molecular Imaging*, 36(10), pp. 1639–1650. doi: 10.1007/s00259-009-1156-3.

Veronese, M. *et al.* (2018) 'Kinetic modelling of [11C]PBR28 for 18 kDa translocatorprotein PET data: A validation study of vascular modelling in the brain usingXBD173 and tissue analysis', *Journal of Cerebral Blood Flow & Metabolism*. SAGE Publications, 38(7), p. 1227. doi: 10.1177/0271678X17712388.

Versijpt, J. *et al.* (2005) 'Microglial imaging with positron emission tomography and atrophy measurements with magnetic resonance imaging in multiple sclerosis: A correlative study', *Multiple Sclerosis*. Mult Scler, 11(2), pp. 127–134. doi: 10.1191/1352458505ms1140oa.

Villa, A. *et al.* (2016) 'Estrogens, Neuroinflammation, and Neurodegeneration.', *Endocrine reviews*. The Endocrine Society, 37(4), pp. 372–402. doi: 10.1210/er.2016-1007.

Villa, A. *et al.* (2018) 'Sex-Specific Features of Microglia from Adult Mice.', *Cell reports*. Elsevier, 23(12), pp. 3501–3511. doi: 10.1016/j.celrep.2018.05.048.

Vomacka, L. *et al.* (2017) 'TSPO imaging using the novel PET ligand [18F]GE-180: quantification approaches in patients with multiple sclerosis', *EJNMMI Research*. Springer Verlag, 7(1). doi: 10.1186/s13550-017-0340-x.

Vowinckel, E. *et al.* (1997) 'PK11195 binding to the peripheral benzodiazepine receptor as a marker of microgila activation in multiple sclerosis and experimental autoimmune encephalomyelitis', *Journal of Neuroscience Research*. John Wiley & Sons, Ltd, 50(2), pp. 345–353. doi: 10.1002/(SICI)1097-4547(19971015)50:2<345::AID-JNR22>3.0.CO;2-5.

Welton, T. *et al.* (2015) 'Functionally Relevant White Matter Degradation in Multiple Sclerosis: A Tract-based Spatial Meta-Analysis', *Radiology*. Radiological Society of North America Inc., 275(1), pp. 89–96. doi: 10.1148/radiol.14140925.

Wheeler-Kingshott, C. A. M. and Cercignani, M. (2009) 'About "axial" and "radial" diffusivities', *Magnetic Resonance in Medicine*. John Wiley and Sons Inc., 61(5), pp. 1255–1260. doi: 10.1002/mrm.21965.

Wimberley, C. *et al.* (2018) 'Impact of endothelial 18-kDa translocator protein on the quantification of 18 F-DPA-714', *Journal of Nuclear Medicine*. Society of Nuclear Medicine Inc., 59(2), pp. 307–314. doi: 10.2967/jnumed.117.195396.

Witte, M. E. *et al.* (2014) 'Mitochondrial dysfunction contributes to neurodegeneration in multiple sclerosis', *Trends in Molecular Medicine*. Trends Mol Med, pp. 179–187. doi: 10.1016/j.molmed.2013.11.007.

Yaqub, M. *et al.* (2012) 'Optimization of supervised cluster analysis for extracting reference tissue input curves in (R)-[11C]PK11195 brain PET studies', *Journal of Cerebral Blood Flow and Metabolism*. J Cereb Blood Flow Metab, 32(8), pp. 1600–1608. doi: 10.1038/jcbfm.2012.59.

Yasuno, F. *et al.* (2008) 'Increased Binding of Peripheral Benzodiazepine Receptor in Alzheimer's Disease Measured by Positron Emission Tomography with [11C]DAA1106', *Biological Psychiatry*. Elsevier, 64(10), pp. 835–841. doi: 10.1016/J.BIOPSYCH.2008.04.021.

Zanotti-Fregonara, P. *et al.* (2019) 'Automatic extraction of a reference region for the noninvasive quantification of translocator protein in brain using 11C-PBR28', *Journal of Nuclear Medicine*. Society of Nuclear Medicine Inc., 60(7), pp. 978–984. doi: 10.2967/jnumed.118.222927.

Zimmer, E. R. *et al.* (2017) '[18F]FDG PET signal is driven by astroglial glutamate transport', *Nature Neuroscience*. Nature Publishing Group, 20(3), pp. 393–395. doi: 10.1038/nn.4492.

TURUN
YLIOPISTO
UNIVERSITY
OF TURKU

ISBN 978-951-29-8484-8 (PRINT)
ISBN 978-951-29-8485-5 (PDF)
ISSN 0355-9483 (Print)
ISSN 2343-3213 (Online)

Painosalama Oy, Turku, Finland 2021